The Resistance and Propulsion Committee

Final Report and Recommendations to the 29th ITTC

1. INTRODUCTION

1.1 Membership and meetings

The members of the Resistance and Propulsion Committee of the 29th ITTC were:

- Richard Pattenden (Chair)
  QinetiQ, United Kingdom
- Nikolaj Lemb Larsen (Secretary)
  FORCE, Denmark
- João L. D. Dantas
  IPT, Brazil
- Bryson Metcalf
  Naval Surface Warfare Center, Carderock Division, USA
- Wentao Wang
  China Ship Scientific Research Centre, China
- Yasuhiko Inukai
  Japan Marine United Corporation, Japan
- Tokihiro Katsui
  Kobe University, Japan
- Seok Cheon Go
  HHI, South Korea
- Haeseong Ahn
  KRISO, South Korea
- Patrick Queutey
  ECN, France
- Devrim Bulent Danisman
  Istanbul Technical University, Turkey
- Yigit Kemal Demirel
  University of Strathclyde, United Kingdom
- Aleksey Yakovlev
  Krylov State Research Centre, Russia

Four meetings were held during the term of the committee:

- QinetiQ, Gosport, United Kingdom, 16-18 January 2018.
- Japan Marine United Corporation, Yokohama, Japan, 23-24 October 2018.
- FORCE, Copenhagen, Denmark, 8-9 May 2019.
- KRISO, Daejeon, South Korea, 14-16 January 2020.

1.2 Tasks

The 28th ITTC recommended the following tasks for the 29th ITTC Resistance and Propulsion Committee:

1. Update the state-of-the-art for predicting the performance of different ship concepts emphasizing developments since the 2017 ITTC Full Conference. The committee report should include sections on:

a. The potential impact of new technological developments on the ITTC, including, for example superhydrophobic materials, new types of propulsors (e.g. hybrid propulsors), azimuthing thrusters, cycloidal propellers, propulsors with flexible blades and rim drives.

b. New experimental techniques and extrapolation methods

c. New benchmark data

d. The practical applications of computational methods to performance predictions and scaling.

e. New developments of experimental and computational methods applicable to the prediction of cavitation.

f. The need for R&D for improving methods of model experiments, numerical modelling and full-scale measurements.

2. During the first year, review ITTC Recommended Procedures relevant to resistance, propulsion and performance prediction, including CFD procedures, and a. identify any requirements for changes in the light of current practice, and, if approved by the Advisory Council, update them, b. identify the need for new procedures and outline the purpose and contents of these.

3. Develop a new procedure for wave profile measurement and wave resistance analysis.

4. Develop a procedure for verification and validation of the detailed flow field data.

5. Cooperate and exchange information with the Specialist Committee on Energy Saving Methods on subjects of common interest.

6. Cooperate and exchange information with the Specialist Committee on Ships in Operation at Sea regarding consequences of EEDI, especially with respect to ITTC Recommended Procedures.

7. Investigate the need of change of standard hull and propeller roughness. Develop and propose new roughness correction methods for both hull and propeller.

8. Conduct the validation of the procedure 7.5-02-03-01.7, 1978 ITTC Performance Prediction Method for Unequally Loaded, Multiple Propeller Vessels.

9. Continue with the monitoring of existing full scale data for podded propulsion. If there is available data, refine the existing procedure.

10. Continue the benchmark campaign with regard to the examination of the possibilities of CFD methods regarding scaling of unconventional propeller open water data. Continue comparative CFD calculation project.

11. Continue with monitoring the use of and, if possible, develop guidelines for quasi-steady open water propeller and propulsion model tests.

12. Conduct a survey of cavitation erosion modelling and predicting methods and identify the need of change of ITTC procedures in this respect.

13. Identify the need of the elaboration of the procedure concerning the rim drives model testing and performance prediction. Elaborate the procedure when necessary.

14. Identify the influence of the new FD definition on power prediction.

15. Investigate the need of changing the standard criterion for Re in model tests of propulsors as well as in the aspect of CFD validation.

16. Investigate the need of change of scaling methods with regard to propulsors (including pods).

17. Investigate and describe a propulsor performance in waves, and discuss the scale effects on its modelling.

2. STATE OF THE ART

2.1 Technological developments

Composite propellers are one of the technologies that are gathering attention for improving efficiency and reducing cavitation and noise. Many papers on composite propellers were presented at SMP'19.

Grasso et al. (2019) presented the measurement results for the deformation of composite propellers not only at model scale but also at ship scale, which contributed valuable knowledge on the full scale hydro-elastic behaviour to exploit the full potential of this technology. The Digital Image Correlation (DIC) technique was used for measuring the deformation. This technique is an image analysis method that tracks and correlates the grey value pattern in small square groups of pixels called subsets. The commercial software, Vic3D, was used for the DIC analysis to perform the camera system calibration, calculate the displacements and output the results for post-processing. To filter out the effect of the non-periodic higher frequency blade vibrations, a surface averaging procedure was developed. Model scale tests were conducted using two composite propellers operating in non-uniform flow in a cavitation tunnel, with a wake generator mounted inside the tunnel (Figure 1 and Figure 2). After confirming the accuracy of the measurement system at model scale, the full scale measurements were performed during a sea trial on the Royal Netherlands Navy Diving Support Vessel “Nautilus”, equipped with a flexible composite propeller. The measurement system was composed of two cameras on the rudder and two sets of strobe lights synchronized with the propeller shaft and camera that are mounted on the rudder and on the hull (Figure 3). In spite of more challenging conditions, i.e. underwater visibility, cavitation and vibrations, compared to the model test, excellent measurement quality was achieved and the blade deformations were delivered with an accuracy comparable to the test at model scale (Figure 4).

Shiraishi et al. (2019) developed a different measurement technique for the deformation of a composite propeller. They used combination-line CCD cameras to measure the amount of deformation of a five bladed, highly skewed propeller made from a carbon filled nylon material (Figure 5). From the amount of deformation measured, the deformed 3D blade shape was estimated using an image-registration in which the deformation was assumed to be represented by a rotation matrix and a translation vector (Figure 6). This measurement technique was utilized by Suyama et al. (2019) who conducted an exhaustive study to predict the performance of a composite propeller. They compared calculations using Fluid-Structure Interaction (FSI) analysis, which combines Computational Fluid Dynamics (CFD) and Finite Element Analysis (FEA), with experiments on the performance in uniform flow and wake flow. The amount of deformation for the same highly skewed propeller as Shiraishi et al. was measured. The difference in the performance and the deformation between propellers made from two kinds of material, i.e. aluminium and carbon, could be well predicted and it was concluded that FSI analysis can be useful for a design of a composite propeller.

Figure 1: Camera setup in the cavitation tunnel (Grasso et al., 2019)

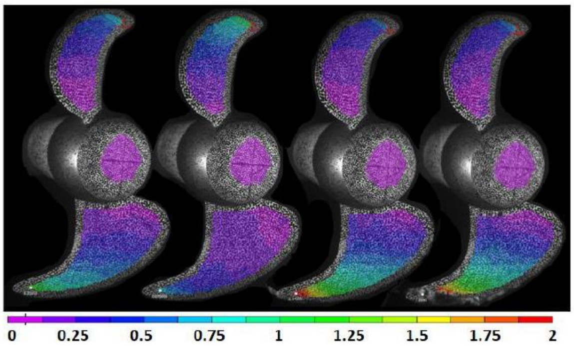

Figure 2: Example of variation in total blade deflection at the tip (Grasso et al., 2019)

Figure 3: Stereo camera setup installed on the port side of the diving support vessel “Nautilus” (Grasso et al., 2019)

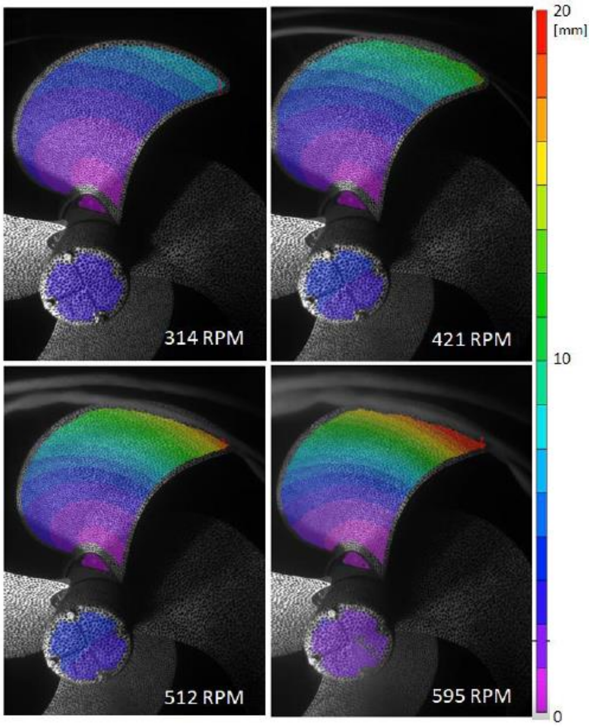

Figure 4: Propeller deflection with only one propeller engaged at increasing RPM (Grasso et al., 2019)

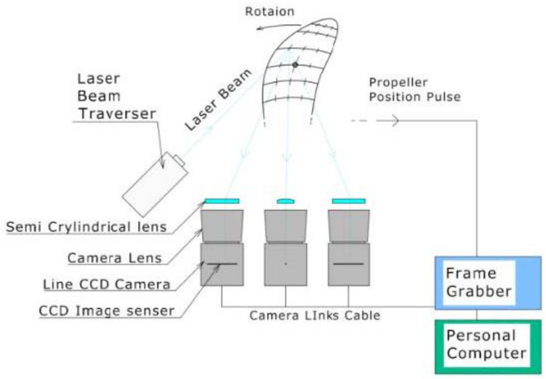

Figure 5: Schematic of measurement system using line CCD cameras (Shiraishi et al., 2019)

Aktas et al. (2019) presented numerical and experimental investigations on a new propeller noise mitigation method, PressurePores^{TM}. This technology implements pressure-relieving holes (PressurePores^{TM}) on marine propellers to mitigate the cavitation induced noise for a more silent propeller. The results showed a significant reduction of cavitation noise (up to 17dB) with the pressure pores while losing only 2% of propeller efficiency.

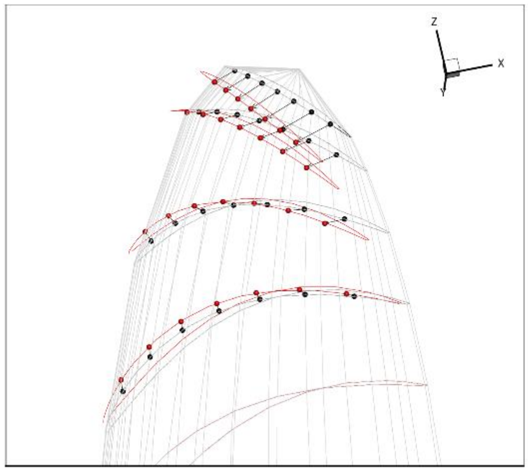

Figure 6: Estimated wing section positions of the model propeller from the deformation measured using line CCD cameras

Figure 7: PressurePores^{TM} as applied on the Princess Royal propeller (Aktas et al., 2019)

Klinkenberg et al. (2017) carried out an experimental campaign to evaluate the performance of a rim-driven tunnel thruster model. The results presented focus on the noise measurements. They found disturbances in signals believed to be due to undesired electromagnetic current, inadequate grounding or engine control switches. Furthermore, for the complex set-up developed in-house, shown in Figure 8, they discussed the challenges and issues encountered during the experiments.

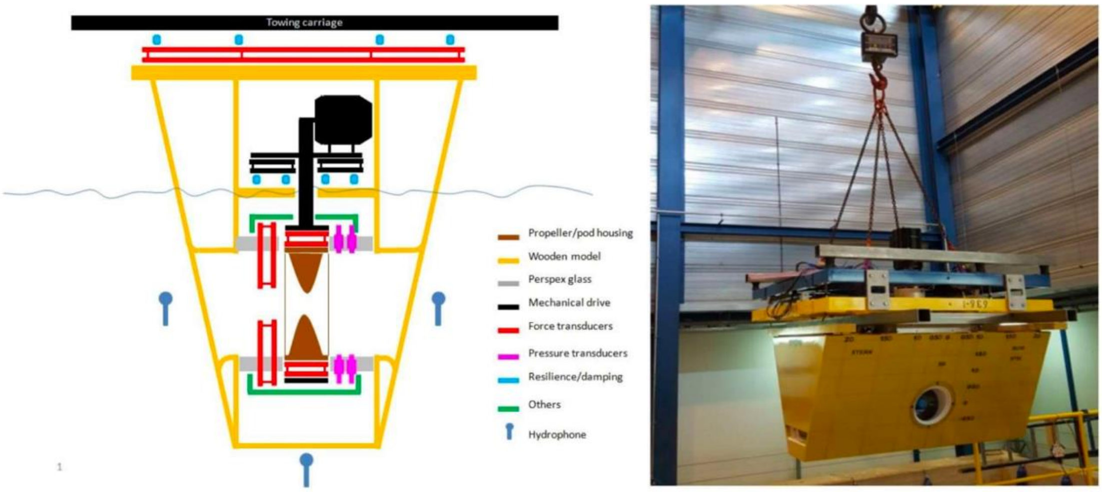

Figure 8: Experimental setup to measure performance of rim driven tunnel thruster (Klinkenberg et al., 2017)

2.2 Experimental techniques and extrapolation methods

Hiroi et al. (2019) conducted the full scale measurement for flows around a duct, fitted to a 63,000DWT bulk carrier, using PIV (Figure 9). Underwater noise and propeller induced pressure fluctuations were also measured in the project. Wake data on the two planes shown in Figure 9 were recorded in 2D2C (2-Dimensions, 2-Components) and transformed afterwards into 0D2C (0-Dimensions, 2-Components) data by spatial averaging. The measured data was compared with RANS simulation by Sakamoto et al. (2020). CFD showed good agreement as shown in Figure 10 and the authors claimed that the surface roughness will be one of the indispensable parameters to be considered for CFD simulations in full scale.

Inukai (2019) conducted the full scale measurement at the stern of a 14,000 TEU container ship using Multi-Layered Doppler Sonar (MLDS) which is an acoustic Doppler sonar capable of measuring relative water velocity at multiple arbitrary depths along an ultra-sonic beam. Although the largest obstacle against the measurements of flow fields at full scale is the complexity and high cost associated with the measurement system, an MLDS is less expensive and easier to install and handle compared with other methods such as LDV or PIV because it uses the same hardware as the commercially available Doppler Sonar. Velocities in six directions of the ultrasonic beam transmitted from the transducer can be measured. They showed that MLDS can measure velocities within a reasonable accuracy and offers good validation data for CFD calculations. Figure 11 shows the measurement area of the MLDS and a comparison of velocities in the ultrasonic beam direction between the measurement and the RANS simulation.

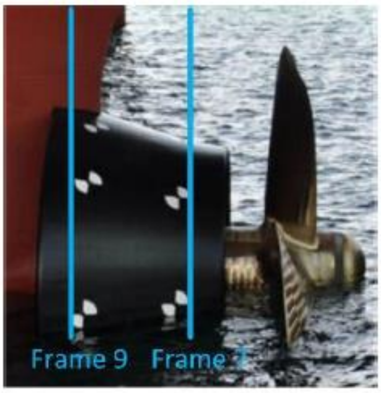

Figure 9: Photo of a duct around which flow was measured using PIV (Hiroi et al., 2019)

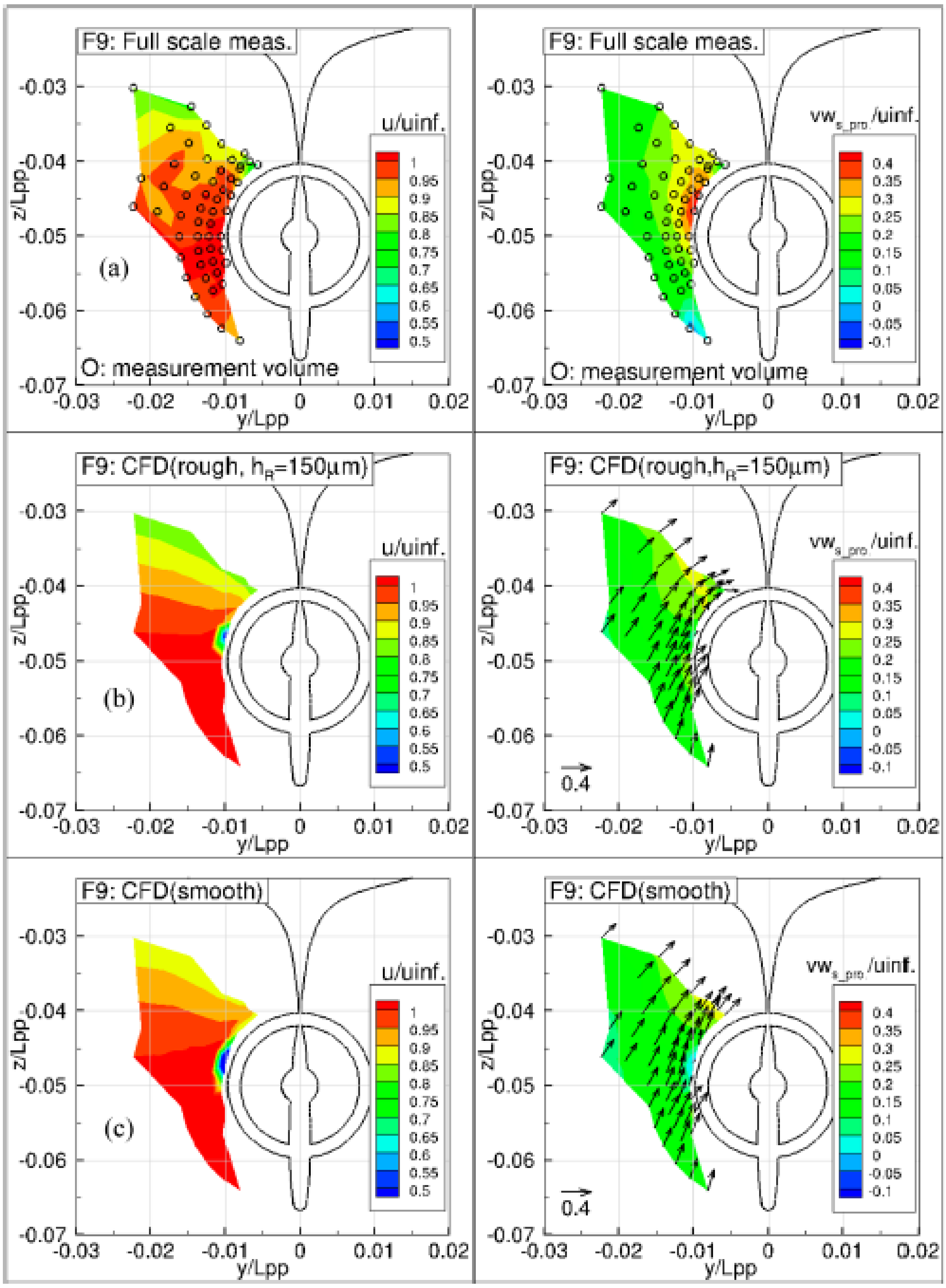

Figure 10: Experimental and computational results of total wake distribution; (a) PIV, (b) CFD with roughness, (c) CFD without roughness (Sakamoto et al., 2020)

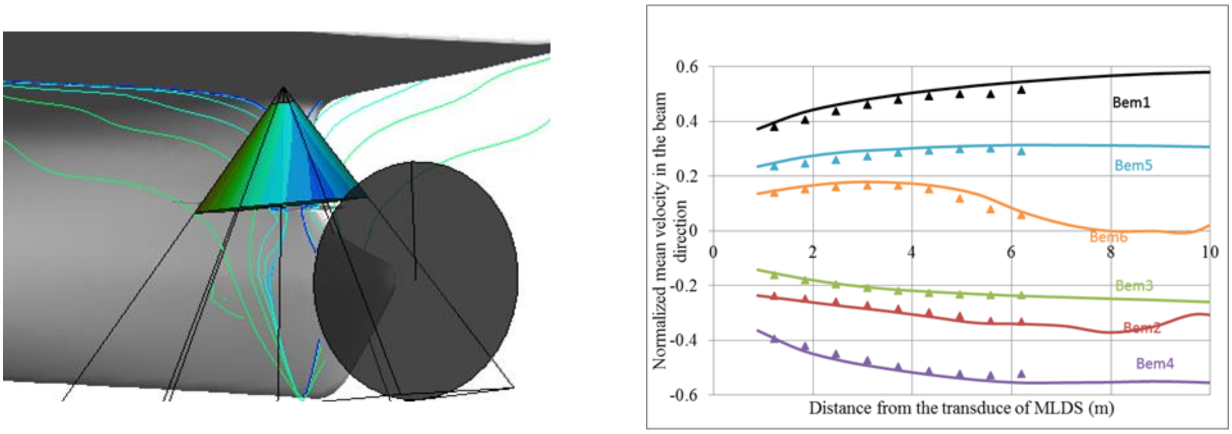

Figure 11: Measurement area by MLDS (left) and comparison of normalized mean velocity in the ultrasonic beam direction between CFD (lines) and measurement (marks) (right) (Inukai, 2019)

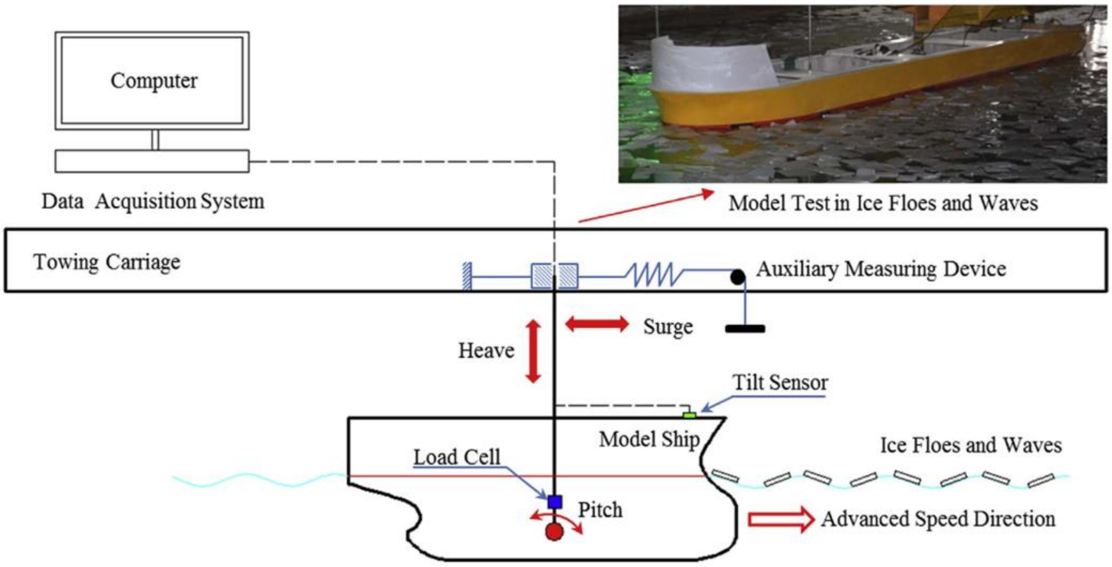

Figure 12: Experimental setup for test in MIZ (Luo et al., 2018)

Ravina and Guidomei (2018) developed an air-bubbling technique for resistance reduction. An original, customised, pneumatic distribution circuit was designed for the air-bubbling and it was applied to different types of flat plates and a hull model. From the towing tests of the plates and hull models, the effective shape of air bubbles is observed while measuring the local skin friction. The result showed that the advantage of air bubbling is more evident at high speed. Also, they concluded that using fewer holes with larger diameters compared favourably to using more holes with a smaller diameter.

Luo et al. (2018) carried out an experimental campaign to investigate the ship-wave-ice interaction in marginal ice zones. Using paraffin as model ice, the ship model test was conducted at a towing tank equipped with a wave generator. The results showed that the motion of the ship model is more unstable in marginal ice zones than in ice floes (Figure 12).

Song et al. (2021a) conducted tank testing of a flat plate and a model ship in smooth and rough surface conditions to examine the validity of using Granville's similarity law scaling (1958; 1987) for predicting the roughness effect on the resistance of a 3D ship hull (Figure 13). Conducting the towing test of the flat plate, the roughness function of the given roughness was determined and used to predict the frictional resistance of the model ship in the rough condition. The total resistance of the model ship was predicted using conventional hypotheses of Froude and Hughes and compared with the experimental result of the rough model ship. The results showed a good agreement.

Demirel et al. (2017) conducted an extensive series of towing tests of flat plates covered with artificial barnacle patches to find the roughness functions of barnacles with varying sizes and coverages. Different sizes of real barnacles, categorised as small, medium and big regarding their size, were 3D scanned and printed into artificial barnacle patches. From the experimental results, they determined the roughness functions of barnacles with varying sizes and coverages (Figure 14).

Song et al. (2021b) investigated the effect of heterogeneous hull roughness on ship resistance. In addition to the homogeneous hull conditions (i.e. smooth and rough conditions), heterogeneous hull roughness conditions (i.e. bow-rough, ¼-aft-rough, ½-bow-rough and ½-aft-rough conditions) were realised by applying sand grit on the hull systematically and towing the Wigley hull model in forward and backward directions. The bow-rough conditions (i.e. ¼-bow-rough and ½-bow-rough) showed larger added resistance compared to the aft-rough conditions (¼-aft-rough and ½-aft-rough) with the same wetted surface area of the roughness region.

Guo et al. (2018) proposed an experimental technique using a stereoscopic underwater particle image velocimetry (SPIV) system to identify the flow characteristics in the wake of a ship model. Using the proposed methodology, the bilge vortex, propeller boss cap vortex, and hook speed contour structure were analysed (Figure 18).

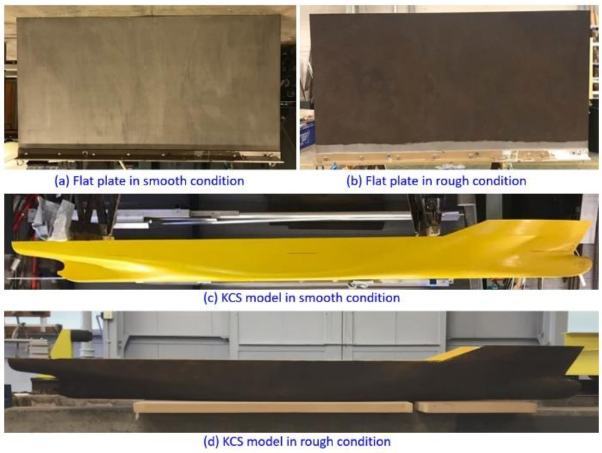

Figure 13: Flat plate and model ship in smooth and rough surface conditions (Song et al., 2021a)

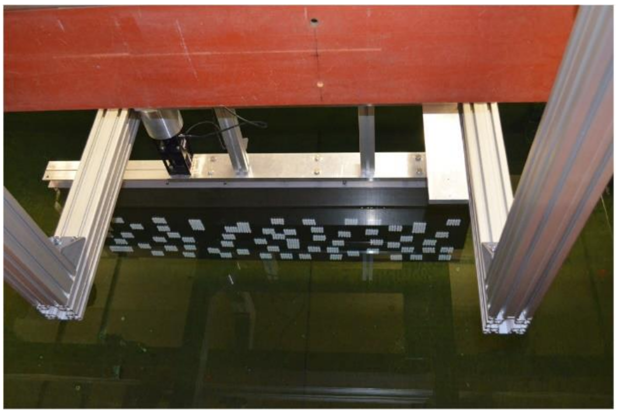

Figure 14: Flat plate with barnacle cluster roughness elements (Demirel et al., 2017)

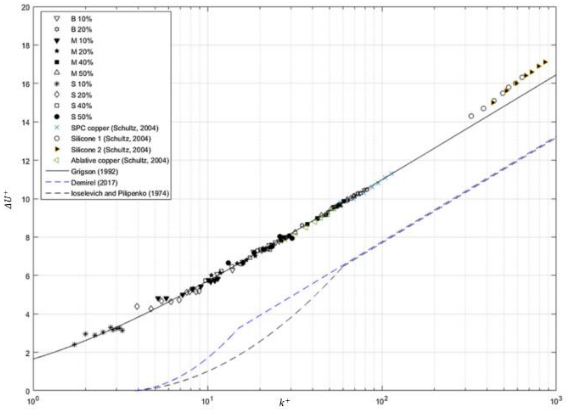

Figure 15: Roughness functions of different barnacle surfaces (Demirel et al., 2017)

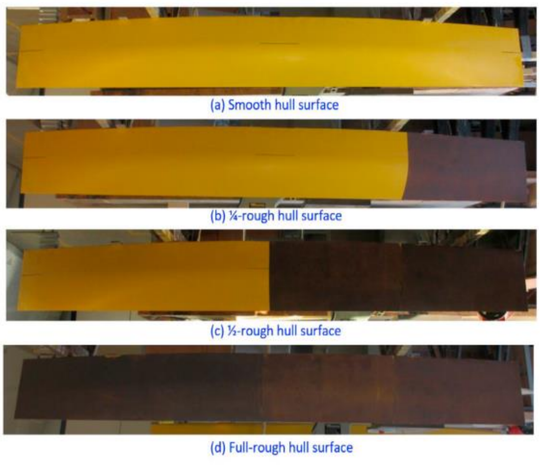

Figure 16: Wigley hull with different surface conditions (Song et al., 2021b)

Figure 17: The towing carriage of the Kelvin Hydrodynamics Laboratory and the Wigley model; (a) ½-bow rough condition, (b) ¼-aft rough condition (Song et al., 2021b)

Dogrul et al. (2020) conducted CFD simulations of a containership (KCS) and a tanker (KVLCC2) at different scales to investigate the scale effects of the ship resistance components and form factors. The results showed that the scale effects of the ship resistance components significantly differ between the two hull types, and these differences lead to different compliances in the resistance extrapolations. They compared the total resistance predictions obtained from different extrapolation methods against the full-scale CFD simulation results. The result showed that the Froude's 2D extrapolation shows a better agreement for KCS than Hughes' 3D extrapolation. Contrarily, for KVLCC2, Hughes' 3D method showed a better agreement than the 2D method (Figure 19).

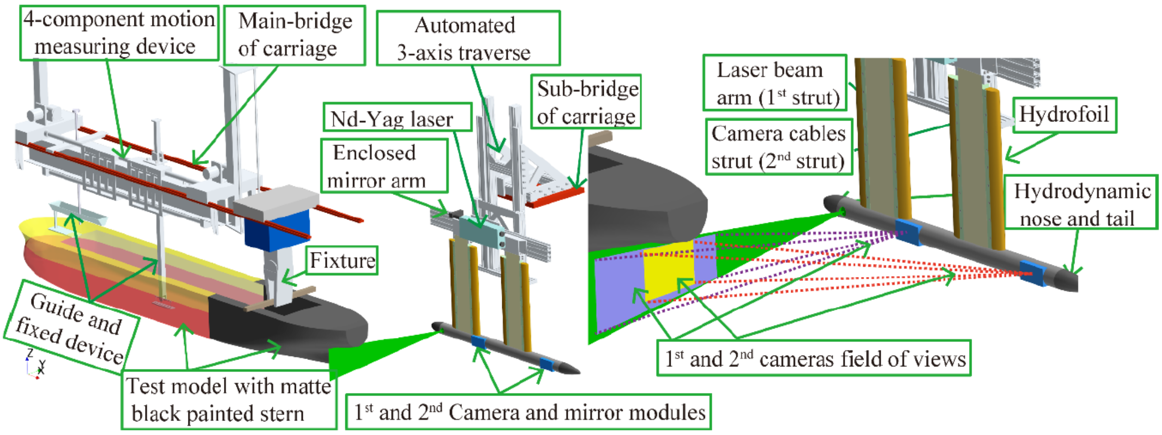

Figure 18: SPIV set up with a test model (Guo et al., 2017)

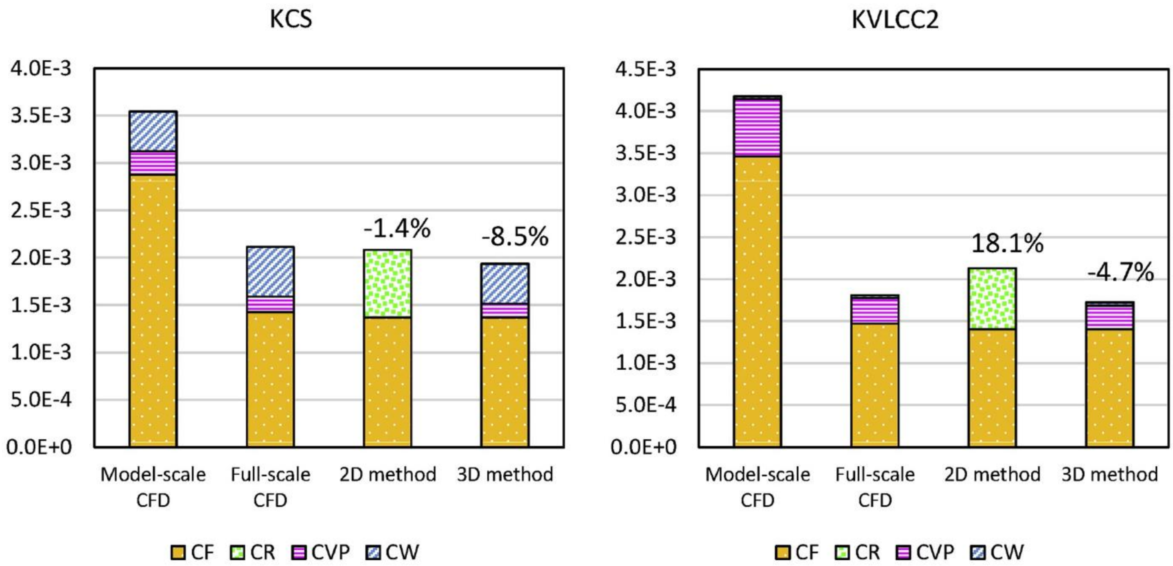

Figure 19: Resistance components from the CFD simulation and the different extrapolation methods for KCS (left) and KVLCC2 (right) (Dogrul et al., 2020)

Ravenna et al. (2019) presented a towing tank study to assess the effect of different configurations of biomimetic tubercles on a flat plate (Figure 20). They used 3-D printed tubercles inspired by humpback whales and the plate was towed at a speed range of 1.5 – 4.5 m/s. The results showed that when these tubercles, where positioned in rows upstream or downstream of the flat plate, the hydrodynamic resistance of the plate was reduced up to 1.3% compared to the bare flat plate.

Charruault et al. (2017) proposed an experimental technique to characterize the free-surface topology and air losses at the cavity closure. A Dot Tracking Algorithm (DTA) based on the Particle Tracking Velocimetry was implemented with a synthetic Schlieren method to measure strong curvature more accurately than with a standard Digital Image Correlation method. It was shown that the capillary waves travelling on the cavity interface could be measured using the newly developed method (Figure 21 and Figure 22).

Figure 20: Flat plate towed at 4.5 m/s (Ravenna et al., 2019)

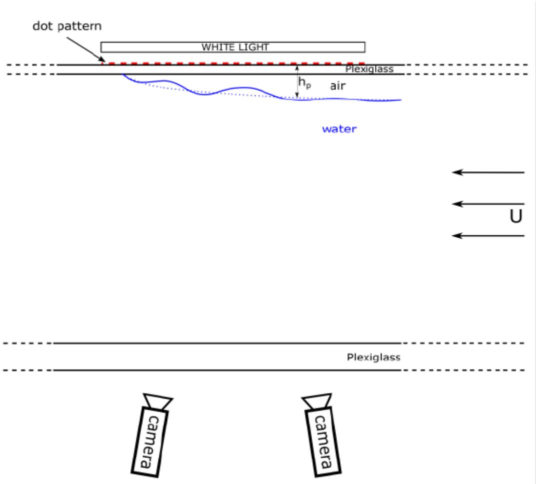

Figure 21: Two cameras in stereo configuration looking at the dot pattern through the bottom of the cavitation tunnel open test section (Charruault et al., 2017)

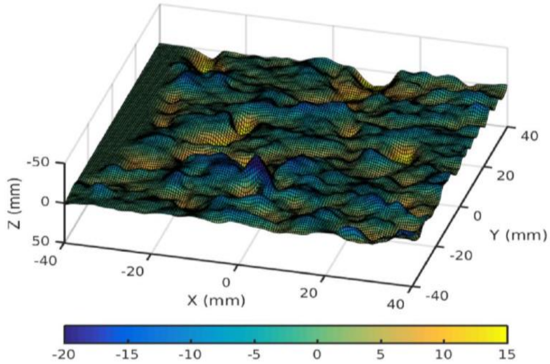

Figure 22: Free surface topology of the cavity closure (Charruault et al., 2017)

Delfos et al. (2017) conducted PIV measurements to investigate the flow characteristics over a smooth compliant coating in a cavitation tunnel at high Reynolds numbers (flow velocities of 1-6 m/s). They used high-speed Background Oriented Schlieren measurements to determine the instantaneous deformation of the compliant coating surface. At velocities of 1-4 m/s, the elastic surface formed large scale undulations that travel with a high velocity over the interface, but their amplitude was lower than the viscous sublayer such that they do not affect the skin friction. On the other hand, at higher speeds, slender trails were observed on top of the undulations and acted as artificial flow-induced roughness increasing the friction (Figure 23).

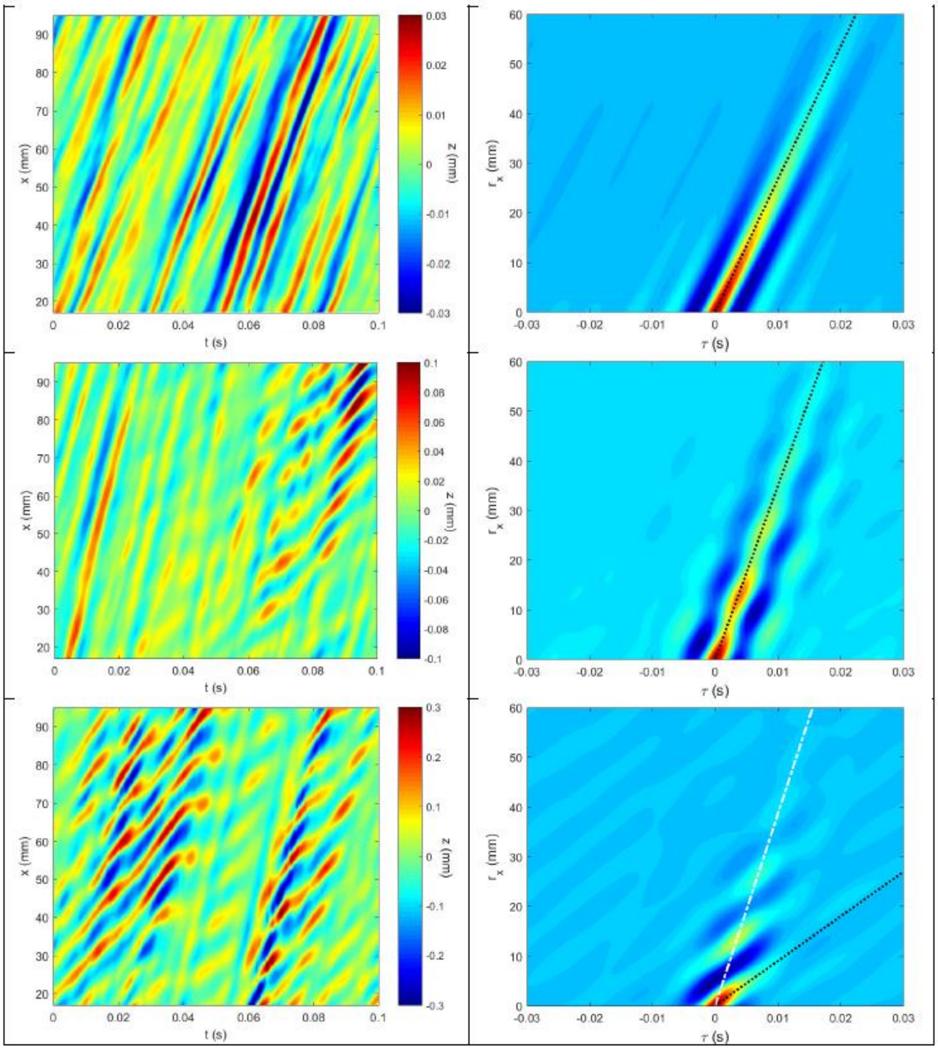

Figure 23: Measurements of surface deformation of compliant coatings by Delfos et al. (2017)

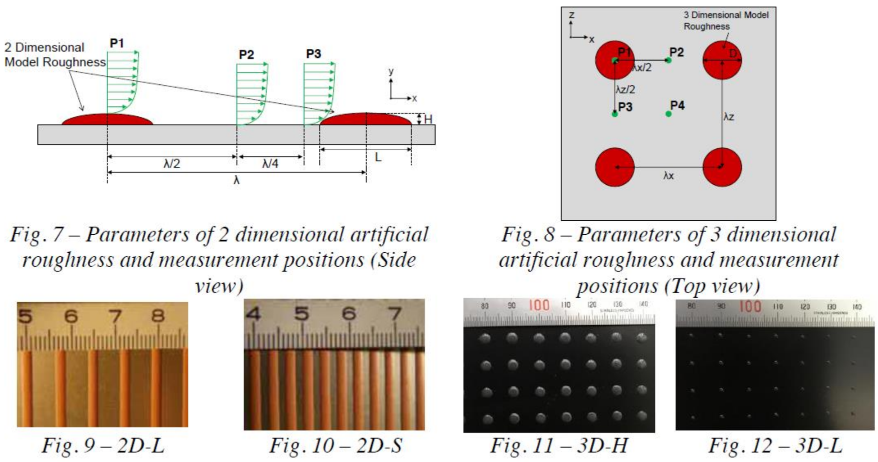

Figure 24: Measurements by Hiroi et al. (2017) of 2D and 3D artificial roughness

Hiroi et al. (2017) used two-dimensional (2D) and three-dimensional (3D) artificial roughness to investigate the relation between skin friction and the geometric roughness parameters such as roughness height, slope and wavelength. Using Laser Doppler Velocimetry (LDV) the turbulent boundary layers over the surfaces with artificial roughness were measured and a comprehensive review was made on the relationship between the roughness parameter and the turbulence statistics (Figure 24).

Guzel (2017) presented an experimental approach to observe the change in hydrodynamic friction due to hydrophobicity. A cylindrical Taylor-Couette flow setup consisting of an inner cylinder that rotates with an angular velocity within a stationary concentric larger outer cylinder has been constructed (Figure 25). The drag reduction due to hydrophobicity was observed over a range of Reynolds numbers in the measured torque on the inner cylinder.

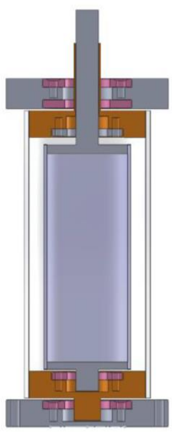

Figure 25: Sketch of the Taylor Couette setup of Guzel (2017)

Greidanus et al. (2017) performed force and PIV measurements of the interaction of smooth compliant coatings with turbulent boundary layer flow at high Reynolds numbers. They found that the skin friction, mean velocity profiles and turbulent statistics are different from the smooth flat plate only at free stream velocities (FSV) beyond the transition of 4.5 m/s (Figure 26).

Fabio et al. (2017) developed a methodology to investigate the interaction between air bubbles and turbulent flow. In order to obtain a simultaneous measurement of the water velocity field and of the bubbles size, shape and orientation, the Particle Image Velocimetry (PIV) has been used, combined with Laser-Induced Fluorescence (LIF). The image analysis allows a proper detection and separation of the two phases with a subsequent accurate analysis of the liquid phase (Figure 27).

Fabbri et al. (2017) developed an experimental technique using a marine biofilm flow-cell in which biofilms can either be cultured under flow or grown statically and then assessed under flow for drag and other properties. Using optical coherence tomography (OCT), the changes of physicomechanical properties of the marine biofilms during flow loading/unloading cycles were observed and compared to simultaneously collected frictional drag properties (Figure 28).

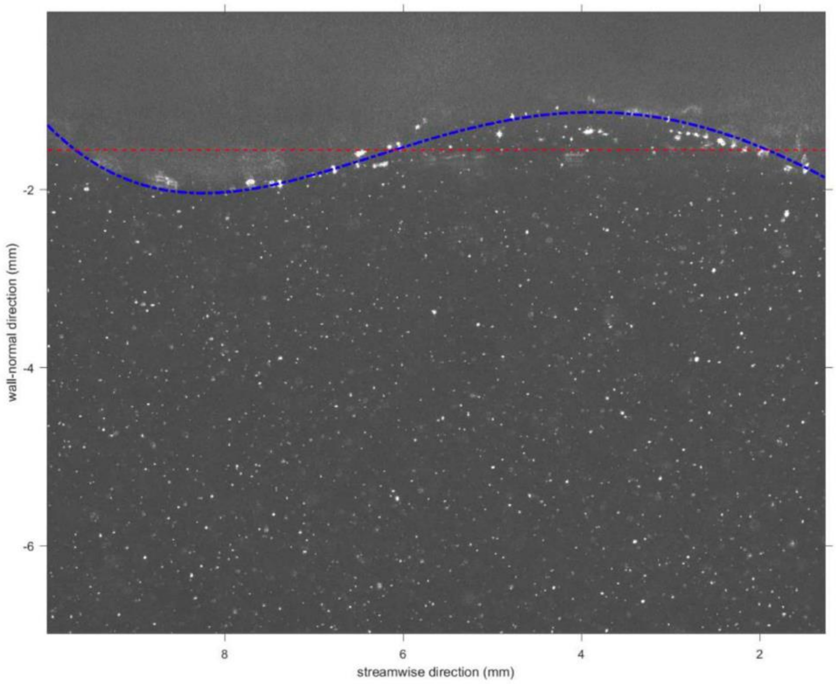

Figure 26: PIV images from measurements of interaction of smooth compliant coatings with turbulent boundary layer flow (Greidanus et al., 2017)

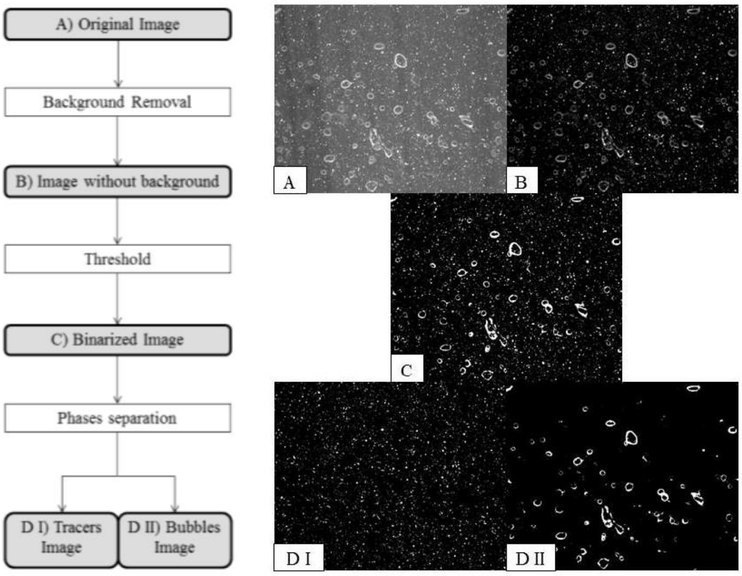

Figure 27: Measurement of interaction between air bubbles and turbulent flow using PIV and LIF (Fabio et al., 2017)

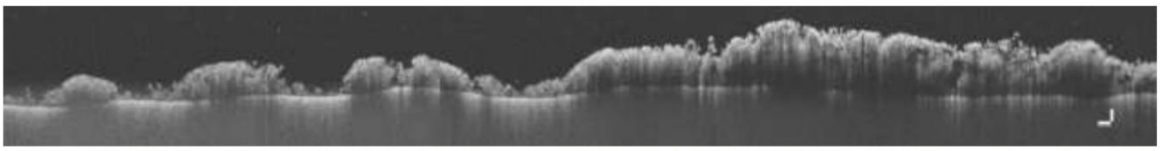

Figure 28: Cross-section of fouling biofilm on a coated panel fully immersed in the flow cell as imaged by optical coherence tomography (Fabbri et al., 2017)

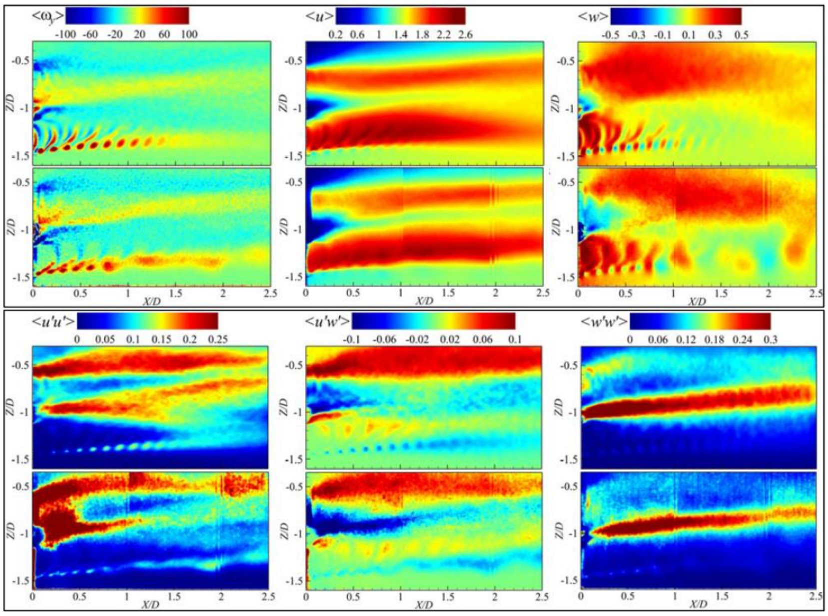

Figure 29: Phase averaged flow behind DARPA Suboff beneath free surface (Wang et al., 2019)

Wang et al. (2019) conducted experiments and CFD simulations of the DARPA Suboff submarine model fitted with the E1658 propeller with different immersion depths. The flow was measured in a phase-locked fashion using particle image velocimetry (PIV) in a cavitation channel, while CFD simulations were modelled with a single-phase level set approach to model the free. Both the experimental and numerical results showed strong interactions between the hull and free surface, producing higher local advance coefficients and blade loads near the free surface (Figure 29).

2.3 New benchmark data

The workshop, held in December 2015 in Tokyo, on CFD in hydrodynamics was the seventh in a series started in 1980 with the objective to assess up-to-date numerical methods of the current CFD codes for ship hydrodynamics (Hino et al., 2021). Three model scale ship hulls were selected with a total of 17 possible test cases specified by the organizers: (i) 5 cases for the KRISO Container Ship (KCS) already used in previous workshops; (ii) 9 cases for the Japan Bulk Carrier (JBC) equipped with a stern duct as an energy saving device (ESD); and (iii) 3 cases for the ONR Tumblehome model 5613 (ONRT) as a preliminary design of a modern surface combatant.

2.3.1 Available experiments

- JBC: towing tank tests at the Tokyo National Maritime Research Institute (NMRI) and Osaka University (OU) including resistance tests, self-propulsion tests and SPIV measurements of stern flow fields. Additional LDV/SPIV data in wind tunnel are available from the Technical University of Hamburg (TUHH).

- KCS: towing tank tests carried out at the Korea Research Institute of Ships and Ocean Engineering (KRISO), self-propulsion tests and also resistance tests at the NMRI. Data for pitch, heave and added resistance are also available from FORCE/DMI measurements.

- ONRT: this modern frigate model is appended with skeg and bilge keels; it also has rudders, shaft and propellers with shaft brackets. Free-running tests include course keeping, zigzag and turning circles in both calm water and regular waves performed at the IIHR Hydraulics Wave Basin Facility.

2.3.2 Participants and Methods

31 organizations have participated in the workshop with 12 submissions from in-house codes, 11 open-source codes and 13 commercial codes. The novelty here is the increase in the number of open-source codes compared with the previous Gothenburg Workshop where there were 14 in-house, 3 open-source and 16 commercial codes. The majority of methods use two-equation k-ω SST or k-ε turbulence models with no-slip wall boundary conditions. Wall-functions are also used, particularly by open-source or commercial codes. The technique of volume of fluid remains the most popular to take into account the free surface. The propellers are traditionally modelled though a body force approximation or represented directly as actual rotating propeller. Discretization is mostly based on finite volume for unstructured grids and pressure based equation to solve the incompressibility.

2.3.3 Results

The summary of the results is taken from the analysis and main conclusions of the various chapters dedicated to the different cases:

JBC: the mean signed comparison error for resistance (Measured-Computed)/Measured is around 1%, the same accuracy reported for the experimental data. The scattering of results is about 2% for towed cases and 4% for self-propulsion. In 2005 the standard deviation was 6% and reduced to 1% in 2010 similar to the 2015 deviations. The effect of the ESD is found to reduce the resistance by 1%, in agreement with the measurements. The accuracy of the methods through grid convergence is still difficult to reach as the order of accuracy is in many cases far from the theoretical order. Concerning the grid size, it is observed that 10M cells are needed to obtain a comparison error below 5% whereas the limit was 3M cells in 2010. It is reasonable to think that the increase in this limit is not so much the absolute need for more points as the increased use of automatic grid generators. To note the better accuracy when wall-functions are used as errors are twice higher with wall resolved.

Conclusions from the analysis of the self-propulsion and ESD performance predictions lead to an averaged absolute error of the model scale delivered power (DP) about 5% to 6%. The experimental value of the DP reduction rate due to the duct is 0.94 whereas the scatter of the predictions is between 0.88 and 1.0. It concludes that CFD estimation of ESD efficiency may not be sufficient for precise reduction of only few percent of this DP.

The major influence on the local flow analysis comes from the turbulence modelling. Non-linear anisotropic closure (EARSM) is now a good compromise although the vorticity is slightly under-predicted in some key stations. For the specific and simplest case of the naked hull no spectacular advantage was noticed with hybrid RANS/LES simulations compared to the best RANS models. However on the case with propeller and without ESD duct, only a hybrid model type was able to capture most of the fine flow details revealed by the phase-averaged measurements. The same comment holds for the ducted propeller about phase-averaged quantities where some URANS computations are in agreement with the measurements. Among the submissions, we would like to highlight the only contribution of wall-resolved LES computation of the double body model (4 billion cells) is in good agreement with measurements and particularly the level of turbulent kinetic energy in the core of the bilge vortex.

KCS: the mean comparison error for all 6 speeds is 0.43% and standard deviation 2.48% with higher error at low Froude simulations. The mean absolute error is 2% which remains in line with the 1.64% of the Gothenburg 2010 workshop. For the self-propulsion submissions the mean K_T and K_Q errors are 0.5% and 3.5% respectively, slightly better than the results of the previous workshop (-0.6% and -4.6%). In this case of captive (fixed rps) test, the body force approach gives slightly better parameters but, as expected, local flow predictions are improved when solving the actual propeller. There were 10 submissions for the assessment of CFD for added resistance of captive test in waves to lead to the overall result of an error of 13%. This error includes the result of the free-running ONRT tests for which the same level of error is observed on the speed loss.

ONRT: with this geometry the new interest in this workshop consisted in the study of free running in head, beam, following and oblique waves. Probably because of the high CPU cost for CFD, there were only 4 submissions, not all of them complete, to be analysed for comparisons with the motions and trajectories measured at IIHR. While high levels of experimental uncertainty are pointed out for some quantities, the numerical uncertainty remains high with a mean error still higher than 5%. Nevertheless, it was concluded that "*in view of the comparable CFD capability for ONRT free running vs. KCS captive conditions, the prognosis for CFD capacity is excellent*". This first call for comparison on such a challenging case for the CFD will continue at the SIMMAN workshop to be held in 2021, during which this geometry will again be proposed as a validation test case.

2.4 Practical applications of computational methods to performance prediction and scaling

Ships intended for operation in shallow-water need to be tested in shallow model basin, but while blockage corrections for tank walls are well understood for deep water, there is no established procedure for applying a blockage correction for tank walls in a shallow-water test. Raven (2019) has proposed a method, based on the hypothesis that the overspeed induced by the tank walls is uniformly distributed across the tank's cross-section, which has been confirmed by computed flow fields. An algebraic equation is obtained for the overspeed induced by the tank walls, separately from that induced by shallow water. The change in volume flux that is required by this equation is obtained from a single potential flow calculation for each depth to be tested. The resulting overspeed is used to correct the resistance curve of the ship. The effects of the tank walls on dynamic sinkage was also studied and found to be substantial.

Computational techniques are increasingly being used to predict full-scale ship and propeller performance. As well as applying the traditional analysis techniques to these predictions, CFD solutions can be used to obtain richer information about the performance. An example of this is the application of energy loss analysis to a CFD prediction of the flow field around a propeller in behind condition as described by Schuiling and Terwisga (2018). In this study the authors propose a method by which the individual components of energy losses can be computed by calculating the integral energy equation on a control volume surrounding the propeller. This gives a breakdown of the losses into axial, rotational and viscous losses, enabling a more informed choice of design modifications, or energy saving device, based on the type and distribution of the losses. The method was demonstrated on a large diameter propeller, which showed a reduction in the axial losses. The use of an asymmetric stern to generate pre-swirl was shown to improve the rotational losses, but also to increase the axial losses.

2.5 Experimental and computational prediction of cavitation

RANS solvers have become a common tool for the prediction of sheet cavitation in the past decade. Recently, there has been a need for more accurate predictions of whole cavitation pattern, e.g. tip vortex cavitation (TVC), in response to various demands, including increasing attention to underwater noise radiated from the propeller, to protect marine mammals. To meet such demands, advanced methods such as LES and DES have been applied to describe more complicated phenomena.

Yilmaz et al. (2019) applied LES to analyse the tip vortex on the INSEAN E779a four bladed propeller with the Schnerr-Sauer cavitation model. To fully capture TVC, they developed a new mesh refinement method, called MARCS, composed of volumetric control method and adaptive mesh method. First, a spiral geometric mesh was generated by the volumetric control method in a region where the TVC may occur. The region was determined using an absolute pressure value specified as the threshold. The spiral mesh is then refined by the adaptive mesh method (Figure 30). Comparing the simulation results with the experiments, it was shown that MARCS could reproduce the structure of TVC much better compared to a conventional mesh treatment (Figure 31).

Shin et al. (2018) used DES to predict TVC on a four bladed propeller with a rudder behind. They refined meshes around TVC using an adaptive mesh method based on the Q-criterion instead of the absolute pressure. They showed that the extent of TVC and the pressure fluctuation became closer to the experimental results by applying the adaptive mesh method. On the other hand, the high-order pressure pulses could not be simulated well because the TVC collapse at the rudder was not reproduced well, which required much finer meshes in the region where TVC interacted with the rudder. In order to accurately simulate TVC, the mesh generating strategy is most important and the adaptive mesh method is useful to effectively generate fine meshes around TVC.

The usage of LES and DES is shown in many papers in SMP’19. For example, Bhatt el al. (2019) calculated thrust break-down on a five bladed propeller using LES, and Kumar el al. (2019) and Paskin et al. (2019) evaluated tip vortices over a three dimensional hydrofoil with LES and DES respectively. All of them verified the accuracy of the calculations by comparisons with the model tests.

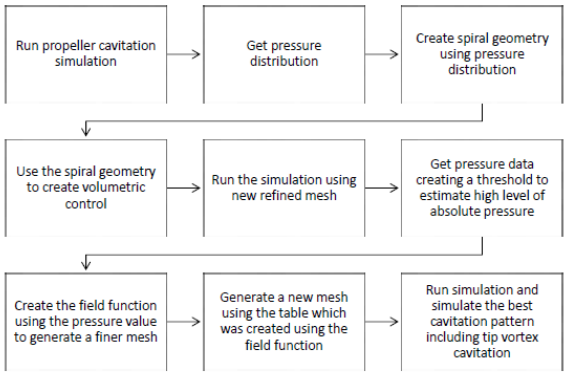

Figure 30: Flowchart summarizing new Mesh Adaption and Refinement approach for cavitation simulation (MARCS)

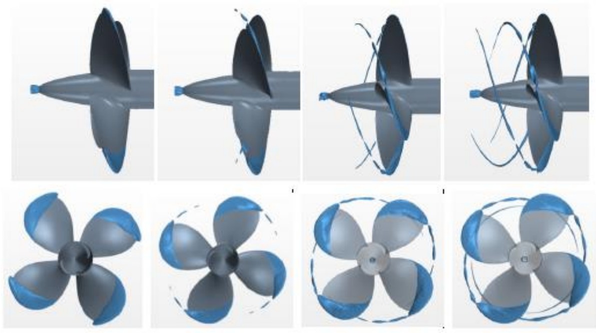

Figure 31: Improvement of tip vortex cavitation extension (From left to right; Result without mesh refinement, with tube refinement, with spiral geometry refinement and with mesh adaption refinement MARCS)

Zhang et al. (2019) presented a post processing technique against the obtained high speed images of a cavitating propeller. A phase congruency method was applied instead of the conventional brightness-gradient based method to detect the edges of cavitation structures, which enables the detailed illustration of the interface topology of the propeller cavitation. The weak tip vortex cavitation that is not apparent in the high speed images can be clearly detected (Figure 32). There are two methods of cavitation inception detection: the acoustic technique and optical or visual technique. It is known that those give different criteria for the inception, while this post processing technique might be used to explain the discrepancies between them.

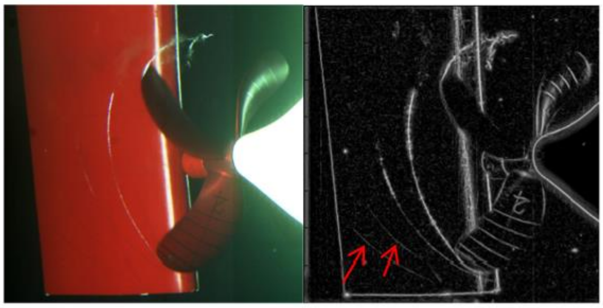

Figure 32: Cavitation topology obtained using the edge detection method (Zhang et al., 2019)

3. DEVELOPMENT OF PROCEDURE FOR WAVE PROFILE MEASUREMENT AND WAVE RESISTANCE ANALYSIS

The RPC committee was requested to develop a new procedure on wave profile measurement and wave resistance analysis. Generally, the purpose of observing, measuring or simulating the wave profile for a model ship at a given speed in a towing tank is to evaluate the ship hull form, and to reduce the wave resistance by modifying the ship hull form. Quantitative measurement techniques of wave height around the model ship free surface field include intrusive and non-intrusive techniques. Resistive and capacitive type wave gauges are widely used as intrusive methods. While non-intrusive techniques include optical sensors, acoustic sensors, radar, imaging methods, and combined laser-scanner and video hybrid systems. Although quantitative wave profile measurement is now mainly used for CFD validation, there is still a need to incorporate it in routine towing tank resistance tests to estimate the wave resistance in a more rapid way.

As a complementary procedure to resistance test in towing tank within ITTC recommended procedures, the main purpose of the new procedure is to provide guidance on the towing tank wave profile measurement and to analyze the wave pattern resistance. Since the single wave profile measurement is relatively rare in the commercial towing tank test, in order to incorporate the wave profile measurement with the routine resistance test, the widely used longitudinal wave cut method together with the Newman-Sharma Method for wave pattern resistance analysis is recommended for the procedure. An example of a wave pattern resistance calculation from wave profile measurement data is demonstrated in the appendix of the procedure. The recommended procedure is suggested to be numbered with 7.5-02-02-04, which is under the category of Resistance 7.5-02-02.

As for the further investigation on the model ship wave measurement, it is suggested for the next ITTC term to review the state-of-the-art of high Froude number surface ship wave breaking, which is multi-phase complex flow and is also difficult for both quantitative measurement and CFD simulation.

4. VERIFICATION AND VALIDATION OF DETAILED FLOW FIELD DATA

4.1 Introduction

This document does not pretend to provide an exhaustive answer to the question of Verification and Validation (V&V) of detailed flow field analysis in the area of ship hydrodynamics for resistance and propulsion. Instead, a review of recent published studies is presented for most advanced Computational Fluid Dynamics (CFD) results with comparison to advanced Experimental Fluid Dynamics (EFD) measurement, not only for global integrated quantities such as the forces or trajectories but also for local quantities of the flow field including turbulence.

First of all, a brief reminder of the V&V objective is given, then what is meant by the notion of local and global data in relation to existing procedures, and finally what is practiced in complex situations to address and to analyse detailed flow field data.

4.2 Code verification and validation

Verification concerns the code verification for correct coding of the model implementation. The solution verification is aimed at estimating the numerical error/uncertainty of a given solution whereas the validation process is concerned with numerical model meaning the modelling errors/uncertainties.

For the estimation of the numerical uncertainty, a set of geometrically similar grids is required, where grid properties remain the same and the refinement ratio be constant in the computational domain. The task of generating a series of embedded grids by coarsening a fine grid or refining a coarse grid is feasible with most of structured grid generators.

The CFD error related to the discretization error is the difference between the exact solution of the PDE and the exact (round-off-free) solution of the algebraic equations used. The possible sources of numerical error to consider for accurately control the precision of a physical model are:

- Round-off errors: its influence is commonly neglected.
- Iterative error (to solve the couplings/segregated equations and the non-linearities): its influence is often neglected assuming the condition of the residuals “low enough” for all the quantities.
- Discretization error (or solution error due to incomplete grid convergence): it is computed from a series of systematically refined grids from which the exact solution is extrapolated and the uncertainty can be evaluated from the computed error.

The ITTC procedure 7.5-03-01-01 “Uncertainty Analysis in CFD Verification and Validation Methodology and Procedures” provides details for estimating the uncertainty of a simulation. A brief but comprehensive note by Celik et al. (2008) is intended to provide guidelines for authors.

4.3 Global and averaged variables

The aforementioned ITTC procedure is commonly used to assess and to justify the results of the simulations, and quite often based on integrated (or global) quantities such as forces. This is the regular practice for simulation where a steady solution is expected. However the numerical uncertainty of unsteady flow simulations in industrial activity remains a non-trivial task, Eça et al (2019): this makes it necessary to control both iterative error and statistical error (induced by initial conditions) even before addressing discretization errors, i.e. grid/time refinement.

The procedure also gives indication for estimating errors for “Point Variables”. This is a way to estimate error and uncertainty on local flow details over a distribution of grid points. Thus, an L2-norm can be used to compute the solution changes within the profile-averaged quantity. As an example the ITTC procedure 7.5-03-03-02 “Practical Guidelines for RANS Calculation of Nominal Wakes” highly recommends the computational results to be presented in accordance with the format proposed in the ITTC procedure 7.5-02-03-02 “Nominal Wake Measurement by a 5-Hole Pitot Tube”. In this case the computed wake field on the propeller plane is interpolated along specific radius and circumferential angles. In this way, such a guidance is followed by Bakica et al (2019) to assess ship-propulsion using CFD.

For further research as an alternative to produce manually geometrically similar series of meshes for convergence studies, which is not straightforward with unstructured grid generators, Wackers et al (2017) shown that the technique of adaptive grid refinement can produce converged local-flow solutions: the numerical accuracy of the computed wake flows is sufficient to assess modelling errors due to turbulence models on meshes with acceptable numbers of cells. The technique was validated in the propeller plane of the KVLCC2 bare hull for both the velocity and the turbulent kinetic energy fields. However, this approach for V&V on non-local and global quantities is still an ongoing research topic. The next section is intended to illustrate code verification, in comparison with detailed EFD in complex situations, where the verification process is almost unfeasible.

4.4 Detailed investigations of the flow field

The present challenge of CFD applied to ship hydrodynamics concerns ship powering, manoeuvring and sea-keeping. In this context CFD has reached a high level of fidelity to address such complex situations: the SIMMAN 2008 and 2014 Workshops only covered calm water manoeuvring situations, the Tokyo 2015 CFD Workshop included free running course keeping in waves as a test case for the first time, and the SIMMAN 2021 workshop will also focus on manoeuvring in waves.

Concerning CFD about these most advanced studies of free-running ships and moving propellers and rudder the desired exercise to conduct a grid convergence analysis has never been done in the literature. This is due to complexity and cost of computations, Carrica et al (2014, 2016), Wang et al (2018), Hashimoto et al (2019): coarsening a grid may be impossible and refining is prohibitively expensive. On the EFD side for currently available data about free-running ships, only the propeller revolution speed is known very accurately during calm water tests and the uncertainty is estimated on the motions and on the forces. Bottiglieri (2016) estimates the random error based on repeated tests and the uncertainty is found as a combination of systematic and random uncertainties representing the propagation of errors within the tracking system and the deviation between repeat trials. In Sanada et al. (2013, 2014) the statistical convergence error on measurements is derived from repeated test results to know how many runs should be performed to get the converged mean trajectories for PIV measurements: for the ONR Tumblehome model the statistical convergence errors are almost converged when the sample size is over twelve. For zigzag manoeuvres of the KCS container, Carrica et al (2016), the repeatability error that contributes to experimental uncertainties of thrust, torque, motions and propeller RPM at self-propulsion is calculated based on ten experiment runs.

Going back to simpler cases for thorough V&V analysis the Tokyo 2015 Workshop the result of the Japanese Bulk Carrier (JBC) case is that the resistance predictions using the finest grids are within 1% of the measured data both with and without the energy saving device. An exhaustive presentation of the JBC test data from NMRI is available in Hirata (2015).

On the other hand, the flow around this JBC hull appears to be difficult to predict accurately with statistical turbulence closures. Compared to measurements, all RANS simulations are able to predict a satisfactory agreement for the mean longitudinal component of the velocity in the core of the vortex whereas the level of turbulent kinetic energy (TKE) is generally underestimated by at least a factor of four. During this workshop the apparent contradiction from a RANS point of view between high levels of TKE and vorticity was removed with hybrid RANS-LES modelling by Abbas et al (2015), Kornev et al (2011), and later by Visonneau et al (2016) using a similar LES closure. On the same case Nishikawa (2015) presented successful fully-resolved LES simulations but at the cost of 39 billion grid points during 2.4 million hours of CPU time.

This highlights how important it is to support research activities focused on detailed analysis either by experiments and high-fidelity simulations. As noted above on the JBC case, the development of more sophisticated turbulence models requires the analysis of TKE and vorticity budgets.

For such needs, Falchi et al (2014) published the results of measurements of a catamaran in steady drift conditions which is typical of naval vessel operating in off-design conditions. The paper introduces a detailed review in literature about the SPIV (Stereo-Particle Image Velocimetry) adopted to acquire the three velocity components in a plane (mean and fluctuating components). Therefore mean vorticity field as well as velocity and vorticity fluctuations are available in five transversal planes and their interaction with the free surface. Possible sources of uncertainty are considered to state that instantaneous velocity field error is about 3% of the mean velocity and 12% of the exact value on the second-order statistical moments. For CFD validation the EFD dataset is available for downloading under request.

On these EFD basis, the results of CFD assessment for these static drift conditions has been done by Broglia et al (2019). The originality of the study is that the validation is based on cross-comparisons between three different CFD codes with different grid strategies and various turbulence modelling, from the Spalart-Allmaras model to hybrid RANS-LES. Assessment of numerical predictions focuses on the onset and propagation of the vortical structures, axial velocity and vorticity, TKE distribution and interaction with the free surface and loads. At a general level the loads are correctly predicted within the numerical uncertainty and differences occur among the turbulence model adopted. Only RANS simulations have been compared to the EFD cases with drift angle and measurement planes. To shortly summarize the validation exercise, the predicted TKE from RANS in the core of the fore body keel vortex is underestimated by at least one order of magnitude than experiments.

Yoon et al (2014) presented the results of experiments for the DTMB model in straight ahead and static drift conditions using a tomographic particle image velocimetry (TPIV) system. This allows detailed description the flow volume structures in specific region of interest and, for example the second invariant Q can be computed from EFD. As reported in Bhushan et al (2019) it was then possible to assess CFD in these conditions about the overall vortex structures with comparison of 3D predicted structures to TPIV measurements. Here again, the originality of the study is that the validation process is based on different codes and it appears that if full Reynolds stress transport model could improve unsteady RANS prediction, only hybrid RANS-LES models of the study are able to explain the high level of TKE from the sonar dome powered by instabilities and therefore higher production from the resolved turbulence.

5. INTERACTION WITH SHIPS IN OPERATION AT SEA COMMITTEE

The specialist committee on Ships in Operation at Sea (SOS) found an inconsistency in the load variation test (LVT) in the current Recommended Procedure 7.5-02-03-01.4. Figures 4 and 5, which are used for a calculation of the load variation coefficient of the ship speed ξ_V, are derived from different data sets.

The Resistance and Propulsion Committee (RPC) and the SOS calculated load variation factors for the SSPA benchmark (Werner, 2018), according to the Procedure. The data has been analysed using the ITTC 1978 performance prediction method version 0, as published in 1999, in the same way as the SOS.

The load variation factors calculated are summarized in Table 1. The load variation coefficient of the delivered power, ξ_P, and the coefficient of the shaft revolution speed, ξ_n, are identical between SSPA, the SOS and the RPC, while ξ_V is slightly different. A reason of the difference is supposed to be that the ξ_V is derived by an interpolation of an interpolation. However, ξ_V doesn't affect EEDI and thus this slight difference can be considered negligible. In conclusion, the load variation factors derived from the same data set are almost the same among all facilities. The RPC replaced Figure 4 and 5 in the current procedure with new ones derived from the same dataset and described the detail of the calculation as an appendix of Recommended Procedure 7.5-02-03-01.4.

Table 1: Comparison of load variation factors between SSPA, the SOS and the RPC for the SSPA benchmark case

	SSPA	SOS	RPC
ξ_P	-0.19	-0.19	-0.19
ξ_n	0.25	0.25	0.25
ξ_V	0.33	0.34	0.32

Table 2: Difference of subscripts between ITTC and ISO

No.	Description	ISO	ITTC	New ITTC (proposal)
1	Full scale resistance without overload	R_{id}	R_0	
2	Added resistance coefficient	C_{TSadd}	C_{TAadd}	
3	Propulsive efficiency in ideal condition	η_{Did}	η_D	η_{D0}
4	Propulsive efficiency considering the load variation effect	η_{Dms}	η_{DM}	η_D
5	Delivered power in ideal condition	P_{Did}	P_{D0}	
6	Propeller shaft speed in ideal condition	n_{id}	n	

Differences in the names of coefficients between the RP 7.5-02-03-01.4 and the International Standard, ISO15016 (2015), was also investigated. Six different subscripts between ITTC and ISO were identified as shown in Table 2. The committee does not consider it to be a problem that ITTC and ISO have their own subscripts because they have a consistency within each document. However, η_{DM} of No.4 in ITTC is inadequate because the subscript "M" represents "Model scale" in the procedure but is not case for η_{DM}.

Thus, the committee replaced η_D of No.3 with η_{D0} of which subscript "0" means "in ideal condition" and η_{DM} of No.4 with η_D.

6. HULL AND PROPELLER ROUGHNESS

6.1 Introduction

The ship hull or propeller surface roughness due to coatings or biofouling have a significant influence on the ship performance. The effects of hull surface roughness due to the coatings are often taken into account in the total resistance prediction as the roughness allowance ΔC_F which is defined by the Townsin formula with the following formulation.

$$\Delta C_F = 0.044\left[\left(\frac{k_S}{L_{WL}}\right)^{\frac{1}{3}} - 10\cdot Re^{-\frac{1}{3}}\right] + 0.000125 \quad (1)$$

In this formulation, the standard value of hull surface roughness k_S is defined to be 150 μm in case that no measured data is available.

This roughness height may not be a correct representation for modern hull coatings and recent research pointed out that the effective roughness of the coated hull surfaces in real life is much lower than this. Each type of coating may follow a different roughness function model, which makes the use of a single roughness height parameter difficult.

6.2 Roughness effects on ship resistance and propulsion

The impacts of hull roughness on ship resistance have been noted since the experiments of Froude (1872, 1874). McEntee (1915) conducted towing tests to investigate the effect of biofouling on frictional drag. Flat plates were coated with anticorrosive paints and exposed in the Chesapeake Bay. After 12 months, the frictional resistance of the plates increased up to four times due to the barnacles on the surface. Hiraga (1934) reported the effect of biofouling on the resistance of a towed brass plate coated with Veneziani composition. The plate was towed after 24 days of immersion and showed a 20% increase in the total drag with grown slime and barnacles on the surface. Lewthwaite et al. (1985) carried out an experiment measuring the boundary layer velocity profiles on a 23m fleet tender. An 83% increase in the frictional resistance and a 15% reduction in ship speed were observed over the 2-year exposure. Haslbeck (1992) conducted a full-scale trial on a Knox class frigate which was coated with an ablative antifouling paint. The delivered power and ship speed were measured after 22 months moored in Pearl Harbour. With a slime film and little macrofouling on the hull, an 18% increase in the delivered power was observed. Schultz (2004) carried out towing tests using flat plates exposed to seawater and concluded that the most dominant effect on resistance was the height of the largest barnacles on the plates. Andrewartha et al. (2010) conducted an experimental study to investigate the effect of biofilm on skin friction using a recirculating water tunnel. The test plates were deployed in the open channels of a hydroelectric power station (Tarraleah Power Scheme, Tasmania, Australia) for varying durations for biofilm growth. They measured up to a 99% increase in the drag of the test plates due to the biofilms on the plates. Li et al. (2019) investigated the effect of marine biofilm on the surfaces coated with different sized cuprous oxide (Cu_2O) particles. In order for the biofilms to develop under 'in-service' conditions, the test panels were installed on a detachable twin strut system. The strut system was deployed under the moon-pool plug of a catamaran research vessel, *Princess Royal*, and exposed in the sea for various periods (Figure 33). The frictional drag of the test panels was measured using a turbulent flow channel after every 6-week deployment period. The result showed an up to 83% increase in frictional drag due to the biofilm developed for 6 months.

There have also been investigations into the roughness effect on propeller performance. Bengough and Shepheard (1943) reasoned that the case of HMS Fowey which failed to reach its designed speed can be attributed to its fouled propeller. When subsequently docked, the propellers were found to be almost completely covered with calcareous tubeworms. The target speed could be finally achieved after cleaning the propeller. McEntee (1916) conducted experiments on artificially roughened model propellers to compare the efficiencies of similar propellers in different surface conditions. A

Figure 33: Testing panels installed on the twin strut assembly (left) and the strut system deployed under the moon-pool plug (right) (Yeginbayeva and Atlar, 2018)

model propeller was painted and stippled while the coating was wet to roughen the surface. The efficiency loss was about 20% due to the roughened surface. In another test, they used a propeller covered with ground cork, which resulted in an efficiency drop of 35%. Taylor (1943) insisted that even the ships operating with a propeller in moderately good condition can suffer a power loss in order of 10%. Townsin et al. (1981) recognised that propeller fouling can be as destructive as hull fouling but the remedy is much cheaper. Mosaad (1986) claimed that although the impact of propeller fouling may seem less severe than hull fouling, the losses per unit area are much greater. Mutton et al. (2005) compared the propeller open water performances in intact and damaged coating conditions and showed reduced propeller efficiency under the damaged scenarios. Korkut and Atlar (2012) conducted experiments to examine the roughness effect of foul release coatings on the propeller open water performances.

6.3 Roughness function

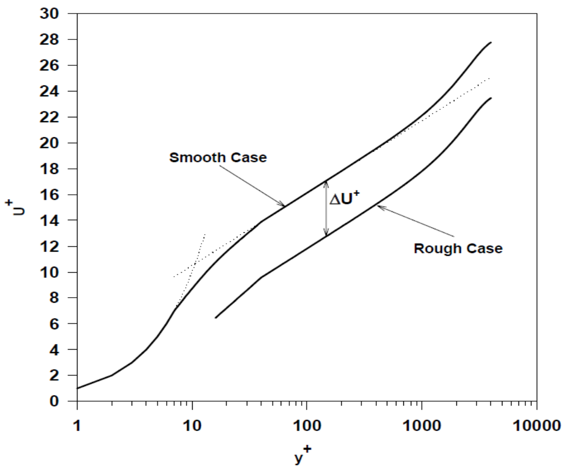

Figure 34: The roughness effect on velocity profile, adapted from Schultz and Swain (2000)

The roughness function, ΔU^+, represents the downward shift of the velocity profile due to the surface roughness in the turbulent boundary layer (Figure 34). Once the roughness function of a given surface is known, it can be utilised with the boundary layer similarity law analysis or Computational Fluid Dynamics (CFD) based methods to predict the added resistance due to the rough surface. The roughness functions can be determined from experiments either directly or indirectly. While the direct method requires the costly measurement of the boundary layer profiles, indirect methods are generally simpler and require less expensive equipment. Granville (1987) derived three indirect methods to estimate the roughness function of arbitrarily rough surfaces. However, the roughness functions are not universal and thus they have to be determined for individual roughness types.

Schultz (2004) has compared the frictional resistance of several coatings in the unfouled, fouled, and cleaned conditions by carrying out flat plate towing tests. The roughness function for the unfouled coatings showed reasonable collapse to a Colebrook-type roughness function when the centreline average height $k=0.17R_a$ was used as the roughness length scale. An excellent collapse of the roughness function for the barnacle fouled surfaces was obtained using a new roughness length scale based on the barnacle height and percent coverage.

Yeginbayeva and Atlar (2018) have investigated the hydrodynamic performance of typical coatings under in-service conditions of roughened ships' hull surfaces. They have presented comprehensive and systematic experimental data on the boundary layer and drag characteristics of antifouling coating systems with different finishes. The coating types investigated were linear-polishing polymers, foul-release and controlled-depletion polymers. The roughness functions were collected with a 2-D laser Doppler velocimetry (LDV) system in a large circulating water tunnel. The roughness length scale defined by the peak-to-trough height ($k=0.14R_t$) and combination of root mean square roughness and spatial distribution of height parameters presented a satisfactory correlation with ΔU^+ for coatings in the transitionally rough flow regimes. They have pointed out that further studies to explore the adequacy of the correlation for fully rough regimes is required.

Katsui et al. (2018) have shown roughness functions for various painted rough surface based on the experimental results using rotating cylinders. The obtained roughness function depends on the roughness Reynolds number, and it also depends on both the roughness wave height and wave length fraction to its height which are obtained FFT analysis for measured paint surface profiles.

Lee et al. (2015) investigated the performance of a new skin-friction reducing polymer named FDR-SPC (Frictional Drag Reduction Self-Polishing Copolymer). The drag-reducing functional radical such as PEGMA (Poly(ethylene) glycol methacrylate) has been utilized to participate in the synthesis process of the SPC. In the high-Reynolds number flow measurement with a flush-mounted balance and an LDV (Laser Doppler Velocimeter), the skin friction of the present FDR-SPC is found to be smaller than that of the smooth plate in the entire Reynolds number range, with the average drag reduction efficiency being 13.5% over the smooth plate.

Demirel et al. (2017) conducted an extensive series of towing test of flat plates covered with artificial barnacle patches to find the roughness functions of barnacles with varying sizes and coverages. Different sizes of real barnacles, categorised as small, medium and big regarding their size, were 3D scanned and printed into artificial barnacle patches. From the experimental results, they determined the roughness functions of barnacles with varying sizes and coverages. The roughness functions collapsed to the Colebrook-type roughness function of Grigson (1992).

6.4 Prediction methods for roughness effect

6.4.1 Similarity law analysis

The boundary layer similarity law scaling method, which was proposed by Granville (1958), has been widely used to predict the increased ship resistance due to hull roughness. The benefit of using this method is that once the roughness function, ΔU^+, of the surface is known, the skin friction with the same roughness can be extrapolated for flat plates with arbitrary lengths and speeds.

Schultz (2004) predicted the increases in the frictional resistance of a 150 m flat plate with different antifouling surfaces in unfouled, fouled and cleaned conditions, using the similarity law analysis. The increase in the frictional resistance of the surfaces in fouled condition ranged from 50% for an SPC TBT coating to 217% for a silicone coating. Using the same method, Schultz (2007) predicted the power penalty of an *Oliver Hazard Perry class* frigate of 144 m with different coating and fouling conditions. The increase in the required shaft power at a constant speed (30 knots) due to the heavy calcareous fouling condition was 59%, while the speed loss at a fixed power was 10.7%. Schultz et al. (2011) also analysed the overall economic impact of hull fouling on a mid-sized naval surface ship based on the resistance predictions using the similarity law analysis. The results indicate that the primary cost associated with fouling is due to increased fuel consumption attributable to increased frictional drag and the cost related to hull cleaning and painting is much lower than the fuel costs.

Demirel et al. (2019) presented practical added resistance diagrams based on the similarity law analysis to be used for predicting the increases in the frictional resistance and effective powers of the ships due to the use of a range of coating and biofouling conditions (Figure 29). Roughness effects of a range of representative coating and fouling conditions on the frictional resistances of flat plates were predicted across a range of ship lengths and speeds. The added resistance diagrams were then used to predict the resistance and powering penalties of different ships including DTMB 5415, KCS, JBC and KVLCC2.

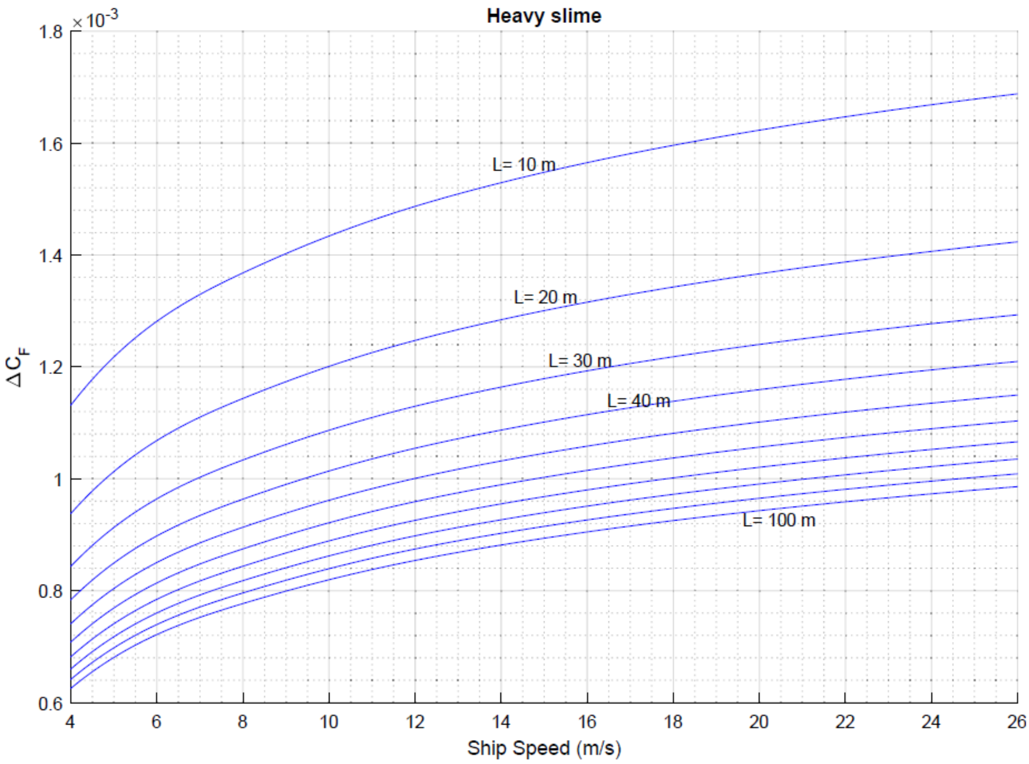

Figure 35: Added resistance diagram generated by Demirel et al. (2019)

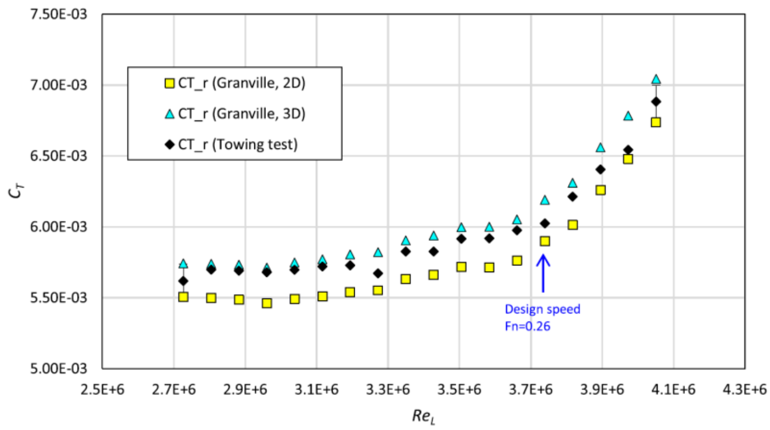

Figure 36: Total resistance predictions based on the similarity law analysis and the experimental data (Song et al., 2021a)

However, there have been questions regarding the validity of the similarity law analysis for predicting the total resistance of a 3D hull, because of its assumption of flat plate. In other words, this method only considers the roughness effect on the frictional resistance, while recent studies claim that the hull roughness affects the pressure-related resistance components as well as the frictional resistance (Farkas et al., 2018).

Recently, Song et al. (2021a) examined the validity of the similarity law scaling method for predicting the total resistance of a 3D hull. They conducted towing tests using a flat plate and a ship model in the smooth and sand-grit surface conditions. The roughness function of the sand-grit was determined from the flat plate test result using the overall method of Granville (1987). The frictional resistance of the ship model was predicted using the similarity law scaling with the obtained roughness function. The total resistance of the model ship was predicted using conventional hypotheses of Froude and Hughes (namely, 2D and 3D methods) and compared with the experimental result of the rough model ship. The total resistance predictions from the 3D method showed better agreement with the experimental result compared to the 2D method, suggesting that the resistance prediction can be more accurate when the roughness effect on the viscous pressure resistance is considered (Figure 36).

Monty et al. (2016) proposed a new prediction approach based on the boundary layer similarity law. The advantage of this approach is that the procedure can cope with varying roughness heights along the flat plate. Using the newly proposed method, they predicted the effect of tubeworm fouling on an FFG-7 Oliver Perry class frigate and a very large crude carrier, which showed 23% and 34% increases in total resistance respectively.

Katsui et al. (2018) have shown a method to evaluate the performance of the paints to reduce the added frictional resistance in full-scale ship Reynolds number. Simultaneous non-linear ordinary differential equations are developed to calculate the hydrodynamic frictional resistance of a flat plate based on the momentum equation and Coles' wall wake law which is the similarity law of the velocity distribution in the turbulent boundary layer. The effects of the roughness of the painted surface are taken into account by adding the roughness function to Coles' wall wake law. The calculated local frictional stress coefficients on the painted surfaces agreed well with the measured ones. The total frictional resistance coefficients of a painted surface in the actual ship scale Reynolds number can be evaluated considering various kinds of paints and the effects of the paint surface profile.

Mieno et. al. (2021) investigated the similarity law of added friction due to painted rough surface based on rotating cylinder tests. They have shown a relation between the friction increase rate and roughness Reynolds number and pointed out that friction increase rate depends not only on roughness height but also on roughness wave length. The roughness parameters of a painted surface which are related with roughness height and wavelength are measured by portable 3D hull roughness analysis which is developed by Mieno et. al. (2020).

6.4.2 CFD approaches

Recently, Unsteady Reynolds Averaged Navier-Stokes (URANS) based CFD simulations have been widely used to predict the added resistance due to surface roughness. The mainstream is using modified wall-functions by employing the roughness function in the CFD model.

Song et al. (2020b) validated the modified wall-function approach for predicting the added resistance of a 3D hull, which had been only validated for flat plates with zero pressure gradient. The flat plate and the KRISO Container Ship (KCS) model of Song et al. (2021a) were modelled in CFD simulations in both smooth and rough surface conditions using the modified wall-function approach. The simulation result showed a good agreement and thus demonstrated the validity of the CFD approach for predicting the roughness effect on 3D hulls.

Demirel et al. (2017b) conducted CFD simulations to predict the effect of marine coatings and biofouling on ship resistance on the full-scale 3D KCS hull. Different coating and fouling surfaces were modelled using a modified wall-function approach. The roughness effects of such conditions on the resistance components and effective power of the full-scale 3D KCS model were then predicted. The increase in the effective power of the full-scale KCS hull was predicted to be 18.1% for a deteriorated coating or light slime whereas that due to heavy slime was predicted to be 38% at a ship speed of 24 knots.

Farkas et al. (2018, 2019) conducted CFD simulations to investigate the effect of biofilm on the resistance a full-scale KCS, using a modified-wall function with the implementation of the roughness functions of diatomaceous biofilm of Schultz et al. (2015). By comparing the 3D KCS simulations with and without the presence of free surface, they decomposed the ship resistance into individual components. The result showed that the total resistance and frictional resistance of KCS increase with the presence of biofilm, whereas the wave-making resistance showed decreases.

Seok and Park (2020) also used the modified wall-function approach to analyse the variation in resistance performance of three different containership models. The simulation results were compared with the predictions based on Townsin's formula (Townsin and Dey, 1990) and showed a satisfactory agreement.

Song et al. (2019) conducted full-scale KCS simulations with different barnacle fouling conditions using the modified wall-function approach. They employed the roughness functions of barnacles (Demirel et al., 2017a) into the wall-function of the CFD model and conducted towed plate simulations to validate the CFD model against the experimental data. The same approach was used to predict the effect of barnacles on the resistance of a full-scale KCS. The results showed significant increases in the frictional resistance and effective power, up to 93% and 73% respectively, due to the barnacles on the hull. By decomposing the resistance components, they found different roughness effects on different resistance components. For example, the wave-making resistance showed decreases while the viscous pressure resistance increases with the presence of hull fouling. They also investigated the roughness effects on other hydrodynamic characteristics, such as the form factor, wake, velocity field and pressure field around the hull.

Owen et al. (2018) conducted CFD simulations to investigate the effect of biofouling on the open water performances of a model-scale propeller. The modified wall-function approach of Demirel at al. (2017b) was adopted to approximate the surface conditions of different coating and fouling surfaces. The effect proved to be drastic with the most severe fouling condition resulting in an 11.9% efficiency loss at J=0.6 ranging to an alarming 30.3% loss at J=1.2 compared to the smooth condition. The study acts as a proof of concept for the proposed CFD assessment method which can be used as a very practical approach to predicting the impact of realistic conditions on propeller characteristics and energy efficiency. Song et al. (2020c) conducted CFD simulations of a full-scale propeller (KP505) to investigate the effect of propeller fouling on the propeller open water performance, using the same modified wall-function approach as used by Song et al. (2019). They found increases in torque coefficient (10.2%) and decreases in thrust coefficient (-11.1%), which leads to a significant loss in the open water efficiency (19.3%).

Song et al. (2020d) conducted full-scale CFD simulations of self-propelled KCS with hull and/or propeller fouling using the same modified wall-function approach (Song et al., 2019). The roughness effects on the self-propulsion characteristics were investigated at the design speed of the KCS in various configurations of the hull and/or propeller fouling conditions. The result suggested that the required shaft power at the design speed of KCS increases by up to 82% due to the hull and propeller fouling. The roughness effects on the flow characteristics around the hull and propeller were investigated to be correlated with the findings on the roughness effect of the self-propulsion characteristics.

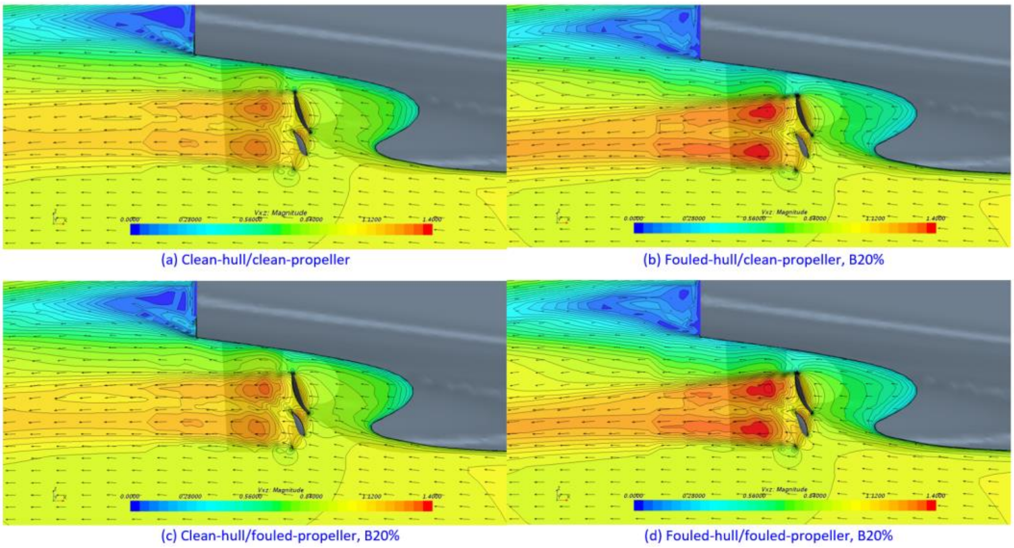

Figure 37: Velocity field around the hull and propeller, with different fouling scenarios (Song et al., 2019)

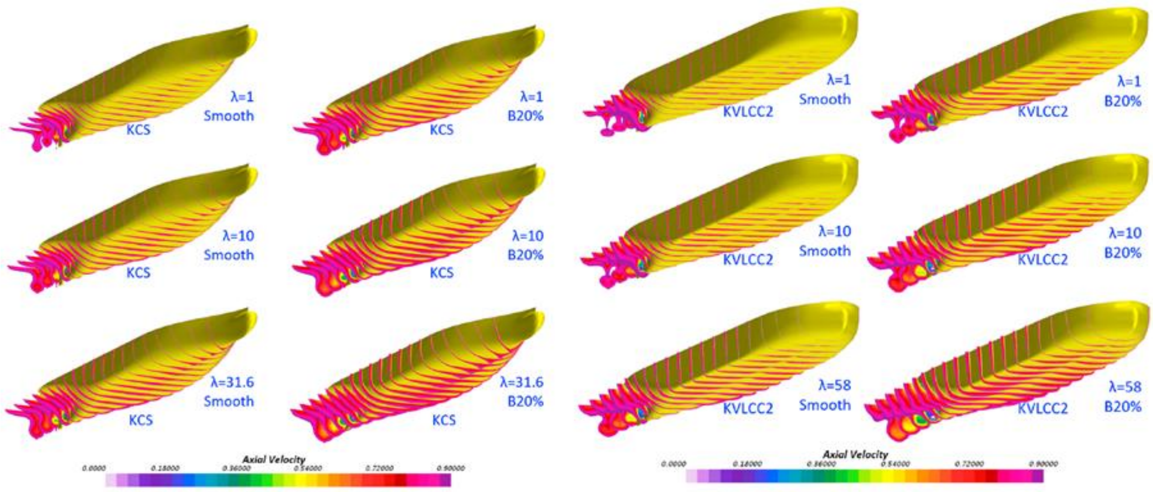

Figure 38: Boundary layer representations around the KCS and KVLCC2 hulls in different hull conditions and scales (Song et al., 2020e)

Song et al. (2020e) continued utilising the CFD method to investigate the effect of biofouling on the resistance of different ship types. A containership (KCS) and a tanker (KVLCC2) were modelled in CFD simulations with various scale factors (i.e. model, moderate and full scales) and speeds. The simulations were conducted with several fouling conditions using the modified wall-function approach. Significant differences in the roughness effects were observed on the resistance components varying with the hull types, lengths and speeds of the ships.

6.5 Conclusion

There is a need to adopt/develop new methods to predict the roughness effect of modern fouling-control coatings and marine biofouling on ship hydrodynamic performance. The similarity law scaling and CFD can be regarded as the most promising potential methods to predict such effects. Both methods require the use of roughness functions of the surfaces in question. The similarity law scaling can be used to predict the effect of roughness on the frictional resistance of flat plates of ship lengths effectively with less computational cost whereas CFD methods can be adopted for accurate prediction of roughness effects on the resistance components, propeller performance characteristics, and hydrodynamics of full-scale 3D ships. While these prediction methods require the roughness functions, there exists no universal roughness function model and no single roughness length scale for all types of marine coatings and biofouling surfaces. Therefore, there is a need to generate a database of roughness functions of modern fouling-control coatings and surfaces representing heterogenous biofouling accumulated on ship hulls and propellers. For this reason, it is recommended that standardised methods for roughness function determination should be adopted by researchers. It would, therefore, be useful to investigate the need for a guideline or procedure for the measurement of roughness functions for different surface finishes or conditions so that this information can be used for predicting the roughness corrections for both hull and propeller.

7. UNEQUALLY LOADED MULTIPLE PROPELLER VESSELS

7.1 Introduction

The objective of this task was to validate the procedure 7.5.02-03-01.7 1978 Performance Prediction Method for Unequally Loaded, Multiple Propeller Vessels proposed from 28th ITTC. Contrary to the single screw vessel or twin screw vessel having identical propellers, each propeller's loading is normally different due to the position of propeller (and as a result, the inflow condition will be different) and the design of propeller for unequally loaded, multiple propeller vessels as shown in Figure 39.

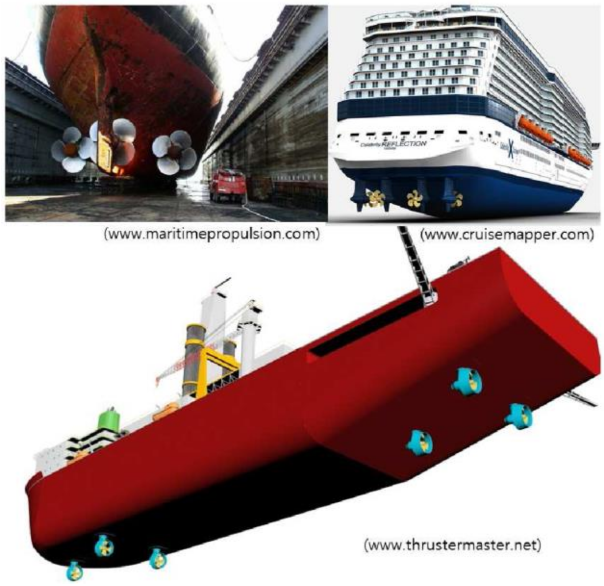

Figure 39: Unequally loaded, multiple propeller vessels

This feature lead to the requirement for the 28th ITTC to implement a new procedure, to consider the different interaction effect between propeller and hull by a new method for thrust deduction factor. By this new method for thrust deduction factor, each propeller's delivered power can be predicted.

To validate this procedure, sea trial data for unequally loaded, multiple propeller vessels is necessary, so that each measured power can be compared with model test prediction value. During the last 4 years, the committee tried to collect sea trial data in the public domain first, and then contacted shipping companies operating this kind of vessel, but unfortunately no sea trial data was available.

The committee has left this validation task as future work until such time as sea trial data becomes available, and decided to make this procedure more comprehensive by adding more graphs, formulae, description and model test data to calculate the thrust deduction factor for unequally loaded, multiple propeller vessels. Through this, the committee expects this recommended procedure and guideline can give more practical guidance for performance evaluation of this kind of vessel.

7.2 Calculation procedure of thrust deduction factor

The unique characteristics of the model test procedure for unequally loaded, multiple propeller vessels is how to get the proper value of thrust deduction factor in the self-propulsion test, the question being how much (i.e. what portion of) resistance is burdened or distributed over each propeller. To answer this, we can devise a factor as shown in Figure 41.

To obtain this factor, some methods were proposed with the assumption that the resistance would be distributed by the ratio of thrust of the propeller or the ratio of power of the propeller (Seo et al, 2011) and the results were compared.

As another way of getting the factor, the 28th ITTC Propulsion Committee proposed the RPG 7.5-02-03-01.7 and suggested load variation tests to calculate the resistance fraction, load fraction and finally the thrust deduction factor of each propeller. The definition of each value is as below;

$$1 - t_i = \gamma_i \frac{R_{TM} - F_D}{T_i} \quad \text{(thrust deduction factor)}$$

$$\gamma_i = \frac{T_i(1-\tau_i)}{\sum_{j=1}^{3} T_j(1-\tau_j)} \quad \text{(load fraction)}$$

$$1 - \tau_i = -\left(\frac{\Delta F}{\Delta T}\right)_i \quad \text{(resistance fraction)}$$

here, $\triangle F$ is the change of towing force and $\triangle T$ is the change of thrust in the load variation test, R_{TM} is the resistance of the model at each speed, corrected for temperature differences between resistance and propulsion tests, and F_D is the tow force expected at each speed for the propelled ship self-propulsion point condition.

In this suggestion, the resistance fraction of the i-th propeller is calculated from the load variation test of that propeller (i.e., the revolutions of i-th propeller only is changed and the other propellers are keeping their revolutions around self-propulsion point). This situation is illustrated in Figure 42 and the slope of the relation (resistance fraction) can be calculated.

To calculate the thrust deduction factor of each propeller, the portion of resistance burdened by each propeller should be defined first and the resistance fraction accounts for artificial distribution of ship resistance by using the ratio of towing force decrease and the corresponding thrust increase of each propeller.

Again, a larger value of (1-resistance fraction) means the thrust force is well transferred to ship's resistance without any significant increase of resistance from the interaction effect between propeller and hull: less interaction effect to resistance means low thrust deduction factor.

The more important consideration is that the ratio of resistance fraction (not the absolute value) determines the thrust deduction factor of each propulsion system by definition. The result from a sample calculation is shown in Figure 40.

Item	$1-\tau_i$	γ_i	t
	[-]	[-]	[-]
Center	1.0	68.7%	0.153
Side	1.0	15.7%	0.153
		31.3%	

Item	$1-\tau_i$	γ_i	t
	[-]	[-]	[-]
Center	0.9	68.7%	0.153
Side	0.9	15.7%	0.153
		31.3%	

Item	$1-\tau_i$	γ_i	t
	[-]	[-]	[-]
Center	0.92	67.1%	0.173
Side	0.99	16.5%	0.110
		32.9%	

Figure 40: Sample calculation

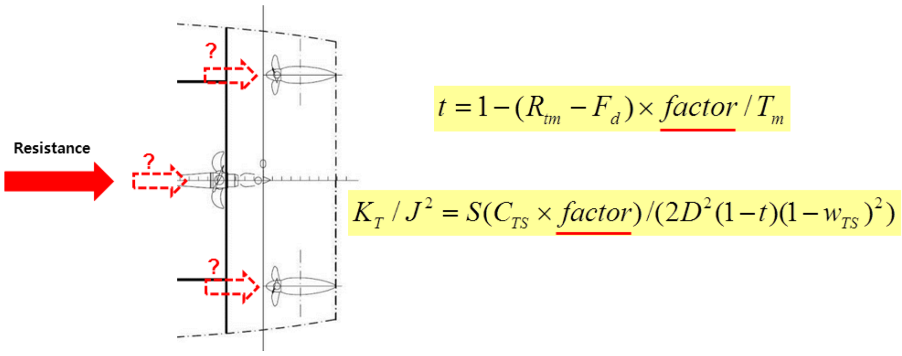

Figure 41: Resistance distribution to each propeller

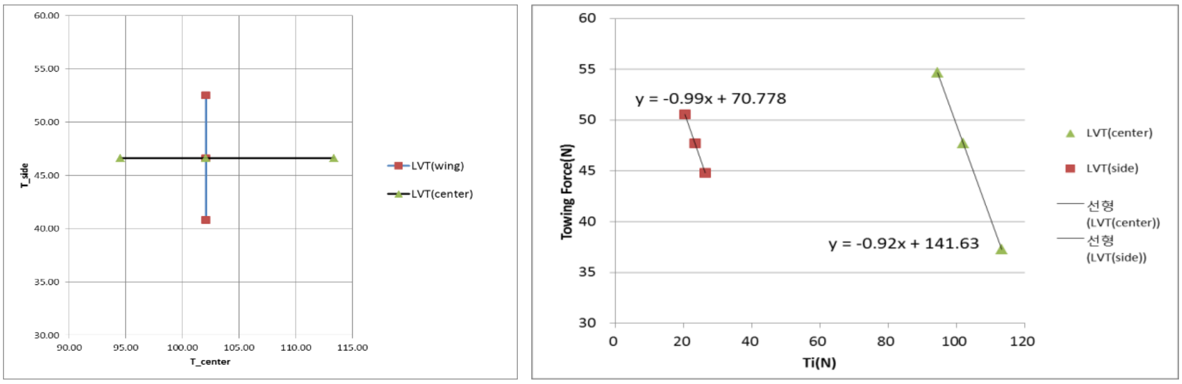

Figure 42: Load variation test to get resistance fraction and sample calculation result

7.3 Sample calculation result based on the proposed procedure

Sample calculations based on the method presented at SMP'11 and 28th ITTC were carried out and compared.

The distributed resistance can be calculated by the definition from SMP'11 and 28th ITTC as below:

$$R_i = \frac{T_i}{\sum_{j=1}^{3} T_j}(R_{TM} - F_D), \quad \text{SMP'11}$$

$$R_i = \frac{T_i(1-\tau_i)}{\sum_{j=1}^{3} T_j(1-\tau_j)}(R_{TM} - F_D), \quad \text{ITTC 28}^{\text{th}}$$

By the definition of thrust deduction factor, if the resistance is distributed by the thrust ratio from SMP'11, the thrust deduction factor of each propeller has the same value and this does not account for the different loading of the propeller or the interaction effect. But if the resistance is distributed by the load fraction, the large value of (1-resistance fraction) accounts for large resistance distribution, low interaction effect and finally low thrust deduction factor. Sample calculation results are as Figure 43.

Even though the two methods showed different values of thrust deduction by the different distribution of resistance, the total sum of delivered power of each propeller was almost the same. This sample calculation is just one example and it is expected that more test cases will help to decide which method can give more accurate results compared to sea trial results.

The 29th ITTC Resistance and Propulsion Committee tried to get sea trial data of unequally loaded, multiple propeller vessels but could not obtain it and it is recommended that the next committee should continue trying to obtain this data to validate the procedure.

Rtmc	Fd
[N]	[N]
173.63	47.71

SM P'11

	Ti	Ri	Ti/T	t
Center	102.1	86.5	68.7%	0.153
Side	23.3	39.5	15.7%	0.153

ITTC 28th

	Ti	Ri	Ti/T	t
Center	102.1	84.4	67.1%	0.173
Side	23.3	41.5	16.5%	0.110

Resistance may be distributed by thrust ratio(from SM P'11)

	Ti/T	t	wts	KT/J2	JTS	etaH	EtaO	EtaD	EHP	DHP	DHP_total		
		-	-						[kW]	[kW]	[kW]		
Center	68.7%	0.153	0.185	0.349	0.785	1.039	0.671	0.691	6325	9159	14599	100.0%	62.7%
Side	15.7%	0.153	0.045	0.131	1.101	0.887	0.591	0.531	2888	5440			37.3%

Resistance may be distributed by "resistance fraction from ITTC 28th

Item	1-τi	γi	t	wts	KT/J2	JTS	etaH	EtaO	EtaD	EHP	DHP	DHP_total		
	[-]	[-]	[-]	-	-	-	-	-	-	[kW]	[kW]	[kW]		
Center	0.92	67.1%	0.173	0.191	0.355	0.782	1.023	0.669	0.678	6178	9106	14546	99.6%	62.6%
Side	0.99	16.5%	0.110	0.045	0.131	1.101	0.932	0.591	0.558	3035	5440			37.4%

Figure 43: Example calculation

8. FULL SCALE DATA FOR PODDED PROPULSION

Podded propulsion is typically installed on large cruise vessels and is also seen on large icebreakers.

Pods are characterized by having an electric engine mounted directly behind a pulling propeller inside an azimuth housing. This has the advantage that there is no gear (reduction or angle gear) and only a very short propeller shaft resulting in a quite effective propulsion seen from the mechanical point of view. The electric power is traditionally generated by diesel gensets and therefore some efficiency loss must be expected. However, for future vessels the electric power could possibly be generated in a more sustainable way e.g. fuel-cells, solar panels etc.

Pods are normally installed in twin or triple formations. For twin installations, both pods will act as a steering device with 360 degree. azimuthing ability. For triple installations, the centre pod could be fixed in angle and therefore only used as propulsion and not steering.

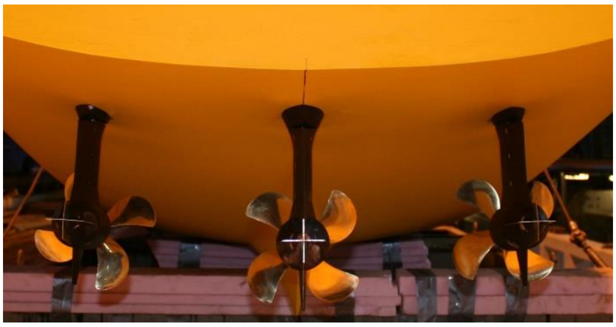

Figure 44. Model scale triple pod installation

The present committee have been in contact with ship owners within the cruise industry. They have the full scale data needed for verification/modification of the current procedure (7.5-02-03-01.3). However, for them it is not possible to share the data with ITTC due to commercial interests even though they would like to from a technical perspective. Seen from this perspective getting full scale data from icebreakers seems to be the way forward since there shouldn't be any commercial restrictions.

9. QUASI-STEADY PROPELLER AND PROPULSION TESTS

The quasi-steady (QS) method is a promising technique for significantly reducing the time required to conduct a propeller open water (POW) test and propulsion test. The QS method is suitable for meeting the growing demands for large series of model tests by ship owners and/or operators, such as trim/draught combination tests. MARIN has studied the method in the past and has shown a good correlation between the QS POW tests and the conventional ones, as shown in the committee report of 28th ITTC. The last committee stated that validation by organisations other than MARIN was a future issue.

During this term, HSVA presented the effectiveness of the QS resistance tests (Larssen, 2018). The QS tests required only a single run to cover the full speed range, saving 4.5 times the time of conventional tests. The towing speed was constantly accelerated until the maximum speed and decelerated until the minimum speed. The hysteresis was removed by averaging of the acceleration and the deceleration data. From two pictures taken during the acceleration and the deceleration, it was found that the deformation along the ship's hull matched well, which indicated a similar pressure distribution on the hull surface during both runs (Figure 45). They conducted both QS tests and conventional tests on the same day and confirmed the deviation of a root mean square value was within only 0.6%, which was comparable to the usual repeatability for conventional tests. Moreover, more than 18 different ships were tested in several different setups. Figure 46 shows the discrete probability density of the deviation between the QS method and conventional test. It shows that the expected value was only 0.07%.

The reliability of the QS method has been confirmed by MARIN and HSVA, and it looks ready to replace the conventional test. However, to develop the guidelines, the limits of applicability, e.g. how large wave making and/or dynamic trim and sinkage are allowed, should be clarified. Since the method has a great potential to replace the conventional test, it is recommended in the next term to conduct benchmark tests and validate the method by more model basins.

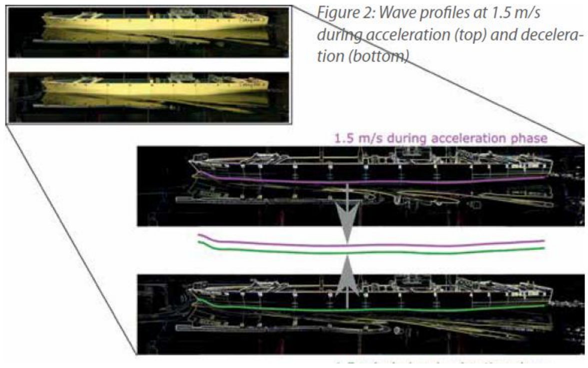

Figure 45: Wave profiles during acceleration (top) and deceleration (bottom)

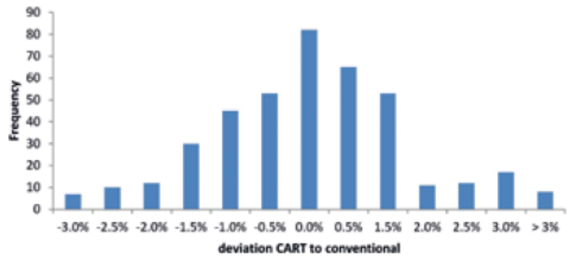

Figure 46: Distribution of discrete deviations of the QS propulsion tests to the conventional tests.

10. CAVITATION EROSION MODELLING AND PREDICTION

10.1 Introduction

Cavitation erosion has long been recognized as a problem in the shipping industry. It degrades propeller performance and imposes high maintenance costs. Thus, accurate prediction of erosion at the design stage is important.

Cavitation erosion on marine propellers and rudders attracted attention as a big issue with the emergence of a new generation of large and fast container ships, ferries and ROPAX vessels in the early 2000s.

Against such a background, the Specialist Committee on Cavitation Erosion on Propellers and Appendages on High Powered/High Speed Ships was organized in the 24th ITTC and developed the RP 7.5-02-03-03.5 "Cavitation Induced Erosion on Propellers, Rudders and Appendages Model Scale Experiments". Then, the Specialist Committee on Cavitation for the 25th ITTC developed the RP 7.5-02-03-03.7 "Prediction of Cavitation Erosion Damage for Unconventional Rudders or Rudders Behind Highly-Loaded Propellers". These were developed from experimental aspects because numerical prediction for cavitation was immature at that time.

Since then, cavitation simulation techniques have advanced greatly due to rapid evolutions in numerical modelling as well as in computational hardware. The state-of-art of the technology has been reported by the following ITTC committees, 26th ITTC (2011), 27th ITTC (2014), and 28th ITTC (2017).

Accordingly, numerical prediction of cavitation erosion is becoming feasible.

10.2 Erosion modelling

Cavitation erosion occurs when impulsive pressure from shock waves and/or microjets generated by bubble collapse exceeds some material threshold, such as its yield stress.

The detailed mechanism is still a subject to be solved, but many researchers have attempted to explain it more accurately. For example, Dular et al. (2019) recently developed a technique on simultaneous observation of one single cavitation bubble collapse and the damage it creates. The dynamics of the bubble created by Nd:YAG laser was observed with two high-speed cameras. They concluded that the most pronounced mechanism is the impact of the microjet when the cavitation bubble implodes near the wall. On the other hand, the influence of the micro-jet diminishes and the collapse of microscopic bubbles in the rebound cloud is more important when the bubble collapses away from the wall.

Although the detail is not fully understood, various cavitation erosion models have been proposed to describe the physical mechanisms.

Fortes-Patella et al. (2004) proposed a model based on the energy balance illustrated in Figure 48. Potential power included in vapour clouds converts into acoustic power by the bubble collapse. The emitted pressure waves interact with the neighbouring solid surface, leading to material damage. Two transfer efficiencies η^{**} and η^{*} are used in the model. η^{**} is a hydrodynamic efficiency between the initial power P_{pot} and the flow aggressiveness power P_{pot}^{mat}, which is a function of the hydrodynamic characteristics (V_{ref}, σ) of the flow and the distance between the vapour structures and the solid surface. η^{*} is a collapse efficiency between P_{pot}^{mat} and pressure wave power P_{wave}^{mat}, which depends mainly on the local pressure and on the initial gas pressure P_{go} within the bubble. Then, the volume damage rate, V_d, was derived by the following formula.

$$V_d = \frac{P_{wave}^{mat}}{\beta \Delta S} \tag{1}$$

Where ΔS is an analysed sample surface and β is a mechanical characteristics of the material.

Dular et al. (2006) proposed a model based on the microjet formation illustrated in Figure 49. Pressure waves emitted from the bubble collapse make a single bubble near the wall oscillate and a microjet occur. The high-velocity liquid jet impact on the wall causes material damage. Through the experiment using hydrofoils, they found that the value of the standard deviation of the grey level in the image of cavitation relates to the time derivative of cavity volume for calculating the pressure wave power P_{wave}. The jet velocity is determined based on the theory developed by Plesset and Chapmann (1971) and the pit depth and the damaged surface area can be estimated using the jet velocity and material property.

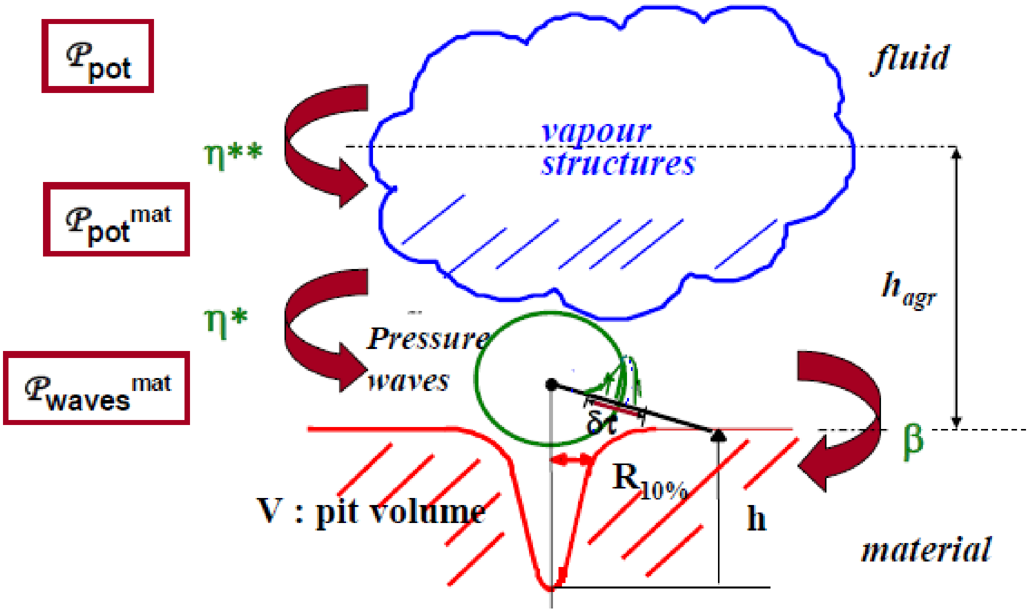

Figure 47: The physical scenario based on the energy balance, Fortes-Patella, et al. (2004)

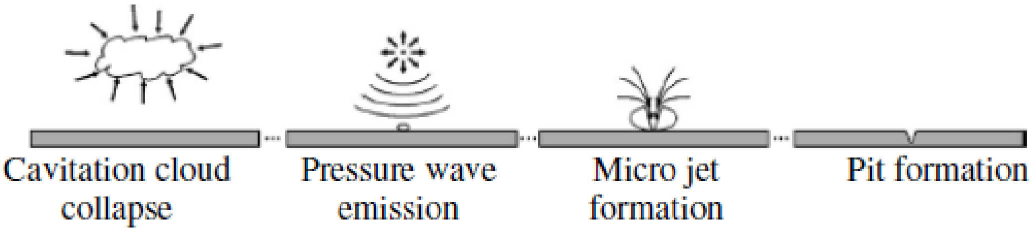

Figure 48: The physical scenario based on the microjet formation, Dular et al. (2006)

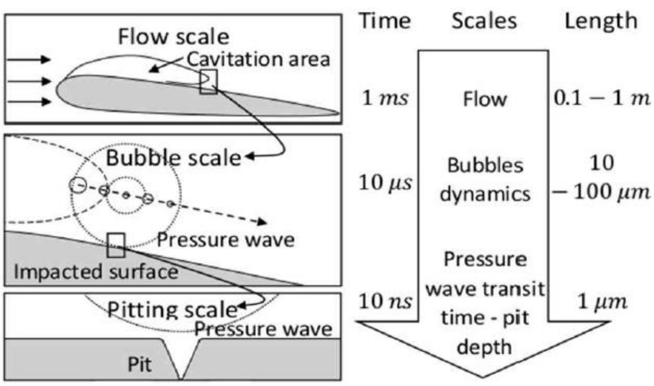

Figure 49: Illustration of time and length scales phenomena induced by cavitation erosion, Leclercq et al (2017)

Melissaris and Terwisga (2019) have recently reviewed the cavitation erosion models published during the last decade. In addition to the abovementioned models, they introduced the concept of the "collapse detector" by Mihatsch et al. (2011), while they addressed that the energy balance model by Fortes-Patella et al. (2004) is the most appropriate for erosion risk assessment using an incompressible pressure based URANS solver.

It is a common concept in all the above models that the process starts with a collapse of vapour structures.

10.3 Numerical approach for erosion prediction

To predict the erosion accurately, one must calculate the whole process from the bubble collapse to the impact of the pressure wave on the surface. However, it is difficult to simulate numerically because a wide range of scale in time and space should be treated in the calculation, as illustrated by Leclercq et al. (2017) in Figure 49. Besides, there are many parameters to be considered, such as water quality and gas content.

Schmidt et al. (2008) attempted to directly solve shock waves emitted from bubble collapse in the flow around the prismatic body and the sphere. However, such a direct simulation requires quite a fine mesh with a small time-step, below one microsecond. The practical implementation with complicated geometry such as a propeller is impractical at the moment.

Alternatively, as a practical solution for assessing erosion, many researchers have proposed erosion indicators derived from the macroscopic flow solved using CFD calculation.

10.4 Erosion indicator

Most indicators relate to pressure *p*, cavity volume *V*, void fraction α and their time derivatives, which are terms for describing the potential power P_{pot} included in the vapor structure. P_{pot} can be calculated as a time derivative of potential energy E_{pot} suggested by Vogel and Lauterborn (1988) as follows:

$$E_{pot} = \Delta p \cdot V \tag{2}$$

$$P_{pot} = \Delta p \cdot \frac{dV}{dt} + \frac{dp}{dt} \cdot V \tag{3}$$

where $\Delta p = (p_d - p_v)$ is the difference between the ambient pressure driving cavity collapse, p_d, and the vapour pressure, p_v. By dividing *Ppot* by a cell volume, V_{cell}, potential power density can be expressed with a void fraction α as follows:

$$\frac{P_{pot}}{V_{cell}} = \Delta p \cdot \frac{d\alpha}{dt} + \frac{dp}{dt} \cdot \alpha \tag{4}$$

Hasuike et al. (2009) applied the following four indicators suggested by Nohmi et al. (2008) to a four bladed propeller whose individual blades have different tip load.

$$\begin{aligned} index1 &= \alpha \cdot max\left[\frac{\partial p}{\partial t}, 0\right] \\ index2 &= \alpha \cdot max[p_d - p_v, 0] \\ index3 &= max\left[-\frac{\partial \alpha}{\partial t}, 0\right] \\ index4 &= max[p_d - p_v, 0] \cdot max\left[-\frac{\partial \alpha}{\partial t}, 0\right] \end{aligned} \tag{4}$$

RANS with *k-ε* turbulence model was used for the cavitation simulation. Cavitation was modelled by Singhal's full cavitation model based on Rayleigh-Plesset equation. In this cavitation model, the pressure fluctuation due to turbulence and the effect of non-condensable gas are taken into account in the mass transfer process. Index 2 could give a reasonable prediction for the area where the paint was peeled in model tests and describe the difference of the damaged area among different blades. Although the absolute values of the indexes have no physical meaning, they showed the possibility to estimate erosion risk qualitatively.

Eskilsson and Bensow (2015) applied three indicators called Discrete Bubble Method (DBM), Gray Level Method (GLM) and Intensity Function Method (IFM) to the case of cavitation over a NACA0015 foil. GLM is an index related to $dV/dt \cdot \Delta p$ and IFM related to dp/dt. DBM is based on the development of advected microscopic bubbles. However, the cavitation pattern was not well simulated by LES with Sauer cavitation model, and none of the methods could predict the erosive behaviour successfully. The authors stressed the need for further work.

Usta et al. (2017) applied GLM and IFM to the case of the King's College-D (KCD)-193 model propeller with five blades. In addition, they proposed the Erosive Power Method (EPM), which focuses on both the derivative of the vapor fraction and the pressure. The cavitating flow was simulated by DES with SST *k*-omega turbulence model. Cavitation was modelled by Schnerr-Sauer(S-S) cavitation model with Reboud correction, which implements a simplified Rayleigh-Plesset equation neglecting the influence of bubble growth acceleration, viscous effects and surface tension effects. All three indicators showed reasonable prediction for the erosion area. Figure 50 shows an example of a comparison of erosion area from model test and EPM. The colours going red and blue in Fig. 4 show the area of high erosion risk. The maximum and minimum scalar values of the erosive intensity are limited with a threshold to make a meaning prediction. Although the threshold was chosen as $1*10^{-7}$-$1*10^{7}$ in this case, how to determine it is unclear. The authors addressed the need for further work to determine the erosion intensity thresholds numerically.

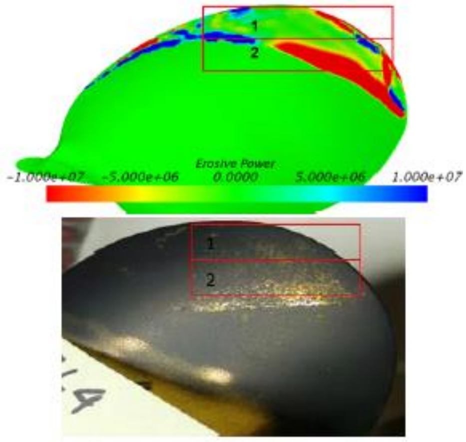

Figure 50: Comparison of erosion area from model test and EPM, Usta et al. (2017)

Melissaris et al. (2018) calculated the cavitating flow over the KCD-193 model propeller by RANS with SST *k*-omega turbulence model. The S-S cavitation model was applied. They investigated the difference of the contribution of the time derivative of pressure $\Delta\alpha \cdot dp/dt$ and the time derivative of void fraction $\Delta p \cdot d\alpha/dt$ to the cavitation aggressiveness. They found that the time derivative of the void fraction contributes more when using the time-averaged local pressure as the driving pressure p, while the time derivative of the pressure contributes more when using the instantaneous local pressure. $\Delta p \cdot d\alpha/dt$ using the time-averaged pressure as the driving pressure shows the best agreements with the paint test. The results shows an importance of a correct definition of the driving pressure for assessing the erosion intensity.

The European project "CaFE (Development and experimental validation of computational models for Cavitating Flows, surface Erosion damage and material loss)" was conducted from 2015 to 2018. Many papers have been published as fruits from the project. The following erosion indicators were developed within the project, Melissaris and Terwisga (2019).

$$\langle \dot{e}_s \rangle_{e_s} = \left(\frac{1}{e_s} \int_0^t \dot{e}_s{}^{n+1} dt \right)^{1/n} \quad (6)$$

$$\langle \dot{e}_s \rangle_f = \left(\frac{1}{T} \int_0^t \dot{e}_s{}^{n+1} dt \right)^{1/(n+1)} \quad (7)$$

where

$$e_s = \int_0^t \dot{e}_s dt = \int_0^t -\Delta p \cdot \frac{\partial \alpha}{\partial t} dt \quad (8)$$

These indicators relate to the time derivative of the void fraction which is the first term of Eq. (4). The indicator $\langle \dot{e}_s \rangle_{e_s}$ averages the local energy impact rate over the surface accumulated energy e_s, amplifying the local extreme events. The indicator $\langle \dot{e}_s \rangle_f$ is normalized by the total impact time T. The parameter n is used to emphasize the peak events.

These indicators were applied to the erosion risk assessment for the KCD-193 model propeller by Melissaris et al. (2019), the Delft twist 11 hydrofoil by Melissaris et al. (2019) and 2D NACA0015 hydrofoil by Schenke et al. (2019). In general, the predicted high erosion risk area agreed well with the paint test. However, there were some cases that the erosion areas were overestimated or underestimated. The authors said that more insight is necessary, especially on the determination of pressure driving cavity collapse, p_d, for calculating Δp in Eq. (8).

10.5 Conclusion

To assess the cavitation erosion risk practically, various erosion indicators have been proposed, which can be derived from macroscopic features of the flow calculated using RANS, DES or LES. Most of them relate to pressure p, cavity volume V, void fraction α and their time derivatives. These indicators are helpful for propeller designers to predict potential erosion areas and locations.

However, it is unclear whether they always give reasonable predictions against various kinds of cavitation pattern. To evaluate the cavitation aggressiveness, some threshold for the indicator is required. Although they influence much on the erosion prediction, how to determine it is also unclear.

To develop the procedure on predicting cavitation erosion, it seems necessary to study further, such as the determination of pressure driving collapse, the influence of the distance between the bubble collapse and the surface, the influence of water quality and so on. Needless to say, the material response and the scale effect, which are not considered in most works, are to be studied as well.

Cavitation erosion modelling is a rapidly developing topic, and further developments should continue to be monitored, and updates to procedures should be considered in future.

11. RIM DRIVE TESTING

The committee was tasked to identify the need to develop a procedure for rim driven propulsor model testing and performance prediction. To understand the need for this and the extent of involvement of ITTC members in rim driven propulsor testing, a questionnaire was prepared and distributed to the ITTC members.

The questionnaire consisted of 39 questions ranging from general questions on the organisation's involvement with rim driven thrusters, to more specific questions on the procedures used to conduct model tests and performance prediction.

Out of 92 organisations to whom the questionnaire was sent, 13 completed responses were received. This immediately indicates that rim driven propulsors are currently of interest to a small group of organisations.

The first question asked whether the organisation was involved in activities related to rim driven thrusters. The responses to this are summarised in Figure 51. A total of 6 organisations are actively involved in these type of devices. A further question then asked what type of activities these organisations carried out on rim driven thrusters. The responses are summarised in Figure 52. Of the respondents, 5 are carrying out model tests, which may include model manufacture, while 3 are involved in design or theoretical studies.

Respondents were then asked whether a specific ITTC procedure should be developed for rim driven thruster testing and performance prediction. The response to this was largely positive, even from some who are not actively involved (Figure 53).

A few publications were identified by the respondents, notably Dang and Ligtelijn (2019), Klinkenberg et al. (2017), Yakovlev et al. (2011) and Sokolov et al. (2012). These may be used to understand some of the key considerations in rim driven thruster testing.

Notably, no respondent was aware of any full scale test data for rim driven thrusters, which seems a significant loss. It is likely that the manufacturers would have such information, and it may be useful for a future committee to try to obtain examples of such data.

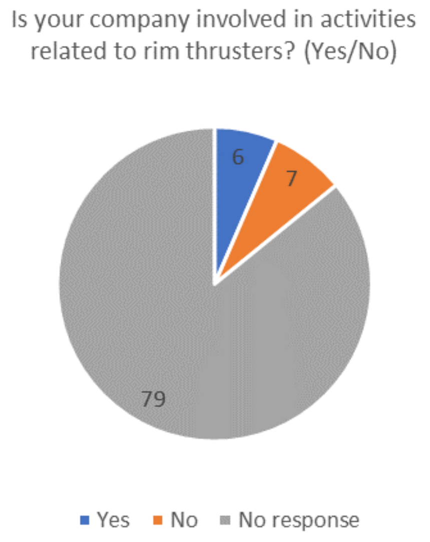

Figure 51: Rim drive responses (question 1)

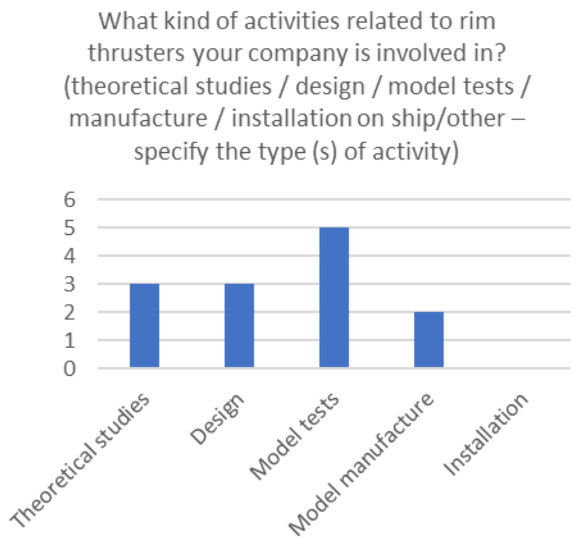

Figure 52: Rim drive responses (question 2)

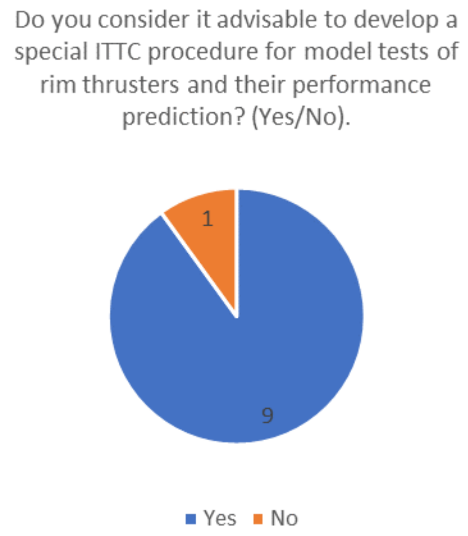

Figure 53: Rim drive responses (question 4)

Model tests are carried out in either a towing tank or a cavitation tunnel, in common with standard propeller testing. Special mounting arrangements are required to support the nozzle, and in some cases a special drive is built to allow measurement of thrust and torque on the blades. If the thruster has a hub, the propeller can be mounted on a standard propeller dynamometer shaft, but this is not possible with hubless designs.

Measured parameters are in line with those expected for a propeller test, including thrust, torque, flow velocity and RPM, as well as the tank/tunnel environmental conditions and perhaps the electrical performance of the motor.

The key challenges that have been reported include isolating the thrust and torque of the thruster blades, scaling issues due to the flow in the gap, friction in the bearings and manufacturing and mounting issues associated with hubless designs.

Thrust is either measured on the whole unit, using load cells or a 6-component balance, or can be measured using a ring-shaped transducer. For a hub-type thruster, the thrust of the rotor can be measured using a standard propeller dynamometer.

Torque can also be measured using the same methods, but can also be derived from the power consumption of the motor, with a correction for friction. The torque of the rim thruster is affected by friction in the gap between the inner and outer ring. This is not Froude scaled. Also the torque on the nozzle may not be negligible so should be measured.

Performance prediction of rim driven thrusters is typically based on model test results, with ITTC blade friction corrections to account for scale. This does not account for the scaling of the gap flow, and currently the only method for assessing the Reynolds number effects in this part of the flow is to use CFD. A number of the respondents mentioned that they use CFD to account for the scale effects.

In summary, there are a number of ITTC members carrying out model tests of rim driven thrusters, and no consistent approach is currently taken to measure the thrust and torque, or to scale the results to make full scale predictions. It is therefore recommended that the next Resistance and Propulsion Committee should work towards developing a new procedure to fill this gap.

12. INFLUENCE OF F_D ON POWER PREDICTION

12.1 Introduction

The objective of this task was to identify the influence of the new F_D definition on power prediction. As is well known, F_D is the skin friction correction in a propulsion test and represents an additional towing force to compensate the difference of resistance between model and ship scale (relatively higher resistance in model scale than ship scale). From this definition, the F_D value can be calculated considering the model scale speed, density of water, wetted surface area and non-dimensional coefficient of resistance in model and ship scale. In practice, some parts of the resistance at ship scale are not included and some parts are added to get a more reliable prediction.

The 28th ITTC general conference accepted to adopt the new F_D definition to enhance the accuracy of powering performance prediction by adding C_A in the formula. However, it did not provide an appropriate basis on whether it actually improves accuracy, so the committee was asked to evaluate the extent of the impact.

12.2 History of F_D definition change

Before looking at the impact of F_D change, the history of previous F_D changes was reviewed and summarized as below:

~ ITTC 24th (2005):

$$F_D = 1/2 \rho_M V_M^2 S_M [C_{FM} - (C_{FS} + \Delta C_F)]$$

$$\Delta C_F = [105(\frac{k_S}{L_{WL}})^{1/3} - 0.64] \times 10^{-3}$$

ITTC 25th (2008) ~ 27th (2014):

$$F_D = 1/2 \rho_M V_M^2 S_M [C_{FM} - (C_{FS} + \Delta C_F)]$$

$$\Delta C_F = 0.044[(\frac{k_S}{L_{WL}})^{1/3} - 10 Re^{-1/3}] + 0.000125$$

ITTC 28th (2017):

$$F_D = 1/2\rho_M V_M^2 S_M[C_{FM} - (C_{FS} + \Delta C_F + C_A)]$$

$$\Delta C_F = 0.044[(\frac{k_S}{L_{WL}})^{1/3} - 10Re^{-1/3}] + 0.000125$$

$$C_A = (5.68 - 0.6logRe) \times 10^{-3}$$

From 2008, the existing (old) $\triangle C_F$ was divided into new $\triangle C_F$ and C_A (i.e., C_{TS} includes new $\triangle C_F$ and C_A, but still (new) $\triangle C_F$ was only included in F_D calculation). This separation had been proposed from 19th ITTC because the existing $\triangle C_F$ has been criticized for not properly reflecting the roughness effect of the hull and was finally adopted by the 25th ITTC in 2008. However, the C_A value left room for continued use of the empirical formula previously used in each towing tank and the standard C_A value was chosen to be similar to those before they were separated.

In addition, it should be noted that despite these changes in the standard procedure, each towing tank adheres to the existing method, taking into account the continuity of their own analysis method.

12.3 How to identify the influence of F_D definition change

As described in last chapter, the history of F_D change was reviewed and the actual value of F_D in propulsion tests with normal size of model ships is as shown in Table 4.

Separation of the old $\triangle C_F$ into the new $\triangle C_F$ and the C_A had to be consistent and the actual value of F_D has a similar level comparing ITTC 28th and ~24th, but comparing 28th and 25th through 27th, there is a considerable difference. If we take the change from 27th to 28th, the typical value of change is as below (Table 3).

Table 3: Change in FD for different ship types

VLCC	-5.6%
Aframax	-10.7%
Suezmax	-9.1%
VLGC	-9.9%
174k LNGC	-3.2%
15.1k CC	2.6%

Table 4: Values of FD for different ship types

Ship Type	Value	ITTC 28th(2017)	ITTC 25th(2008)~27th(2014)	ITTC ~24th(2005)
VLCC (14.5kts)	F_D(N)	14.47	15.33	14.85
	$\triangle C_F$*1000	0.118	0.118	0.169
	C_A*1000	0.092		
Aframax (14.5kts)	Fd(N)	13.70	15.33	14.03
	$\triangle C_F$*1000	0.117	0.117	0.251
	C_A*1000	0.167		
Suezmax (15kts)	Fd(N)	19.46	21.41	19.93
	$\triangle C_F$*1000	0.122	0.122	0.224
	C_A*1000	0.135		
84k LPGC (17kts)	Fd(N)	12.64	14.03	12.72
	$\triangle C_F$*1000	0.137	0.137	0.279
	C_A*1000	0.151		
174k Twin LNGC (19.5kts)	Fd(N)	25.44	26.27	25.36
	$\triangle C_F$*1000	0.152	0.152	0.199
	C_A*1000	0.043		
15.1k CC (22kts)	Fd(N)	36.95	36.02	36.31
	$\triangle C_F$*1000	0.162	0.162	0.152
	C_A*1000	-0.033		

The objective of this study is to identify the impact of this change on the powering performance prediction and this can be achieved through evaluating the corresponding change of propulsion efficiency and propeller revolutions.

To calculate the change of propulsion efficiency and propeller revolutions, the propulsion test data was re-analysed with several values of F_D around the definition from ITTC 27th as shown in Figure 54. This shows the general trend of the change of propulsion efficiency and propeller revolutions along with the change of F_D value and finally can identify the influence of the new F_D definition.

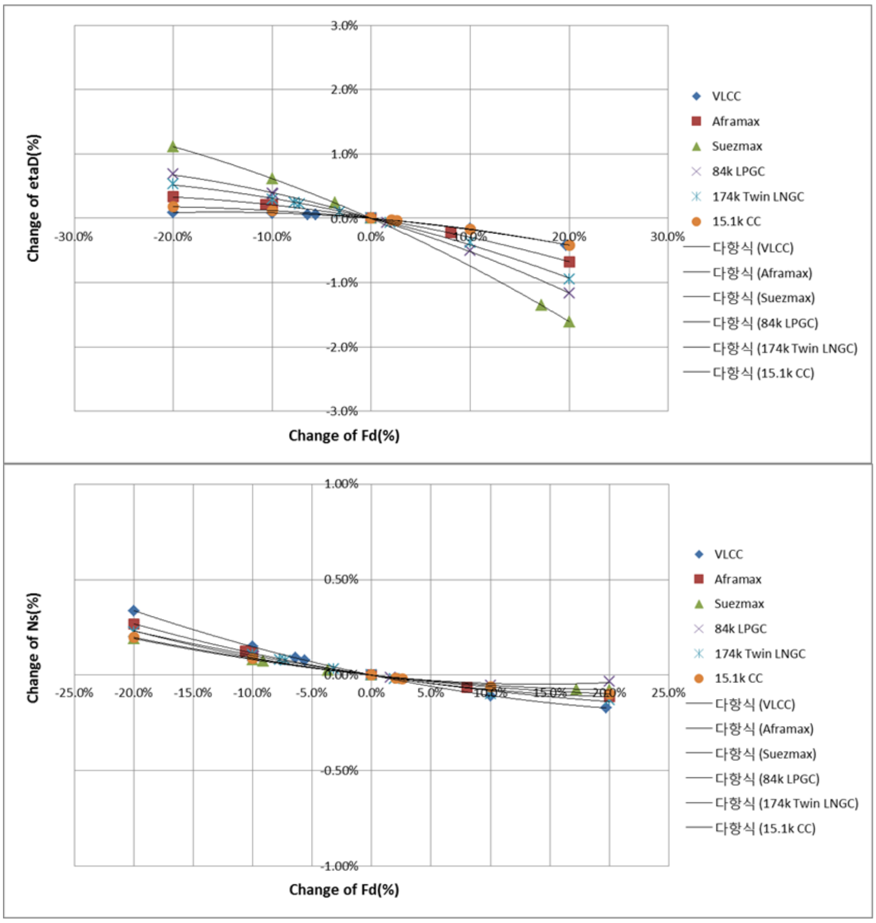

Ship Type	△Fd	△EtaD
VLCC	-5.6%	0.1%
Aframax	-10.7%	0.2%
Suezmax	-9.1%	0.6%
VLGC	-9.9%	0.4%
174k LNGC	-3.2%	0.1%
15.1k CC	2.6%	0.0%

Ship Type	△Fd	△Ns
VLCC	-5.6%	0.08%
Aframax	-10.7%	0.12%
Suezmax	-9.1%	0.07%
VLGC	-9.9%	0.09%
174k LNGC	-3.2%	0.03%
15.1k CC	2.6%	-0.02%

Figure 54: Sample analysis of propulsion test with the different value of F_D

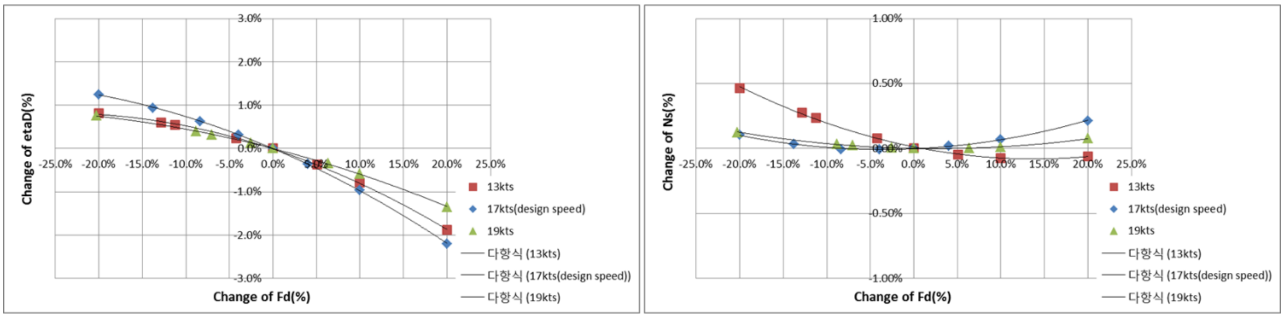

Figure 55: Effect of speed on the change of propulsion efficiency and revolution of propeller

The committee members were asked to re-analyse their own propulsion test data with the different value of F_D and finally 31 cases were collected. During this analysis, the design speed only was chosen and the effect of speed was investigated to be limited, as shown in Figure 55.

12.4 Result of sample calculation on the effect of the new F_D definition

The definition of F_D includes $\triangle C_F$ and C_A and these two parameters are dependent on the ship length and Reynolds number as in Figure 56. There is a wide variety of ship types and speed, so it is necessary to organize them into a single parameter to present the result. The Reynolds number was already included in the definition of friction resistance compensation, so it was used as an independent parameter.

The overall trend of F_D change is shown in Figure 56. First of all, the amount of F_D change itself is relatively small for large and high speed and vice versa. By this trend, the influence of large and high speed vessel on the power prediction is relatively limited. For small and slow vessels, the impact of the F_D definition change on power prediction is considerable and the propulsion efficiency change (EtaD) is about 1~2%. For the revolution of propeller, the impact of the F_D definition change is very limited at around 0.2%.

As a general conclusion, the new F_D definition appears to make a very small difference to the powering prediction compared to the previous definition. Many towing tanks still use the old definition, but should be aware of what the effect of this is on their prediction.

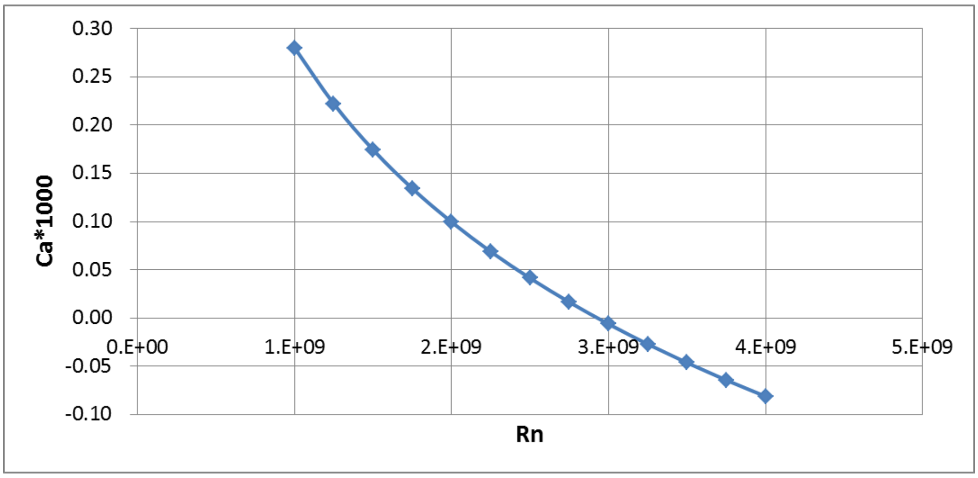

Figure 56: Dependency of Reynolds number on C_A

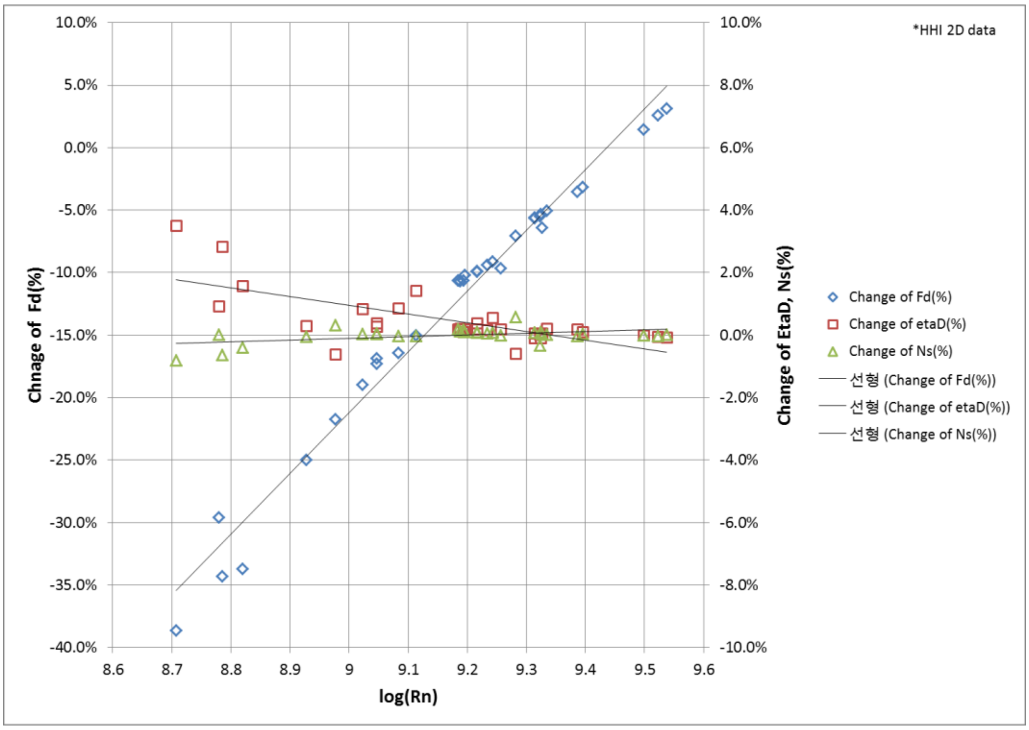

Figure 57: Overall trend of F_D definition change and the impact on the propulsion efficiency and revolution of propeller

13. REYNOLDS NUMBER EFFECTS ON PROPELLER TESTING

As described in the ITTC recommended procedures 7.5-02-03-01.4, “1978 ITTC Performance Prediction Method”, and 7.5-02-03-02.1, “Open Water Test”, the minimum Reynolds number, based on the representative chord length at r/R=0.75, must not be lower than 2×10^5. Some concerns about unstable open water test results and the applicability of corrections for low blade ratio propellers or other unconventional propulsors when the Re is below a critical value have been raised. The 28th ITTC Propulsion Committee suggested that it might be necessary to increase the minimum Reynolds number to at least 3×10^5 to have enough margin to obtain reliable data. An additional literature review for the minimum Re has been conducted during the 29th ITTC term.

From Kim et al. (1985), the variation in K_T and K_Q with Reynolds number is inconsistent at Re<5×10^5 for a propeller model KP088 (D=0.25m, P/D=1.635, Ae/A0=0.779) in the towing tank open water test. There is no difference in terms of the thrust and torque of the propeller due to three different wing section profiles (NACA 66, MAU and NSMB series). The measured values are stabilized when Re≥3×10^5.

Sheng et al (1979) investigated the scale effect by using five propeller models of the same MAU 4-60 profile (P/D=0.788) in towing tank open water tests at Reynolds numbers ranging from 1.2×10^5 to 8.1×10^5. The recommended critical Re was 3.0×10^5. If Re < 2.5×10^5, the scale effect was still evident after ITTC 1978 scale effect correction.

Hasuike et al (2017) presented extensive oil flow visualization and numerical calculations of the scale effect of a series of propellers (27 in total) for a chemical tanker. The blade profiles were parametrically changed. Oil flow visualization of the propeller open water test (POT) and self-propulsion test (SPT), showed flow patterns in SPT condition at Re=2.7×10^5 were similar (laminar and include laminar flow separation) to that in the POT condition at Re= 3×10^5 which was a typical Reynolds number in SPT condition, as shown in Figure 60.

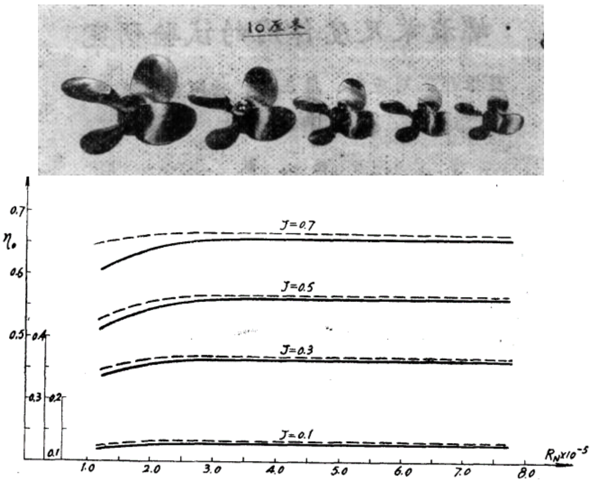

Figure 58: The open water efficiency variation against Re number from Sheng (1979). The dotted lines represented the efficiency after scale effects correction using ITTC1978 method and solid lines represented the model test results.

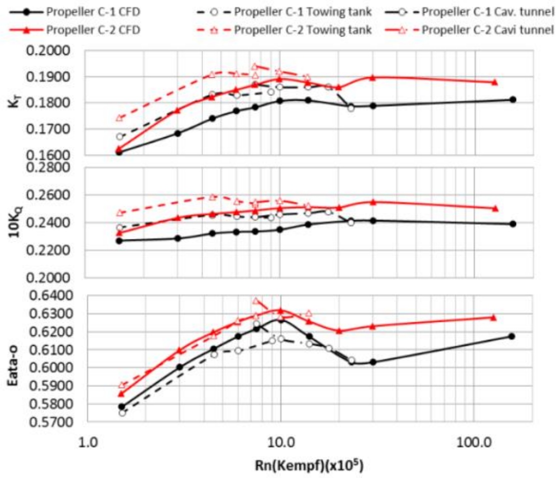

Figure 59: KT 10KQ and Eta0 Variation of Propeller C-1 (D=0.25m, Ae/A0=0.48) and Propeller C-2 (D=0.25m, Ae/A0=0.38) against Reynolds number from Hasuike et al (2017)

.

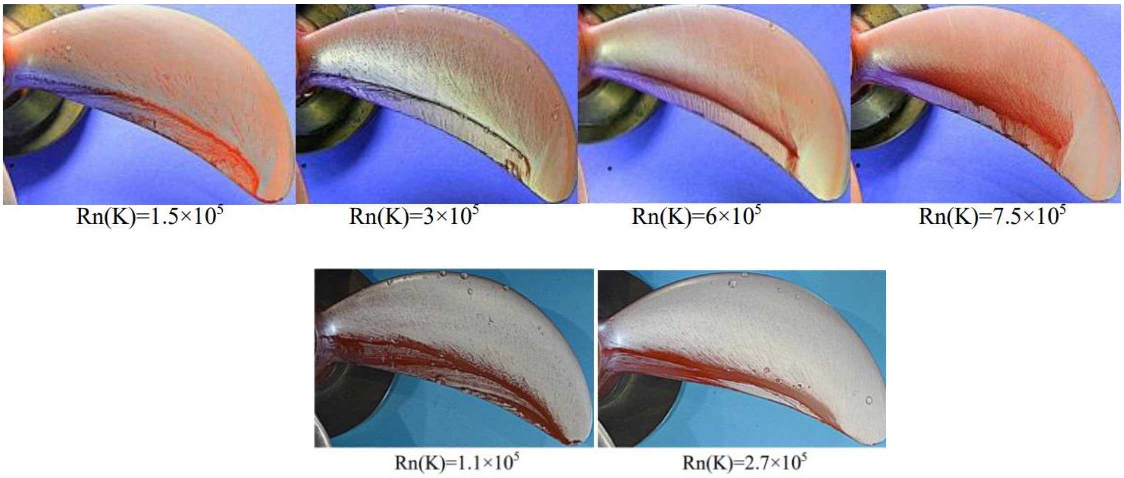

Figure 60: Oil flow visualization results for POT condition (above) and SPT condition (below) of Propeller C-2 (D=0.25m and Ae=0.38) from Hasuike et al (2017)

In the POT condition, K_T and K_Q increase in the range of Re=1.5×10^5 to 4.5×10^5 due to the flow separation extent decreasing gradually. K_T is almost flat and K_Q is decreasing in the range of Re=4.5×10^5 to 7.5×10^5. The range of laminar and turbulent flow is maintained and the thickness of the boundary layer was decreased. The flow characteristics of POT condition are thought to be mainly laminar in the range of Re=1.5×10^5 to 7.5×10^5.

The "2POT method" of ITTC recommended procedure 7.5-02-03-02.1, with the lower Reynolds number corresponding to propulsion factors evaluation and the higher Reynolds number as high as possible, was supported based on such investigation. However, similar laminar-turbulent transition flow, not the laminar flow for the propeller model surface flow at lower Reynolds number POT with corresponding SPT should be achieved by careful investigation. From Lücke et al (2017), the lower Reynolds number POT test should be 40% higher than during flow pattern for small blade area propeller.

Baltazar et al (2019) presented numerical predictions of an open water propeller (P0.7R /D=0.757 and Ae/A0=0.464) at different Reynolds numbers ranging from 10^4 to 10^7 using the RANS code, ReFRESCO V2.1, with two turbulence models, k-ω SST turbulence model and γ-(Re)˜θt transition model. These are shown in Figure 61 and can be compared to paint test results from Boorsma (2000) in Figure 62. The limiting streamlines at outer radii predicted using the k-ω SST turbulence model agreed well with the leading edge roughness (LER) propeller paint test. On the other hand the limiting streamlines predicted using the γ-(Re)˜θt transition model matched the smooth propeller paint test when inlet turbulence quantities were properly selected. From the numerical results at Re=1×10^5 and 5×10^5 and the K_T K_Q trend with Re between 10^4 to 10^7, it seems that 5×10^5 might be the minimum Re.

Yao (2019) presented the CFD investigation on the flow pattern of a PPTC propeller model (D=0.25m, P/D=1.635, Ae/A0=0.779) using commercial codes STAR-CCM+ with transition turbulent model, the Reynolds number ranged from 2.32×10^5 to 3.63×10^7. From Re 2.32×10^5 to 3.48×10^5, the flow pattern on the back side transited from laminar to turbulent in the outer radii closing to trailing edge, while the full scale flow pattern is fully turbulent both on back and face sides. The critical Re for such case is estimated to be around 3.48×10^5.

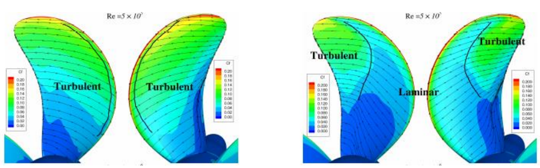

Figure 61: Flow pattern for POT at Re=5×105 using k-ω SST turbulence model (left) and γ-(Re)˜θt transition model (right) from Baltazar et al (2019).

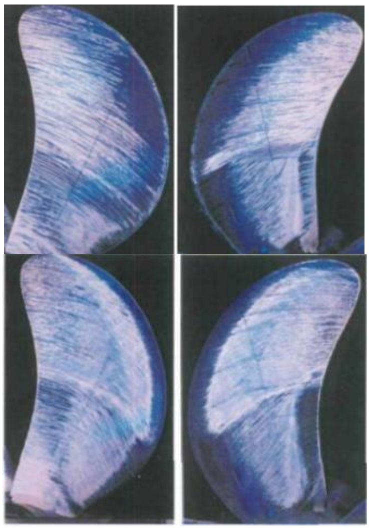

Figure 62: Propeller paint test for at Re=5×105 with (left) and without (right) leading edge roughness (LER) from Boorsma (2000)

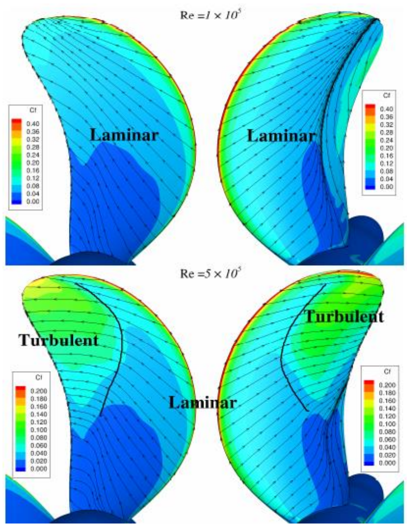

Figure 63: Flow pattern for POT at Re=1×105 (above) and Re=5×105 (below) using γ-(Re)˜θt transition model from Baltazar et al (2019).

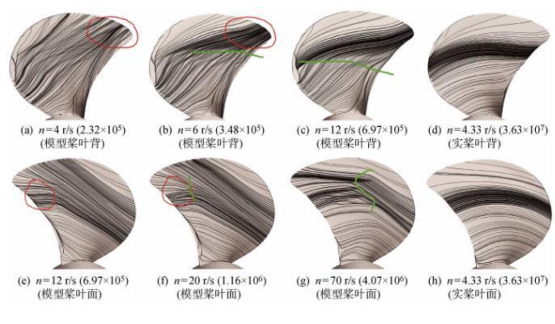

Figure 64: Different Re flow patterns on a PPTC propeller surface from Yao (2019)

Heinke et al (2019) investigated the Reynolds number influence on open water characteristics using four short chord length model propellers. For propeller A (D=0.239m, Ae/A0=0.418) and propeller B (D=0.239m, Ae/A0=0.444), the thrust coefficients are nearly constant, while the torque coefficient decreases linearly with rising Reynolds number if Re is above 5×10^5, as shown in Figure 65. The ITTC 1978 correction method is applicable for consistent full scale propeller open water characteristics when the Re is above 5×10^5.

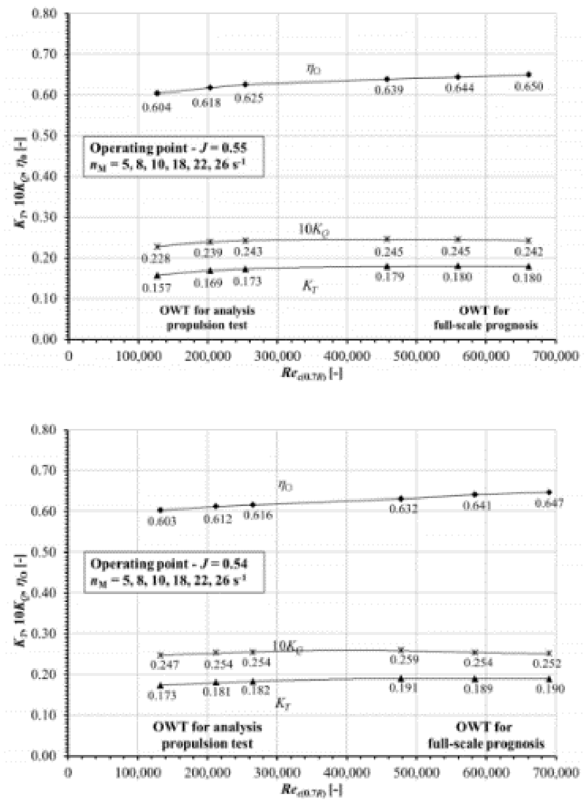

Figure 65: Variation of propeller coefficients of propeller A (left) and propeller B (right) with the Reynolds number from Heinke (2019)

From the above literature review, the minimum Reynolds number (2×10^5) in the present ITTC procedure is probably not sufficient for obtaining stable open water test data. This minimum Reynolds number generally ranges from 3×10^5 to 5×10^5 for different propeller types. This range might not be suitable for other propeller types, like CLT propellers or ducted propellers etc., which should be treated separately.

One specific minimum Reynolds number which is applicable for all propeller types may not be possible. Each model basin is recommended to analyse their specific propeller case and to choose the proper minimum Reynolds number, especially for propulsion factors evaluation purpose. Careful attention should be paid to propeller open water RPM selection to achieve the similar transition or turbulent flow, not fully laminar flow pattern on the propeller model surface, and also for the proper propeller dynamometer range to reach the sufficient measurement resolution. A series of Reynolds number variation open water tests or CFD simulations covering the self-propulsion Reynolds number range is recommended for investigating the Reynolds number dependency. The ITTC procedures 7.5-02-03-01.4, “1978 ITTC Performance Prediction Method”, and 7.5-02-03-02.1, “Open water test”, are recommended to be revised during the 30th ITTC term.

14. SCALING METHODS FOR PROPULSORS

Scaling of open water curves is an important topic since the effect will be directly visible in the speed and power curve.

Today, several empirical methods are used where the ITTC’78 (7.5-02-03-01.4) method is widely adopted by the ITTC members. This method is relatively simple and therefore easy to apply. Of other scaling methods the following can be mentioned: “Strip method”, Streckwall et al. (2013) and “Stone”, Helma (2015). Both are comprehensive to apply and would typically require a software solution. Additionally, for ITTC’78 scaling, only data for one representative chord will be needed where the “other” methods need data for several chords from the root to the tip.

In contrast to the empirical scaling methods, a future solution for scaling of open water curves could be simply to use CFD to predict open water curves at both model scale and full scale and to derive the scale effects from these. The 28th ITTC Propulsion committee presented a CFD open water benchmark study. There 13-14 ITTC members presented CFD open water curves of an unconventional 4-bladed FP propeller and a conventional 5-bladed CP propeller. The results showed some scatter in the curves, especially at the higher J-values corresponding to the operating point in a self-propulsion condition. This could lead to the question of whether CFD is mature enough for detecting open water scale effects.

14.1 Case study

In the below, scale effects (ITTC'78, Strip method and CFD scaled) are investigated for six different propellers designed for the same medium size container vessel. There is an as-built propeller designed for full speed and five retrofit alternatives designed for slow steaming. Additionally, the five new propellers represent 15-years of development in propeller design. The as-built propeller must be designed pre-RANS CFD and the new ones with RANS CFD available.

Figure 66: Original (dark) and the five new (shiny) model propellers

The propellers have the following characteristics / features:

1) Original / lower middle. Six bladed with high area ratio. Typical design for a container vessel delivered before slow steaming.

2) Retrofit / lower right. Four bladed with special tip feature. Slightly larger in diameter relative to original.

3) Retrofit / upper left. Four bladed with special profile feature. Larger in diameter relative to original.

4) Retrofit / upper middle. Six bladed with slender blades and untraditional rake slope. Identical diameter to original.

5) Retrofit / lower left. Four bladed with some tip loading. Larger in diameter than original.

6) Retrofit / upper right. Four bladed with special tip feature. Larger in diameter relative to original.

The scale effect is investigated for the full open water curve. However, in the following only results for J=0.8 are presented. This is around the operating point in a self-propulsion condition.

Figure 67, Figure 68 and Figure 69 show the percentage change from model scale to full scale, for the three scaling methods.

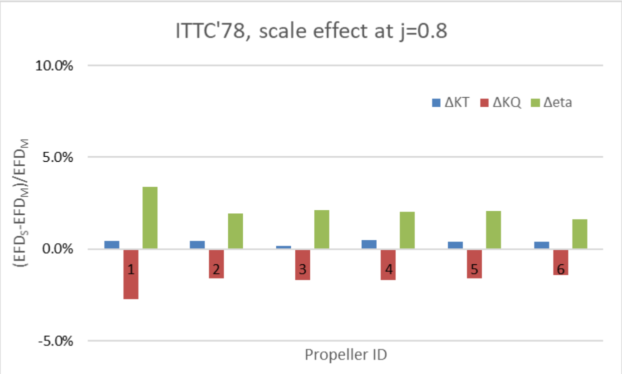

Figure 67: ITTC'78 scaling

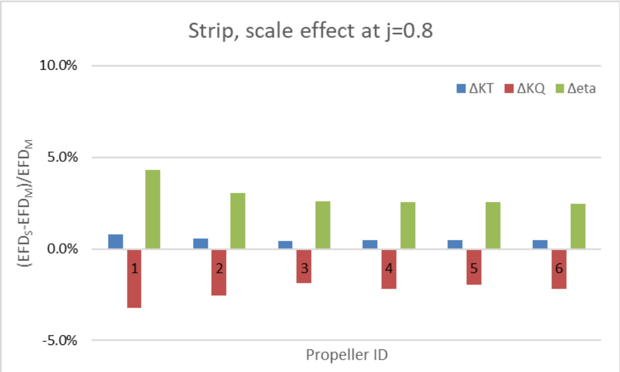

Figure 68: Strip method scaling

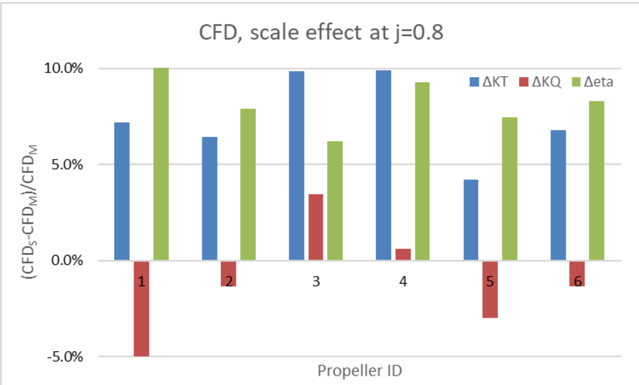

Figure 69: CFD scaling

From the figures it is clearly visible that the result of ITTC'78 and Strip method are in line. That said, the Strip method prescribes slightly larger scale effects for all six propellers. On average (of the six propellers) the scale effect is 0.1% larger for KT and 0.6% for KQ. This might not seem much, but it results in 0.7% (again in average of the six) more efficient propellers at this advance ratio (J=0.8).

The scale effects from CFD scaling is somewhat off in this example compared to the two empirical methods and without doubt it is the CFD scaling that is way too optimistic in this specific example. However, with some progress in CFD open water calculations the method should in theory work, and this could replace any empirical method. CFD open water will require a 3D CAD file of the actual propeller and this is not always available for commercial projects. Additionally, the workload with CFD open water compared to a well-known empirical method is somewhat larger.

15. PROPULSOR PERFORMANCE IN WAVES

15.1 Introduction

A literature study was undertaken to investigate and identify the influences of operating propellers in waves. The influences on the propeller inflow are broken down into two categories; wave dynamics, and induced flows from ship motions in waves.

Wave dynamics refers to a propeller operating in waves, without the influence of a ship, which causes non-uniformity in the propeller inflow as a function of the orbital wave velocities, assuming trochoidal wave theory. Induced flows from ship motions refer to the influences from a hull that is surging, pitching and heaving in waves.

Influences were identified as added resistance, temporal and spatial variations of inflow wakes, ventilation, and shaft speed variation affecting thrust, torque, efficiency, cavitation, and pressure pulses.

15.2 Wave dynamics

McCarthy (1961), illustrated that, for deeply-submerged propellers, fluctuations in the open water thrust and torque in waves is in good agreement with the calm-water uniform-flow performance curves for the propeller, when the mean orbital velocities of the waves are considered in the advance coefficient (Figure 70 and Figure 71).

For the low frequencies of encounter of a propeller in waves, unsteady effects may be neglected in calculating the instantaneous thrust and torque of a propeller in a wave crest or trough.

The results shown indicate that the percentage changes in the propeller's thrust and torque increase with:

1. Increasing average speed coefficient (J_m)
2. Increasing wave height-propeller diameter ratio (a/D)
3. Decreasing propeller speed-wave celerity ratio (V/V_w)
4. Increasing wave height-wave length ratio (a/λ)

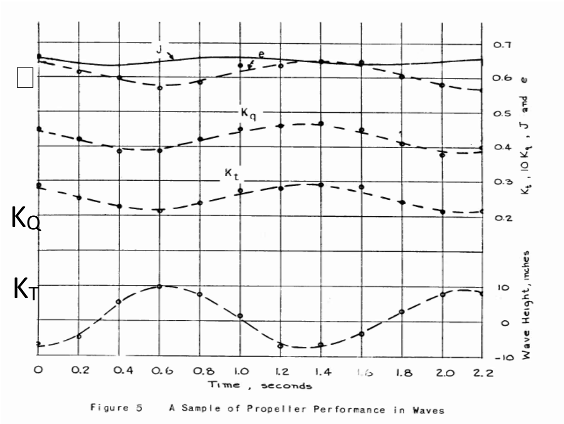

Figure 70: Propeller performance as a function of wave oscillation from McCarthy et al (1961)

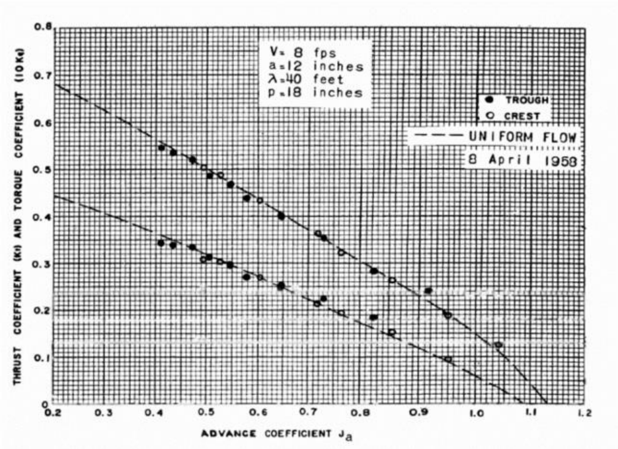

Figure 71: Calm water and wave agreement considering propeller inflow speed from McCarthy et al (1961)

Taskar et al (2016) showed that when K_T, K_Q and efficiency in the presence of waves is plotted against the corresponding advance coefficients, the data points follow the propeller open water curves. From this, we can conclude that the efficiency is primarily affected by the average change in wake fraction and not much by wake distribution (Figure 72).

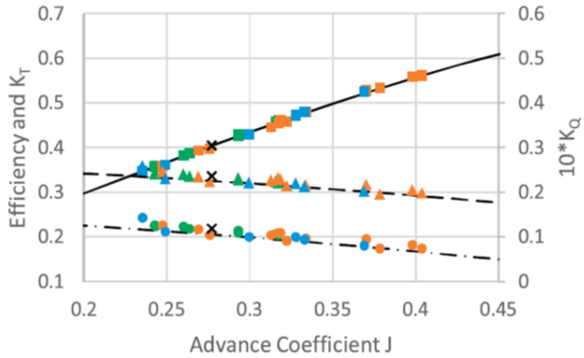

Figure 72: Calm water and wave agreement considering propeller inflow speed from Taskar et al (2016)

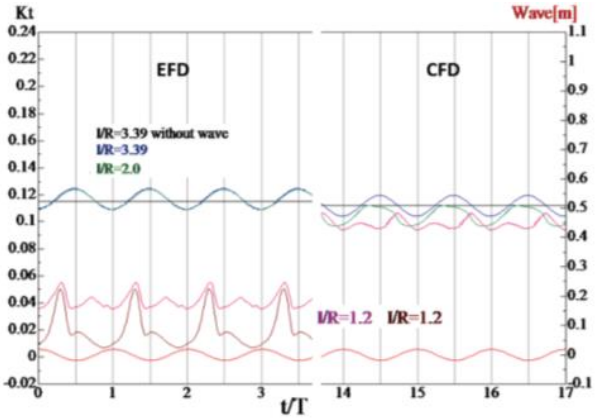

Figure 73: Correlation of K_T from waves and calm water and influence of ventilation for KVLCC2 propeller at J=0.5 from Tokgoz et al (2017)

Tokgoz et al (2017) investigated the depth of propeller immersion in waves and corroborated the results of McCarthy and Taskar for deeply submerged propellers. Due to wave orbital velocities, the minimum thrust is achieved when the wave crest is at the propeller plane. Ventilation was shown to significantly affect the trend of thrust fluctuations where the maximum value of thrust occurs in the wave crest while the minimum values of thrust occur in the wave trough when ventilation occurs. This effect is stronger and more prevalent with the reduced expanded area ratio propeller since the suction pressures are greater at the blades. The influence of ventilation is strongly related to the depth of immersion.

Tokgoz et al (2017) illustrate by computations of KVLCC2 in waves without including the surge motion of the vessel that when surge is essentially zero (region B), the mean values of the EFD and CFD results are comparable. In region A where the ship surges forward the thrust is not comparable. Although the mean levels are different, the characteristics of ventilation on thrust is apparent in both regions (Figure 74 and Figure 75).

Taskar et al (2017) show that the mean wake fluctuations due to the wave orbital velocities are relatively constant and greater than that due to surge regardless of the wavelengths (Figure 76). The mean change in wake is more significant at low ship speeds. The propeller efficiency is dependent on the average wake changes rather than the changes in the wake distribution and is effected the most when the wavelength is close to the ship length.

Hsin, Ching-Yeh et al (2016) concluded that the unsteady flow effects due to the ship wake is more important than that due to the ship motions.

15.3 Ship motions

Taskar et al (2016) showed that cavitation and pressure pulses are directly related to wake distribution, and they depend less on average wake fluctuations. The relative stern motion was only shown to affect the range of Cp_{min} and not the angle of attack; since it only affects the cavitation number, while the wake change can affect both the variables. It was observed that wake change, due to wave orbital velocities and hull interactions, does not significantly affect the amount of cavitation hence cavitation margin should be considered only to handle increased load and relative stern motions.

Taskar et al (2016) additionally revealed that the blade root circulation in short waves was always greater than calm water and generally higher for all other wave conditions. The change in tip circulation, at top dead centre, when operating in waves was equal to or shown to be substantially lower than in calm water.

Taskar et al (2017) found that contrary to the expectation of less hull wake influence for a twin-screw ship, both the cavitation and pressure pulses increased remarkably due to the effect of waves, as did the cavitation volumes.

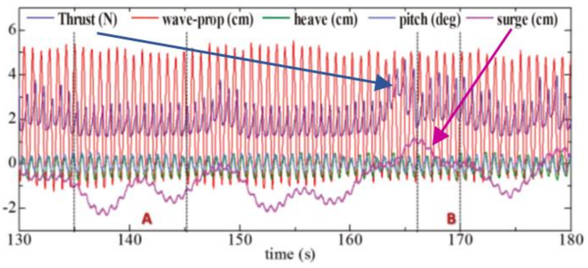

Figure 74: EFD time series of KVLCC2 in λ/L=0.6 illustrating wave height, thrust, and ship motions from Tokgoz (2017):

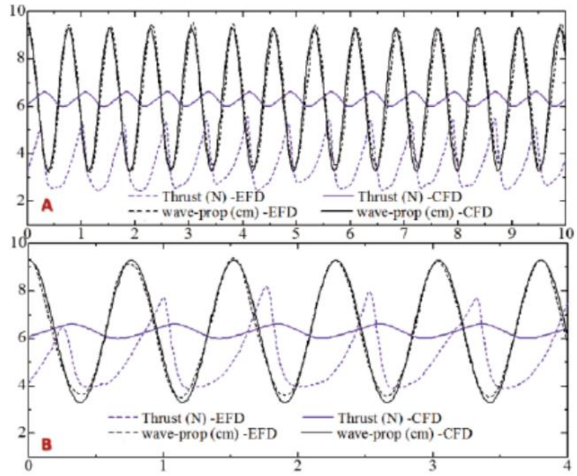

Figure 75: Surging influence on thrust in waves from Tokgoz (2017)

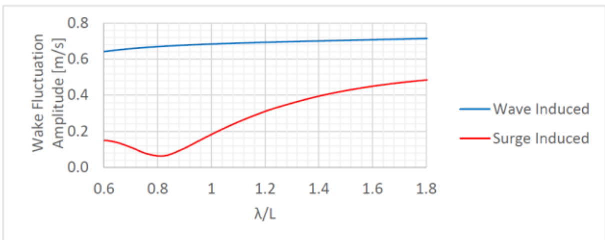

Figure 76: Comparison of the contribution of wave induced and surge induced fluctuation in the wake fluctuation

15.4 Conclusions

Propeller thrust, torque and efficiency are primarily affected by the average change in wake fraction. Propeller cavitation and pressure pulses are primarily affected by variation in the distribution of the wake.

Mean wake fluctuations due to the wave orbital velocities are relatively constant and greater than that due to surge regardless of the wavelengths.

If ventilation is present, the trend of thrust fluctuations significantly alter from deeply submerged conditions and there can be severe reductions in thrust followed by higher harmonics before recovering.

Hub vortex cavitation was found to be more likely to occur while operating in waves than tip vortex cavitation. The hull interaction with the wake changes due to waves resulted in lower levels of cavitation for a single screw in comparison to a twin screw.

It is recommended to perform scaling studies to decipher the level of model hull wake interactions with the wave field when conducting model scale measurements of propellers in waves.

The influence of ventilation on propeller performance is recommended for further evaluation during 30th ITTC term.

16. CONCLUSIONS AND RECOMMENDATIONS

16.1 Task 2

Adopt the updated procedures:

7.5-02-02-01

7.5-02-02-02

7.5-02-02-02.1

7.5-02-02-02.2

7.5-02-03-01.1

7.5-02-03-01.3

7.5-02-03-01.4

7.5-02-03-01.7

7.5-02-03-02.1

7.5-03-01-01

7.5-03-01-02

7.5-03-02-02

7.5-03-02-04

16.2 Task 3

A new procedure has been written on measurement of wave profiles and the calculation of resistance from the wave profile data.

It is recommended that the conference adopt this new procedure. It is also recommended that the next committee should conduct some validation of this new procedure.

16.3 Task 4

A review of the literature on verification and validation of flow field data has been undertaken. However, while verification and validation, including uncertainty analysis, of CFD predictions are commonly performed for integral values such as resistance, it is much less common to find uncertainty studies on flow field quantities.

There are existing procedures on CFD V&V, which includes some description of uncertainty assessment for point data in the flow field. There are also procedures related to the uncertainty of flow measurement e.g. 7.5-01-03-*.

16.4 Task 5

Following interaction with the Specialist Committee on Energy Saving Methods, there is increasing interest in low friction coatings. It is recommended that characterisation of low friction coatings to be treated in a manner consistent with that of roughness effects. Guidelines for model tests of air lubrication, low friction coatings, wind assisted vessels may need to be developed as these technologies evolve.

16.5 Task 6

In collaboration with the Specialist Committee on Ships in Operation at Sea, an inconsistency in the load variation test procedure was identified and resolved.

16.6 Task 7

The ship hull or propeller surface roughness due to coatings or biofouling have a significant influence on the ship performance. The effects of hull surface roughness due to the coatings are often taken into account in the total resistance prediction as the roughness allowance ΔC_F which is defined by the Townsin formula. In this formulation, the standard value of hull surface roughness k_S is defined to be 150 μm in the case that no measured data is available. This roughness height may not be a correct representation for modern hull coatings and recent research pointed out that the effective roughness of the coated hull surfaces in real life is much lower than this. Each type of coating may follow a different roughness function model, which makes the use of a single roughness height parameter difficult.

There is a need to adopt or develop new methods to predict the roughness effect of modern fouling-control coatings and marine biofouling on ship hydrodynamic performance. Similarity law scaling and CFD can be regarded as the most promising potential methods to predict such effects. Both methods require the use of roughness functions of the surfaces in question. Similarity law scaling can be used to predict the effect of roughness on the frictional resistance of flat plates of ship lengths effectively, with less computational cost, whereas CFD methods can be adopted for accurate prediction of roughness effects on the resistance components, propeller performance characteristics, and hydrodynamics of full-scale 3D ships. While these prediction methods require the roughness functions, there exists no universal roughness function model and no single roughness length scale for all types of marine coatings and biofouling surfaces. Therefore, there is a need to generate a database of roughness functions of modern fouling-control coatings and surfaces representing heterogenous biofouling accumulated on ship hulls and propellers. For this reason, it is recommended that standardised methods for roughness function determination should be adopted by researchers. It would, therefore, be useful to investigate the need for a guideline or procedure for the measurement of roughness functions for different surface finishes or conditions so that this information can be used for predicting the roughness corrections for both hull and propeller.

16.7 Task 8

The procedure 7.5-02-03-01.7, 1978 ITTC Performance Prediction Method for Unequally Loaded, Multiple Propeller Vessels, has been revised to make it more comprehensive by adding more explanations and graphs of model test data of a triple shaft vessel. The procedure is not limited to just triple shaft vessels but has been extended to multiple shaft propulsion ship with more general description. One aspect of the task was to validate the procedure using full-scale data, however, despite requests to operators, it was not possible to obtain any suitable data. It is recommended that the next committee should continue trying to obtain this data in order to validate the procedure.

16.8 Task 9

No full-scale data on podded propulsors was available to support this task. It is recommended that a future committee should continue to seek data to be used in the development of the procedures. The majority of podded propulsors are fitted to commercial vessels, which have proved difficult to obtain information from. An alternative approach might be to seek data from government (non-military) owned vessels such as icebreakers.

16.9 Task 10

The results of the benchmark study carried out by the previous committee were considered to be complete, and it was not felt to be worthwhile adding more data to the benchmark dataset. It would be more beneficial in future to perform a benchmark of the full scale and model scale predictions in order to support scaling using CFD.

16.10 Task 11

The reliability of quasi-steady propulsion testing has been confirmed by a limited number of organisations. While a guideline or procedure would clearly be useful, there remain some unknowns, which would need to be clarified before a guideline or procedure could be developed, such as the limitations of applicability of the method. More testing is required to understand these limits. It would therefore be useful for benchmark tests to be carried out to validate the method in more model basins.

16.11 Task 12

The topic of cavitation erosion is one which is receiving much attention, and modelling techniques are developing rapidly. Much of the work has been focussed on the development of cavitation erosion risk indicators based on CFD solutions, which can be used by propeller designers to predict potential erosion areas and locations. However, research is still needed to determine thresholds for these indicators that predict when erosion will occur. A combination of CFD and EFD will be needed to further understand the physical mechanisms and quantities that drive the erosion behaviour.

The ITTC should continue to monitor the progress in this field, and updates to procedures could be considered in future.

16.12 Task 13

A survey has been carried out to determine the level of activity on rim driven thrusters within the ITTC membership. At least six members are actively working with rim driven thrusters, and there is a consensus that a dedicated procedure should be developed for testing them. Specific issues relate to the measurement arrangements for thrust and torque, given the absence of a shaft, and to the scaling from model scale to full scale. This is often done using CFD. It is recommended that the next committee should continue working to develop a procedure, but it is clear that only a few institutions have experience of such testing.

16.13 Task 14

The new F_D definition appears to make a very small difference to the powering prediction compared to previous definitions. Some institutions still use alternative definitions, and should be aware of what the effect of this is on the predictions. Each institution should check their own method against the 28th ITTC definition to understand the impact.

16.14 Task 15

The minimum Reynolds number (2×10^5) in the present ITTC procedure is probably not sufficient for obtaining stable open water test data. This minimum Reynolds number generally ranges from 3×10^5 to 5×10^5 for different propeller types. This range might not be suitable for other propeller types, such as CLT propellers and ducted propellers, which should be treated separately, and it may not be possible to provide a single value that is universally applicable.

A series of Reynolds number variation open water tests or CFD simulations covering the self-propulsion Reynolds number range is recommended for investigating the Reynolds number dependency. The ITTC procedures 7.5-02-03-01.4 1978 ITTC Performance Prediction Method and 7.5-02-03-02.1 Open water test procedures are recommended to be revised during 30th ITTC term.

A benchmark study looking at the effects of Reynolds number on propeller performance measurements could be useful for a future committee to make a more informed assessment, and to propose changes to the procedures.

16.15 Task 16

Alternative methods of propeller scaling tend to be proprietary and not universally applicable, being extremely complicated to implement, so are unlikely to be a viable alternative to the current ITTC procedure. In the long-term CFD is likely to provide an alternative method of scaling unconventional propeller performance, however a limited case study has shown that CFD can over-predict the scale effects compared to other methods. A benchmark study on CFD open-water scaling could therefore be useful.

16.16 Task 17

It is recommended to perform scaling studies to decipher the level of model hull wake interactions with the wave field when conducting model scale measurements of propellers in waves. The influence of ventilation on propeller performance is recommended for further evaluation during 30th ITTC term.

16.17 Proposals for future tasks

1. A benchmark study looking at the effect of Re at model scale, and scaling methods for full scale prediction could be carried out. This could use the two propellers that were provided for the previous benchmark study run by the 28th ITTC. CFD calculations would be run at a range of Re at model scale and full scale, along with open-water model tests at a range of Re.
    - Modern propeller designs with low blade area may suffer from laminar effects in self-propulsion test. A procedure to carry out two open water tests at different Reynolds number has been suggested.
    - Survey how ITTC members tackle this issue, and which scaling method they use for low blade area propellers.
    - Review literature on the subject
    - Suggest modification to recommended procedures.

2. The procedures on CFD verification and validation should be reviewed and updated to ensure that they represent best practise for the types of calculations being required by other ITTC procedures.

3. The requirements for testing and numerical evaluation of high-speed marine vessels should be investigated and the need for updated procedures assessed.

4. The use of CFD to predict full-scale ship performance and the need for validation at full-scale should be investigated.

5. The measurement and prediction of breaking waves should be further investigated.

6. Developments in hull and propeller model manufacturing should continue to be monitored. These would include advances in additive manufacturing techniques and novel materials. The use of 3D scanning techniques to validate the model geometry should also be investigated with a view to updating the procedures.

7. Guidelines should be developed for model testing of low skin friction coatings and air lubrication systems, including scaling laws.

17. REFERENCES

Abbas, N., Kornev, N., 2015, "Computations of the Japan Bulk Carrier Using URANS and URANS/LES Methods Implemented into OpenFOAM Toolkit", Tokyo 2015 CFD Workshop.

Aktas, B., Yilmaz, N., Atlar, M., Sasaki, N. Fitzsimmons, P., Taylor, D., 2019, "Suppression of Tip Vortex Cavitation noise using PressurePoresTM technology: A numerical and experimental investigation", Paper presented at the Sixth International Symposium on Marine Propulsors, smp'19, Rome, Italy, May 2019.

Andrewartha, J., Perkins, K., Sargison, J., Osborn, J., Walker, G., Henderson, A., Hallegraeff, G., 2010, "Drag force and surface roughness measurements on freshwater biofouled surfaces", Biofouling, Vol. 26, pp 487-496.

Bakica, A., Gatin, I., Vukčević, V., Jasak, H., Vladimir, N., 2019, "Accurate assessment of ship-propulsion characteristics using CFD", Ocean Engineering, Vol. 175, pp 149-162, February 2019.

Baltazar J., Rijpkema D., Campos J., 2019, "Prediction of the Propeller Performance at Different Reynolds Number Regimes with RANS", Sixth International Symposium on Marine Propulsors, smp'19, Rome, Italy, May 2019.

Bengough, G.D., Shepheard, V.G., 1943, "The corrosion and fouling of ships", Paper presented at the Marine Corrosion Sub-committee of the Iron and Steel Institute and the British Iron and Steel Federation.

Bhatt, M., Mahesh, K., 2019, "Investigation of propeller cavitation using compressible large eddy simulations", 6th International Symposium on Marine Propulsors smp'19, Rome, Italy, May 2019.

Bhushan, S., Yoon, H., Stern, F., Guilmineau, E., Visonneau, M., Toxopeus, S., Simonsen, C., Aram, S., Kim, S.E., Grigoropoulos, G., 2019, "Assessment of CFD for Surface Combatant 5415 at Straight Ahead and Static Drift β=20°", Journal of Fluids Engineering, Vol. 141, May 2019.

Boorsma, A., 2000, "Improving Full Scale Ship Powering Performance Predictions by Application of Propeller Leading Edge Roughness, Part 1: Effect of Leading Edge Roughness on Propeller Performance". Master's thesis, University of Technology Delft.

Bottiglieri, M.J., 2016, "Uncertainty assessment for free-running model cases at the IIHR wave basin", MSc thesis, University of Iowa.

Broglia, R., Zaghi, S., Campana, E.F., Dogan, T., Sadat-Hosseini, H., Stern, F., Queutey, P., Visonneau, M., Milanov, E., 2019, "Assessment of Computational Fluid Dynamics Capabilities for the Prediction of Three-Dimensional Separated Flows: The DELFT 372 Catamaran in Static Drift Conditions", Journal of Fluid Engineering, Vol. 141, Sept. 2019.

Carrica, P.M., Mofidi, A., 2014, "Simulations of zigzag maneuvers for a container ship with direct moving rudder and propeller", Computers and Fluids, Vol. 96, pp 191–203.

Carrica, P.M., Mofidi, A., Eloot, K., Delefortrie, G., 2016, "Direct simulation and experimental study of zigzag maneuver of KCS in shallow water", Ocean Engineering, Vol. 112, pp 117–133.

Celik, I.B., Ghia, U., Roache, P.J., Freitas, C.J., Coleman, H., Raad, P.E., 2008, "Procedure for Estimation and Reporting of Uncertainty Due to Discretization in CFD Applications", Journal of Fluid Engineering, Vol. 130, July 2008.

Charruault, F., Westerweel, J., Terwisga, T.v., Breugem, W.-P., 2017, "On the drag reduction induced by an air cavity and characterisation of its free surface", Paper presented at the 5th International Conference on Advanced Model Measurement Technology for the Maritime Industry (AMT'17), Glasgow, UK.

Dang, J., Ligtelijn, Th., 2019, "Development of Tunnel Thruster Series Propellers for Low Noise and Vibration", 6th International Symposium on Marine Propulsors smp'19.

Delfos, R., Greidanus, A., Charruault, F., & Westerweel, J., 2017, "Wave characteristics of a compliant coating under a turbulent flow", Paper presented at the 5th International Conference on Advanced Model Measurement Technology for the Maritime Industry (AMT'17), Glasgow, UK.

Demirel, Y.K., Song, S.S., Turan, O., Incecik, A., 2019, "Practical Added Resistance Diagrams to Predict Fouling Impact on Ship Resistance", Ocean Engineering, Vol. 186, 106112, 2019.

Demirel, Y.K., Turan, O. and Incecik, A., 2017, "Predicting the Effect of Biofouling on Ship Resistance Using CFD", Applied Ocean Research, Vol. 62, pp. 100-118.

Demirel, Y.K., Uzun, D., Zhang, Y., Fang, H.C., Day, A.H., Turan, O., 2017, "Effect of Barnacle Fouling on Ship Resistance and Powering", Biofouling, Vol. 33, No. 10, pp. 819-834.

Dogrul, A., Song, S., Demirel, Y.K., 2020, "Scale effect on ship resistance components and form factor". Ocean Engineering, Vol. 209, 107428.

Dular M., Stoffel B., Sirok B., 2006, "Development of a cavitation erosion model", WEAR, Vol. 261, pp 642-655.

Dular M., Pirc Z., Pozar T., Petkovsek R., 2019, "High speed observation of damage created by a collapse of a single cavitation bubble: Development of a cavitation erosion model", WEAR, Vol. 418-419, pp 13-26.

Eça, L., Vaz, G., Toxopeus, S.L., Hoekstra, M., 2019, "Numerical Errors in Unsteady Flow Simulations", Journal of Verification, Validation and Uncertainty Quantification, Vol. 4.

Eskilsson, C., Bensow, R., 2015, "Estimation of Cavitation Erosion Intensity Using CFD: Numerical Comparison of Three Different Methods", Fourth International Symposium on Marine Propulsors SMP'15, Austin, USA.

Fabbri, S., Dennington, S., Stoodley, P., Longyear, J., 2017, "A marine biofilm flow cell for in situ determination of drag, structure and viscoelastic properties". Paper presented at the 5th International Conference on Advanced Model Measurement Technology for the Maritime Industry (AMT'17), Glasgow, UK.

Fabio, D.N., Francisco, A.P., Giovanni, d.M., Fabio, D.F., Rudy, G., Francesco, G., Massimo, M., 2017, "Bubble size and velocity measurements in high void fraction bubbly flows using PIV-LIF technique". Paper presented at the 5th International Conference on Advanced Model Measurement Technology for the Maritime Industry (AMT'17), Glasgow, UK.

Falchi, M., Felli, M., Grizzi, S., Aloisio, G., Broglia, R., Stern, S., 2014, "SPIV measurements around the DELFT 372 catamaran in steady drift", Exp. Fluids, Vol. 55, No. 1844.

Farkas, A., Degiuli, N., Martić, I., 2018, "Towards the prediction of the effect of biofilm on the ship resistance using CFD", Ocean Engineering, Vol. 167, pp 169-186.

Farkas, A., Degiuli, N., Martić, I., 2019, "Impact of biofilm on the resistance characteristics and nominal wake", Proceedings of the Institution of Mechanical Engineers, Part M: Journal of Engineering for the Maritime Environment.

Fortes-Patella, R., Reboud, J.L. and Briancon-Marjollet, L., 2004, "A Phenomenological and Numerical Model for Scaling the Flow Aggressiveness in Cavitation Erosion", EROCAV Workshop, Val de Reuil, France.

Froude, W., 1872, "Experiments on the surface-friction experienced by a plane moving through water". In The collected papers of William Froude. British Association for the Advancement of Science: Institution of Naval Architects, 1955.

Froude, W., 1874, "Report to the Lords Commissioners of the Admiralty on Experiments for the Determination of the Frictional Resistance of Water on a Surface, Under Various Conditions".

Granville, P.S., 1958, "The frictional resistance and turbulent boundary layer of rough surfaces". Journal of Ship Research, Vol. 2, No. 3, pp 52-74.

Granville, P.S., 1987, "Three Indirect Methods for the Drag Characterization of Arbitrarily Rough Surfaces Flat Plate", Journal of Ship Research, Vol. 31, No. 1, pp 70-77.

Grasso, N., Hallmann, R., Schlocz, T., Zondervan, G., Maljaars, P., Schouten, R., 2019, "Measurements of the hydro-elastic behaviour of flexible composite propellers in non-uniform flow at model and full scale", 6th International Symposium on Marine Propulsors smp'19.

Greidanus, A., Delfos, R., Westerweel, J., 2017, "Fluid-structure interaction of compliant coatings under turbulent flow conditions: force and PIV analysis". Paper presented at the 5th International Conference on Advanced Model Measurement Technology for the Maritime Industry (AMT'17), Glasgow, UK.

Grigson, C.W.B., 1992, "Drag Losses of New Ships Caused by Hull Finish", Journal of Ship Research, Vol. 36, pp 182–196.

Guo, C.-Y., Wu, T.-C., Luo, W.-Z., Chang, X., Gong, J., She, W.-X., 2018, "Experimental study on the wake fields of a Panamax Bulker based on stereo particle image velocimetry", Ocean Engineering, Vol. 165, pp 91-106.

Güzel, B., 2017, "Experimental investigation of hydrophobic effects on drag reduction". Paper presented at the 5th International Conference on Advanced Model Measurement Technology for the Maritime Industry (AMT'17), Glasgow, UK.

Hashimoto, H., Yoneda, S., Omura, T., Umeda, N., Matsuda, A., Stern, F. and Tahara, Y., 2019, "CFD prediction of wave-induced forces on ships running in irregular stern quartering seas", Ocean Engineering, Vol. 188, 2019.

Haslbeck, E.G.B., 1992, "Microbial biofilm effects on drag-lab and field". Proceedings of the Ship Production Symposium.

Hasuike, N., Okazaki, M., Okazaki, A., Fujiyama, K., 2017, "Scale effects of marine propellers in POT and self-propulsion test conditions", Fifth International Symposium on Marine Propulsors smp'17, Espoo, Finland, June 2017.

Hasuike, N., Yamasaki, S., Ando, J., 2009, "Numerical Study on Cavitation Erosion Risk of Marine Propellers Operating in Wake Flow", Proceedings of the 7th International Symposium on Cavitation CAV2009, Michigan, USA.

Heinke, H., Hellwig-Rieck, K., Lübke, L., 2019, "Influence of the Reynolds Number on the Open Water Characteristics of Propellers with Short Chord Lengths", Sixth

International Symposium on Marine Propulsors smp'19, Rome, Italy, May 2019.

Helma, S., 2015, "An Extrapolation Method Suitable for Scaling of Propellers of any Design", Fourth International Symposium on Marine Propulsors smp'15, Austin, Texas, USA.

Hino, T., Stern, F., Larsson, L., Visonneau, M., Hirata, N., Kim, J., 2021, "Numerical Ship Hydrodynamics: An assessment of the Tokyo 2015 Workshop", Springer.

Hiraga, Y., 1934, "Experimental investigations on the resistance of long planks and ships", Zosen Kiokai, Vol. 55, pp 159-199.

Hirata, N., 2015, "JBC test data in NMRI", Tokyo 2015 CFD Workshop.

Hiroi, T., Kawashima, H., Sawada, Y., Fujisawa, J., Mieno, H., 2017, "Experimental investigation of the effect of geometric roughness parameters on turbulent boundary layer by LDV measurements". Paper presented at the 5th International Conference on Advanced Model Measurement Technology for the Maritime Industry (AMT'17), Glasgow, UK.

Hiroi, T., Winden, B., Kleinwachter, A., Ebert, E., Fujisawa, J., Kamiirisa, H., Damaschke, N., Kawakita, C., 2019, "Full-Scale On-board Measurements of Wake Velocity Profiles, Underwater Noise and Propeller Induced Pressure Fluctuations", The Japan Society of Naval Architecture and Ocean Engineers, Vol. 29, pp 193-198.

Inukai, Y., 2019, "Full Scale Measurement of The Flow Field at The Stern by Using Multi-Layered Doppler Sonar (MLDS)", 6th International Symposium on Marine Propulsors smp'19, Rome, Italy.

ISO, 2015, "Ships and marine technology – guidelines for the assessment of speed and power performance by analysis of speed trial data", ISO15016 second edition.

ITTC, 2017, "Propulsion Committee Final Report", 28th ITTC Full Conference Proceedings, Vol. 1, Wuxi, China.

Katsui, T., Tanaka, H., 2018, "The Evaluation Method of the Hydrodynamic Frictional Resistance for the Painted Rough Surface", Proceedings of the ASME 2018 37th International Conference on Ocean, Offshore and Arctic Engineering, OMAE2018-77693.

Kim, K., Lee, C., 1985, "Influence of Reynolds Number on Propeller Open Water Characteristics", Korea Institute of Machinery & Materials Report.

Klinkenberg, Y., Bosman, R., Dang, J., Ligtelijn, D., 2017, "Advanced measurements of rim-driven tunnel thrusters". Paper presented at the 5th International Conference on Advanced Model Measurement Technology for the Maritime Industry (AMT'17), Glasgow, UK.

Korkut, E., Atlar, M., 2012, "An experimental investigation of the effect of foul release coating application on performance, noise and cavitation characteristics of marine propellers". Ocean Engineering, Vol. 41, pp 1-12.

Kornev, N., Taranov, A., Shchukin, E. and Klein-sorge, L., 2011, "Development of hybrid URANS-LES methods for flow simulations in the ship stern area", Ocean Engineering, Vol. 38, Issue 16, pp. 1831–1838.

Kumar, P., Mahesh, K., 2019, "Large Eddy Simulation of flow over a confined elliptic hydrofoil", 6th International Symposium on Marine Propulsors smp'19.

Larssen J., Kluwe, F., 2018, "Seven in One Sweep – Constantly Accelerated Resistance

Test (CART)", HSVA Newswave 2018, Issue 1.

Leclercq, C., Archer, A., Fortes-Patella, R., Cerru, F., 2017, "Numerical Cavitation Intensity on a Hydrofoil for 3D Homogeneous Unsteady Viscous Flows", Journal of Fluid Machinery and Systems, Vol. 10, No. 3, pp 254-263.

Lee, I.W., Park, H., Chun, H.H., 2015, "Drag Reduction Performance of FDR-SPC (Frictional Drag Reduction Self-Polishing Copolymer)", Proc. of International Symposium on Turbulence and Shear Flow Phenomena (TSFP-9), Vol. 5A-1.

Lewthwaite, J., Molland, A., Thomas, K., 1985, "An investigation into the variation of ship skin frictional resistance with fouling", Transactions of Royal Institution of Naval Architects, Vol. 127, pp 269-284.

Li, C., Atlar, M., Haroutunian, M., Norman, R., Anderson, C., 2019, "An investigation into the effects of marine biofilm on the roughness and drag characteristics of surfaces coated with different sized cuprous oxide (Cu2O) particles", Biofouling, pp 1-19.

Lücke T., Streckwall H., 2017, "Experience with Small Blade Area Propeller Performance", Fifth International Symposium on Marine Propulsors smp'17, Espoo, Finland.

Luo, W.-Z., Guo, C.-Y., Wu, T.-C., & Su, Y.-M., 2018, "Experimental research on resistance and motion attitude variation of ship–wave–ice interaction in marginal ice zones", Marine Structures, Vol. 58, pp 399-415.

McCarthy, J.H., Norley, W.H., Ober, G.L., 1961, "The performance of a fully submerged propeller in regular waves, David Taylor Model Basin, Report No. 1440.

McEntee, W., 1915, "Variation of frictional resistance of ships with condition of wetted surface", Trans. Soc. Nav. Arch. Mar. Eng., Vol. 24, pp 37-42.

McEntee, W., 1916, "Notes from Model Basin", Transactions of the Society of Naval Architects and Marine Engineers.

Melissaris T., Bulten N., van Terwisga T., 2018, "On Cavitation Aggressiveness and Cavitation Erosion on Marine Propellers using a URANS Method", Proceedings of the 10th International Symposium on Cavitation, Baltimore, USA.

Melissaris T., van Terwisga, T., 2019, "On the Applicability of Cavitation Erosion Risk Models with a URANS Solver", Journal of Fluids Engineering, Vol. 141.

Melissaris. T., Bulten, N., Oprea, I., 2019, "The necessity of accurate prediction of cavitation behaviour for fuel efficient propellers", Sixth International Symposium on Marine Propulsors SMP'19, Rome, Italy.

Mieno, H., Katsui, T., 2020, "Development of a portable 3D hull roughness analyser", Journal of Marine Science and Technology, Vol. 25, pp 498–509.

Mieno, H., Katsui, T., 2021, "Experimental investigation of added frictional resistance by paint rough surface using a rotating cylinder", Journal of Marine Science and Technology, Vol. 26, pp 1–15.

Mihatsch, M.S., Schmidt, S.J., Thalhamer, M., Adams, N., 2011, "Numerical Prediction of Erosive Collapse Events in Unsteady Compressible Cavitating Flows", Fourth International Conference on Computational Methods in Marine Engineering, Lisbon, Portugal.

Monty, J.P., Dogan, E., Hanson, R., Scardino, A.J., Ganapathisubramani, B., Hutchins, N., 2016, "An assessment of the ship drag penalty arising from light calcareous tubeworm fouling", Biofouling, Vol. 32, No. 4, pp 451-464.

Mosaad, M.A.A.-R., 1986, "Marine propeller roughness penalties", PhD thesis, Newcastle University, Newcastle Upon Tyne.

Mutton, R.J., Atlar, M., Anderson, C.D., 2005, "Drag Prevention Coatings for Marine Propellers". Paper presented at the 2nd International Symposium on Seawater Drag Reduction, Busan, Korea.

Nishikawa, T., 2015, "Application of Fully resolved Large Eddy Simulation to Self-Propulsion Test Condition of Double-Model KVLCC2", 14tth International Conference on Computer and IT Applications in the Maritime Industries (COMPIT'15), pp.191-199.

Nishikawa, T., 2015, "Application of fully resolved large eddy simulation to Japan Bulk Carrier with an energy saving device", Tokyo 2015 CFD Workshop.

Nohmi, M., Iga, Y., Ikohagi, T., 2008, "Numerical Prediction Method of Cavitation Erosion", Proceedings of FEDSM2008, Jacksonville, USA.

Owen, D., Demirel, Y.K., Oguz, E., Tezdogan, T., Incecik, A., 2018, "Investigating the Effect of Biofouling on Propeller Characteristics Using CFD", Ocean Engineering, Vol. 159, pp. 505-516.

Paskin, L., Visonneau, M., Guilmineau, E., Wackers, J., 2019, "Computational Modeling of Turbulent Flows on the Tip Vortex of a Marine Propeller's Blade", 6th International Symposium on Marine Propulsors smp'19.

Plessett, M.S., Chapman, R.B., 1971, "Collapse of an initially spherical vapour cavity in the neighbourhood of a solid boundary", Journal of Fluid Mechanics, Vol. 47, pp 283-290.

Raven, H., 2019, "A method to correct shallow-water model tests for tank wall effects", Journal of Marine Science and Technology, Vol. 24, No. 2.

Ravenna, R., Marino, A., Song, S., Demirel, Y. K., Atlar, M., Turan, O., 2019, "Experimental Investigation on the Effect of Biomimetic Tubercles on the Hydrodynamics of a Flat Plate". Paper presented at the Sixth International Conference on Advanced Model Measurement Technology for The Maritime Industry (AMT'19), Rome, Italy.

Ravina, E., Guidomei, S., 2018, "Experimental Investigation on Resistance Reduction by Means of Air-Bubbling Technique".

Sakamoto, N., Kobayashi, H., Ohashi, K., Kawanami, Y., Winden, B., Kamiirisa, H., 2020, "An overset RaNS prediction and validation of full scale stern wake for 1,600 TEU container ship and 63,000 DWT bulk carrier with an energy saving device", Applied Ocean Research, Vol. 105.

Sanada, Y., Tanimoto, K., Takagi, K., Gui, L., Toda, Y., Stern, F., 2013, "Trajectories for ONR Tumblehome maneuvering in calm water and waves", Ocean Engineering, Vol. 72, pp 45–65.

Sanada, Y., Elshiekh, H., Toda, Y., Stern, F., 2014, "Effects of Waves on Course Keeping and Maneuvering for Surface Combatant ONR Tumblehome", The 30th Symposium on Naval Hydrodynamics, Hobart, Tasmania, Australia.

Schenke, S., Melissaris, T., van Terwisga, T., 2019, "On the Relation between the Potential Cavity Energy and the Acoustic Power Signature caused by Periodic Vapor Cavity Collapses", Sixth International Symposium on Marine Propulsors SMP'19, Rome, Italy.

Schmidt, S., Sezal, I., Schnerr, G., 2008, "Numerical Analysis of Shock Dynamics for

Detection of Erosion Sensitive Areas in Complex 3-D Flows", Cavitation: Turbo-machinery & Medical Applications WIMRC FORUM 2008, Warwick University, UK.

Schuiling, B., Terwisga, T., 2018, "Energy loss analysis for a propeller operating behind a ship", 32nd Symposium on Naval Hydrodynamics, Hamburg, Germany.

Schultz, M.P., 2004, "Frictional Resistance of Antifouling Coating Systems", Journal of Fluids Engineering, Vol. 126, No. 6, pp 1039-1047.

Schultz, M.P., 2007, "Effects of coating roughness and biofouling on ship resistance and powering". Biofouling, Vol. 23, No. 5, pp 331-341.

Schultz, M.P., Bendick, J.A., Holm, E.R., Hertel, W.M., 2011, "Economic impact of biofouling on a naval surface ship". Biofouling, Vol. 27, No. 1, pp 87-98.

Seo, H., Go, S., Lee, S., Kwon, J., 2011, "A Study on the Powering Performance of Multi-axes Propulsion Ships with Wing Pods", SMP'11, Hamburg, Germany.

Seok, J., Park, J.-C., 2020, "Numerical simulation of resistance performance according to surface roughness in container ships". International Journal of Naval Architecture and Ocean Engineering, Vol. 12, pp 11-19.

Sheng, Z., et al, 1979, "Experimental study on propeller scale effects" (in Chinese), Journal of Shanghai Jiaotong University.

Shin, K., Andersen, P., 2018, "CFD Analysis of Propeller Tip Vortex Cavitation in Ship Wake Fields", 10th Symposium on Cavitation (CAV2018).

Shiraishi, K., Sawasda, Y., Arakawa, D., Kumura, K., 2019, "A Study on Deformation Measurements and Hydrodynamic Investigation of the Flexible Composite Marine Propeller", 6th International Symposium on Marine Propulsors smp'19.

Sokolov, M., Marinich N., 2012, "Experimental study on hydromechanic properties of hubless propeller in RIM-drive propulsion system", 10th International Conference on Hydrodynamics, St. Petersburg, Russia.

Song, S., Dai, S., Demirel, Y. K., Atlar, M., Day, S., Turan, O., 2021a, "Experimental and Theoretical Study of the Effect of Hull Roughness on Ship Resistance". Journal of Ship Research, Vol. 65, No. 1, pp 62-71.

Song, S., Demirel, Y.K., Atlar, M., 2019, "An investigation into the effect of biofouling on the ship hydrodynamic characteristics using CFD", Ocean Engineering, Vol. 175, pp 122-137.

Song, S., Demirel, Y.K., Atlar, M., 2020c, "Propeller Performance Penalty of Biofouling: Computational Fluid Dynamics Prediction". Journal of Offshore Mechanics and Arctic Engineering, Vol. 142, No. 6.

Song, S., Demirel, Y.K., Atlar, M., 2020d, "Penalty of hull and propeller fouling on ship self-propulsion performance", Applied Ocean Research, Vol. 94.

Song, S., Demirel, Y.K., Atlar, M., Dai, S., Day, S., Turan, O., 2020b, "Validation of the CFD approach for modelling roughness effect on ship resistance". Ocean Engineering, Vol. 200.

Song, S., Demirel, Y.K., De Marco Muscat-Fenech, C., Tezdogan, T., Atlar, M., 2020e, "Fouling effect on the resistance of different ship types", Ocean Engineering, Vol. 216.

Song, S., Ravenna, R., Dai, S., DeMarco Muscat-Fenech, C., Tani, G., Demirel, Y. K., Atlar, M., Day, S., Incecik, A., 2021b, "Experimental investigation on the effect of heterogeneous hull roughness on ship resistance", Ocean Engineering, Vol. 223.

Streckwall, H., Greitsch, L., Scharf, M., 2013, "An advanced Scaling Procedure for Marine Propellers", Third International Symposium on Marine Propulsors smp'13, Launceston, Australia.

Suyama, N., Fujita, S., Kumura, K., Shiraishi, K., Sawada, Y., Kawakita, C., 2019, "Study on Method to Predict Performance of Composite Propeller Using FSI Analysis", 6th International Symposium on Marine Propulsors smp'19.

Taskar, B., Yum, K.K., Steen, S., Pedersen, E., 2016, "The effect of waves on cavitation and pressure pulses", Applied Ocean Research, Vol. 60, pp 61-74.

Taskar, B., Steen, S., Eriksson, J., 2017, "Effect of waves on cavitation and pressure pulses of a tanker with twin podded propulsion", Applied Ocean Research, Vol. 65, pp 206-218.

Taylor, D.W., 1943, "The speed and power of ships: a manual of marine propulsion", Washington: U.S. G.P.O.

Tokgoz, E., Takasu, S., Wu, P-C., Toda, Y., 2017, "Computation and Experiment of Propeller Thrust Fluctuation in Waves for Propeller Open Water Condition", Journal of JASNAOE, Vol. 25, pp 55-62.

Townsin, R.L., Byrne, D., Svensen, T.E., Milne, A., 1981, "Estimating the technical and economic penalties of hull and propeller roughness", Trans SNAME, pp 295-318.

Usta, O., Aktas, B., Maasch, M., Turan, O., Atlar, M., Korkut, E., 2017, "A study on the numerical prediction of cavitation erosion for propellers", Fifth International Symposium on Marine Propulsors SMP'17, Espoo, Finland.

Visonneau, M., Deng, G., Guilmineau, E., Queutey, P., Wackers, J., 2016, "Local and Global Assessment of the Flow around the Japan Bulk Carrier with and without Energy Saving Devices at Model and Full Scale", Proceedings of the 31st ONR Symposium on Naval Hydrodynamics, Monterey, California, September 2016.

Vogel, A., Lauterborn, W., 1988, "Acoustic transient generation by laser-produced cavitation bubbles near solid boundaries", Journal of The Acoustical Society of America, Vol. 84, pp 719-731.

Wackers, J., Deng, G., Guilmineau, E., Leroyer, A., Queutey, P., Visonneau, M., Palmieri, M., Liverani, A., 2017, "Can adaptive grid refinement produce grid-independent solutions for incompressible flows?"", Journal of Computational Physics, Vol. 344, pp 364-380.

Wang, J., Zou, L., Wan, D., 2018, "Numerical simulations of zigzag maneuver of free running ship in waves by RANS-Overset grid method", Ocean Engineering, Vol. 162, pp 55–79.

Wang, L., Martin, J. E., Carrica, P. M., Felli, M., Falch, M., 2019, "Experiments and CFD for DARPA Suboff Appended with Propeller E1658 Operating Near the Surface". Paper presented at the Sixth International Symposium on Marine Propulsors, smp'19, Rome, Italy.

Werner, S., 2018, "Derivation of load variation factors – an example case", SSPA-Report No: RE70178533-01-00-A, SSPA.

Yakovlev, A., Sokolov, M., Marinich, N., 2011, "Numerical design and experimental verification of a RIM-driven thruster", Second International Symposium on Marine Propulsors smp'11, Hamburg, Germany.

Yao, H., Zhang, H., 2019, "Improvement of scaling method recommended by ITTC at lower Reynolds Number Range" (in Chinese), Journal of Shanghai Jiaotong University, Vol. 53, No. 1.

Yeginbayeva, I.A., Atlar, M., 2018, "An Experimental Investigation into the Surface and Hydrodynamic Characteristics of Marine Coatings with Mimicked Hull Roughness Ranges", Biofouling, Vol. 34, No. 9, pp. 1001-1019.

Yilmaz, N., Atlar, M., Khorasanchi, M., 2019, "An improved Mesh Adaption and Refinement Approach to Cavitation Simulation (MARCS) of Propellers", Ocean Engineering, Vol. 171, pp 139-150.

Yoon, H., Gui, L., Bhushan, S., Stern, F., 2014, "Tomographic PIV Measurements for a Surface Combatant at Straight Ahead and Static Drift Conditions", 30th Symposium on Naval Hydrodynamics, Hobart, Tasmania, Australia.

Zhang, C., Lu, F., Lu, L., 2019, "High-speed visualization of cavitation evolution around a marine propeller", Journal of Visualization, Vol. 22, Issue 2, pp 273-281.